University of Alberta

Investigation of Periotest® and Osstell® Instruments for Measuring Craniofacial Implant Integrity

by

Stephen Joseph Hurst ©

A thesis submitted to the Faculty of Graduate Studies and Research in partial fulfillment of the requirements for the degree of Master of Science.

Department of Mechanical Engineering

Edmonton, Alberta

Fall 2002

National Library
of Canada

Acquisitions and
Bibliographic Services

395 Wellington Street
Ottawa ON K1A 0N4
Canada

Bibliothèque nationale
du Canada

Acquisitions et
services bibliographiques

395, rue Wellington
Ottawa ON K1A 0N4
Canada

Your file Votre référence

Our file Notre référence

The author has granted a non-exclusive licence allowing the National Library of Canada to reproduce, loan, distribute or sell copies of this thesis in microform, paper or electronic formats.

The author retains ownership of the copyright in this thesis. Neither the thesis nor substantial extracts from it may be printed or otherwise reproduced without the author's permission.

L'auteur a accordé une licence non exclusive permettant à la Bibliothèque nationale du Canada de reproduire, prêter, distribuer ou vendre des copies de cette thèse sous la forme de microfiche/film, de reproduction sur papier ou sur format électronique.

L'auteur conserve la propriété du droit d'auteur qui protège cette thèse. Ni la thèse ni des extraits substantiels de celle-ci ne doivent être imprimés ou autrement reproduits sans son autorisation.

0-612-81411-4

Canada

University of Alberta

Library Release Form

Name of Author:	**Stephen Joseph Hurst**
Title of Thesis:	**Investigation of Periotest® and Osstell® Instruments for Measuring Craniofacial Implant Integrity.**
Degree:	**Master of Science**
Year this Degree Granted:	**2002**

Permission is hereby granted to the University of Alberta Library to reproduce single copies of this thesis and to lend or sell such copies for private, scholarly or scientific research purposes only.

The author reserves all other publication and other rights in association with the copyright in the thesis, and except as herein before provided, neither the thesis nor any substantial portion thereof may be printed or otherwise reproduced in any material form whatever without the author's prior written permission.

Stephen J. Hurst

Stephen J. Hurst
PO Box 5662
High River AB
T1V 1M7

Date: July 5/2002

University of Alberta

Faculty of Graduate Studies and Research

The undersigned certify that they have read, and recommend to the Faculty of Graduate Studies and Research for acceptance, a thesis entitled **Investigation of the Periotest® and Osstell® Instruments for Measuring Craniofacial Implant Integrity** submitted by **Stephen Joseph Hurst** in partial fulfillment of the requirements for the degree of **Master of Science**.

Gary Faulkner

Dr. Gary Faulkner (Supervisor)

Dr. Don Raboud (Co-Supervisor)

Dr. J. Wolfaardt (External)

Ken Fyfe

Dr. Ken Fyfe (Chair)

Date: July 4/02

Abstract

Use of osseointegrated implant retained facial prostheses have greatly increased quality of life for those individuals who have missing or lost parts of the face that cannot be autogenously reconstructed. The technique developed by Per-Ingvar Brånemark requires a healing period of 3-4 months after implant installation. This period is designed to safely accommodate the remodeling cycle in humans prior to loading the implant with a prosthesis. To safely reduce this healing period requires the ability to monitor changes in the interface between the implant and supporting tissue. The Periotest® and Osstell® instruments have been used to measure changes in the interface without a good understanding of which instrument has more favorable resolution, repeatability, and sensitivity.

This study investigates the ability of the Periotest® and Osstell® instruments to measure implant integrity by first understanding instrument operation, then measuring several in vitro and in vivo implant systems, and finally, applying a mathematical model to better understand parameters which affect the motion of the implant system.

The conclusions from this study show the Periotest® instrument may be improved by modifying the post-processing of the transducer signal. With this improvement, both the Periotest® and Osstell® instruments have similar capabilities of detecting changes in implant system geometric and material parameters.

Dedication

To all those people who have more confidence in me than I do

Acknowledgments

I am reminded of a quote by Benjamin Franklin:

> *Tell me, and I forget.*
>
> *Teach me, and I may remember.*
>
> *Involve me, and I learn.*

The past 18 months have been some of the most involved learning I have ever experienced. During this time, I have been frustrated, confused, depressed, and happy. My friends and family have provided motivation, inspiration, and most of all, hope the end was near (just kidding). Thanks for your patience and guidance – without it this research would not be possible.

Dr. Gary Faulkner, Dr. Don Raboud, Dr. J. Wolfaardt
Don, Albert, Bernie, Ian, Dave, Terry, Dirk, Rick, Tuula
Demetri, Kajsa, Kristin, Ryan, Karla Collinge, Tonya, Dave Lario, Jason Hawirko
Jonathon Levesque
Shannon, Michelle, Susanne, Dr. Ray, Rhonda K., Rhonda H., Jane
Joyce, Marcie, Dianne, Sandy
Dr. DiToppa, Claudette, Jan

AND MOST OF ALL, Thanks Mom and Dad.

Table of Contents

Chapter 1 – Introduction 1
  1.1 Introduction and Literature Review 1
  1.2 Problem Statement and Thesis Outline 9
Chapter 2 - Materials and Methods 16
  2.1 Introduction 16
  2.2 General Equipment and Procedures 17
    2.2.1 Implant Systems 17
    2.2.2 Transducer Signal Recording Apparatus 20
    2.2.3 Development of MATLAB Code to Replicate Periotest® PTV 21
    2.2.4 Development of MATLAB Code to Replicate Osstell® ISQ 23
    2.2.5 Instrument Measurement Protocol 25
  2.3 In Vitro Periotest® Studies 26
    2.3.1 Investigation of Periotest® Transducer Signal 26
    2.3.2 Investigation of Periotest® Resolution, Repeatability, and Sensitivity 28
    2.3.3 Repeatability of the Periotest® Transducer Signal 29
    2.3.4 Estimation of Clinical Periotest® Repeatability 29
    2.3.5 Response of Implant System to the Periotest® 30
    2.3.6 Effect of Changing Supporting Material Stiffness on PTV 33
    2.3.7 Investigation of In Vitro FRB-10 Disc Plate Effects 33
  2.4 In Vitro Osstell® Studies 34
    2.4.1 Investigation of Osstell® Resolution, Repeatability, and Sensitivity 34
    2.4.2 Estimation of Clinical Osstell® Repeatability 35
    2.4.3 Response of Implant System to Osstell® 35
  2.5 In Vivo Study 36
    2.5.1 Periotest® Training Block 36
    2.5.2 Measurement Protocol 37
Chapter 3 – Results and Discussion 51
  3.1 Introduction 51
  3.2 Understanding Instrument Operation 52
    3.2.1 Periotest® Measurements 52
    3.2.2 Osstell® Measurements 56
  3.3 Estimate of Periotest® Repeatability and Resolution 56
    3.3.1 Existing Periotest® PTV 57
    3.3.2 MATLAB PTV 57
  3.4 Estimate of Osstell® Repeatability and Resolution 59
  3.5 Effect of Geometric Implant System Variables 61
    3.5.1 Effect of Abutment Length on Periotest® 61
    3.5.2 Osstell® Sensitivity to Changes in Abutment Length 65
    3.5.3 Minimum Measurable Change of Abutment Length 67
    3.5.4 Effect of Engagement Length on Periotest® and Osstell® 68
    3.5.5 Effect of Implant Diameter on Periotest® and Osstell® 74
  3.6 Mathematical Model of Implant System Motion 76
    3.6.1 Correlation of Model and Experiments 82
    3.6.2 Possible Second Mode of Vibration 86
  3.7 In Vivo Results 88

Chapter 4 – Conclusions and Recommendations 103
 4.1 Conclusions 103
 4.2 Recommendations 104
List of References 107
Appendix A – MATLAB Code for Periotest® 110
Appendix B – MATLAB Code for Osstell® 112
Appendix C – Pre-Amplified Periotest® Transducer 115
Appendix D – Strain Gauge Response to Periotest® 122
Appendix E – Strain Gauge Response to Osstell® 129
Appendix F – Periotest® Response to Abutment Length: Giannitsios et. al. Model (2001) 136
Appendix G – Periotest® Response to Abutment Length 139
Appendix H – Osstell® Response to Abutment Length 142
Appendix I – Periotest® Response to Engagement Length 145
Appendix J – Osstell® Response to Engagement Length 148
Appendix K– Periotest® and Osstell® Response to Implant Diameter 151
Appendix L – Giannitios et. al. Model(2001) 154
Appendix M – Least Squares Fit of Periotest® Data 158
Appendix N – Theoretical Modal Analysis 159
Appendix O – In Vivo Patient Measurements 162

Table of Figures

Figure 1-1: Schematic Cross-Section View of A Two-Piece Implant System 11
Figure 1-2: Schematic of Implant System for a Bone Anchored Hearing Aid® 11
Figure 1-3: Response of Implant System to Periotest® Rod Strike 12
Figure 1-4: Transducer Recording for a Complete Periotest® Measurement Sequence. 12
Figure 1-5: Periotest® Accelerometer Response for a Single Strike with Implant System 13
Figure 1-6: Periotest® Instrument Variables 13
Figure 1-7: Osstell® Transducer Lead Connected to an Abutment 14
Figure 1-8: Schematic of Implant System Variables 15
Figure 1-9: Schematic of Implant System Variables with Influence of Bone Loss 15
Figure 2-1: Schematic of Two-Piece Brånemark Implant System 39
Figure 2-2: Digital Acquisition System 39
Figure 2-3: Sample of Periotest® Transducer Signals 40
Figure 2-4: Sample Osstell® Transducer Signal 40
Figure 2-5: Verification of Constant Time-Step Approximation in MATLAB Code 41
Figure 2-6: Sample Osstell® Signal – Showing Resonant Frequency 41
Figure 2-7: Control of Azimuthal Direction for In Vitro Measurements 42
Figure 2-8: Periotest® Accelerometer Verification using Independent Accelerometer Mounted to a Shaker Table 42
Figure 2-9: Comparison of Periotest® Accelerometer Signal Sampled After an Input Amplifier to an Independent Accelerometer 43
Figure 2-10: Comparison of Periotest® Accelerometer Signal Sampled Before an Input Amplifier to an Independent Accelerometer Signal 43
Figure 2-11: Periotest® In Vitro Experimental Apparatus 44

Figure 2-12: Multiple Responses of the Periotest® Transducer when Evaluating a Ø4mm Intra-Oral Brånemark Implant in FRB-10 to an Engagement length of 8.72mm 44
Figure 2-13: Sample of Strain Gauge and Periotest® Signals 45
Figure 2-14: Periotest® and Strain Gauge Response of a Ø4mm Intra-Oral Brånemark Implant Mounted in FRB-10 to an Engagement Length of 1.68mm 45
Figure 2-15: Positive Displacement of Abutment When Periotest® Rod moving Outwards 46
Figure 2-16: Single Degree of Freedom System 46
Figure 2-17: Response of a Strain Gauged Abutment, attached to a Ø4mm Intra-Oral Brånemark Implant Installed in FRB-10 to an Engagement Length of 8.72mm, to the Periotest® 47
Figure 2-18: Modification Process of In Vitro Disc Number 11 47
Figure 2-19: Additional Clamping Apparatus 48
Figure 2-20: Strain Gauged Abutment Response to Osstell® Measurement 48
Figure 2-21: Use of Periotest® Training Block During In Vivo Study 49
Figure 2-22: Flow Chart of In Vivo Protocol 50
Figure 3-1: Periotest® and Strain Gauge Response of a Ø4mm Intra-Oral Brånemark Implant Mounted in FRB-10 to an Engagement Length of 1.68mm 90
Figure 3-2: Response of Ø4mm Intra-Oral Brånemark Implant in FRB-10 to an Engagement Length of 8.72mm 91
Figure 3-3: Response of Ø4mm Intra-Oral Brånemark Implant in FRB-10 to an Engagement Length of 5.72mm 91
Figure 3-4: Response of Ø4mm Intra-Oral Brånemark Implant in FRB-10 to an Engagement Length of 1.68mm 91
Figure 3-5: Response of Ø3.75mm Extra-Oral Brånemark Implant in FRB-10 to an Engagement length of 4.78mm 92
Figure 3-6: Response of Ø3.75mm Extra-Oral Brånemark Implant in FRB-10 to an Engagement length of 3.83mm 92
Figure 3-7: Response of Ø3.75mm Extra-Oral Brånemark Implant in FRB-10 to an Engagement length of 2.78mm 92
Figure 3-8: Response of Ø3.75mm Extra-Oral Brånemark Implant in FRB-10 to an Engagement length of 1.87mm 92
Figure 3-9: Response of Ø3.75mm Intra-Oral Brånemark Implant in FRB-10 to an Engagement length of 5.62mm 93
Figure 3-10: Response of Ø3.75mm Intra-Oral Brånemark Implant in FRB-20 to an Engagement length of 5.62mm 93
Figure 3-11: Strain Gauge and Osstell® Recording Transducer Simultaneous Responses (shown on top and bottom, respectively) 94
Figure 3-12: Representative Periotest® Response to Changes in Abutment Length for Ø3.75mm Brånemark Intra-Oral Implants installed in FRB-10 94
Figure 3-13: Representative Osstell® Response to Changes in Abutment Length for Ø3.75mm Brånemark Intra-Oral Implants installed in FRB-10 95
Figure 3-14: Periotest® Response to Changes in Engagement Length and Striking Height for Ø3.75mm Brånemark Intra-Oral Implants installed in FRB-10 95
Figure 3-15: Osstell® Response to Changes in Engagement Length and Striking Height for Ø3.75mm Brånemark Intra-Oral Implants installed in FRB-10 96
Figure 3-16: Representative Periotest® Response to Changes in Implant Diameter for Brånemark Intra-Oral Implants installed in FRB-10 to an Effective Engagement Length of 5.72mm 97

Figure 3-17: Representative Osstell® Response to Changes in Implant Diameter for Brånemark Intra-Oral Implants installed in FRB-10 to an Effective Engagement Length of 5.72mm 97
Figure 3-18: Giannitsios et. al.(2001) Model of Vibrating Implant System 98
Figure 3-19: FBD/MAD of Implant Model Proposed by Giannitsios et. al.(2001) 98
Figure 3-20: Response of Periotest® Pre-Amplified Transducer Signal to Changes in Effective FRB-10 Disc Diameter – Thin Plate Study 99
Figure 3-21: Response of Periotest® to Axial Evaluation of Implant System – Thin Plate Study 99
Figure 3-22: Response of Perpendicular Periotest® Evaluation of In Vitro Disc Number 6 with and without Additional Clamping – Thin Plate Study 100
Figure 3-23: Mode Shapes for Ø3.75mm Intra-Oral Brånemark Implant Installed in FRB-10 to an Engagement Length of 5.62mm (Not drawn to scale) 100
Figure 3-24: Pre-Amplified Periotest® Response for Ø3.75mm Intra-Oral Brånemark Implant, with 10mm Abutment, and Installed in FRB-10 to an Engagement Length of 5.62mm – Curve Fit Using A Damped Sine 101
Figure 3-25: Second Frequency Component for Figure 3-24 101
Figure 3-26: Representative Periotest® In Vivo Measurements 102
Figure 3-27: Representative Osstell® In Vivo Measurements 102

List of Tables

Table 1-1: Correlation of PTV to Miller Mobility Index 5
Table 2-1: Implant/FRB-10 Disc Combinations Considered in the In Vitro Study 18
Table 2-2: List of Abutments 19
Table 2-3: Comparison of PTVs from Periotest® and MATLAB Code 23
Table 2-4: Osstell® Instrument and MATLAB Determine Resonant Frequencies 24
Table 3-1: Natural Frequencies of the Implant System Measured Using A Strain Gauged Abutment 55
Table 3-2: Properties of Existing Periotest® and MATLAB Measurement Values 58
Table 3-3: PTVs from Periotest® and MATLAB Code for In Vitro Disk Number 6 59
Table 3-4: MATLAB and Osstell® Resonant Frequency Standard Deviations 60
Table 3-5: Linear Regression Results for MATLAB PTV/Abutment Length Plots 63
Table 3-6: Linear Regression Results for Osstell® ISQ/Abutment Length Plots 66
Table 3-7: Minimum Detectable Abutment Length using the Periotest® or Osstell® 67
Table 3-8: Linear Regression Results for MATLAB PTV/Engagement Length/Striking Height Plots 69
Table 3-9: Linear Regression Results for Osstell® ISQ/Engagement Length/Striking Height Plots 71
Table 3-10: Minimum Detectable Engagement Length* Changes 73
Table 3-11: Variable Definitions for Giannitsios et. al. (2001) Model 78
Table 3-12: Least Squares Results for In Vitro Implant Systems 83
Table 3-13: Natural Frequencies of Implant System 87

Chapter 1 – Introduction

1.1 Introduction and Literature Review

Human trauma can result from many experiences in our daily lives. One of the most traumatic experiences is the loss of portions of our most distinguishable feature – our face and head. These losses may be caused by congenital or acquired conditions and can take the form of removed, absent, or deformed teeth, eyes, ears, and noses, as well as permanent loss of hearing. Whether these alterations are caused by a vehicle collision, birth defect, industrial accident, or removal of a cancerous tumor, the effect is the same: both functional and psychosocial losses leading to a loss of quality of life.

To treat these losses, prostheses are constructed and retained in place of the missing or lost facial structures. Prosthesis construction combines both science and art. Retention of the prosthesis is accomplished using titanium screws, called implants, installed in bone proximal the facial defect. A typical implant system is composed of an implant and an abutment, as shown in Figure 1-1. The abutment is attached to the implant using a screw and transfers the loads from the prosthesis to the implant. Examples of these systems include an orbital prosthesis that connects to implant/abutment systems located in the orbital rim, a Bone Anchored Hearing Aid® (BAHA®, Entific Medical Systems, Götenburg, Sweden) that is attached to an implant/abutment system installed in the temporal bone, as shown in Figure 1-2, and prosthetic teeth attached to implants in the mandible or maxilla. With facial prostheses, the color and final shape are primarily determined by the artistic talents of the clinician. With the constructed prosthesis connected to the implant/abutment system, the goal is that the person can return to a more normal lifestyle with a corresponding improvement in quality of life.

Osseointegrated implants systems are presumably installed for the lifetime of the individual and rely on a rigid connection between the implant and the bone to withstand loads transferred from the prosthesis to the implant. Typical loads applied to the implant are caused by routine removal of prostheses for cleaning, and functional loads, such as forces and moments resulting on prosthetic teeth systems during mastication of food. These loads transferred to the implant and supporting tissue are believed to influence the response of bone adjacent the implant. Initially, premature loading of implants was believed to cause failures and led to standard installation procedures of waiting approximately three to four months – one healing period of human bone – for the bone to heal around the implant before the prosthesis was connected. Today, more work is being undertaken in the belief that earlier loading of the implant may positively influence the bone response and allow earlier connections of the prosthesis.

To avoid an increase in implant failures and allow the patient to wear his or her prosthesis sooner requires the ability to monitor the 'health' or integrity of the interface between the bone and implant. This ability is especially crucial when monitoring the interface during the first stages of bone healing to decide how the loading of the implant affects the bone and adjust prosthesis design and use accordingly to avoid implant failures. In addition, the concept of progressive loading becomes meaningful. Failing implants could be identified and unloaded until safe to resume loading.

Several different approaches to measuring implant integrity have been attempted. These measurement techniques include the use of radiography, sound, and manual perturbation of the implant system. The measuring techniques are developed to monitor minute changes in the interface properties between the implant and bone and may be used over time for repeated measures assessment. Therefore, it is important that the measuring technique is repeatable and has a resolution and sensitivity capable of detecting these changes in the interface properties that may forewarn of an implant failure.

Radiography distinguishes between the varying qualities and quantities of tissue surrounding the implant. To measure implant integrity, an image of the implant surrounded by supporting tissue is subjectively interpreted based on the amount and type of tissue in contact with the implant. It is important to note that the image only has two dimensions and cannot return reliable information about implant integrity in other planes without multiple measurements. Because of the resolution and sensitivity of this technique, changes in implant integrity are difficult to detect (Elias, Brunski, & Scarton 1996; Kaneko 1993; Ichikawa et. al. 1994; Derhami et. al. 1995), and may lead to incorrect assessment of the interface and premature loading of the implant (Olivé & Aparicio 1990). In addition, the reproducibility of radiographic images is questionable (Walker et. al. 1997; Meredith et. al. 1996). However, radiography has been used in several studies as a comparison for manual perturbation methods of measuring implant integrity (Salonen et. al. 1993; Truhlar et. al. 1994; Haas et. al. 1995; Aparicio 1997; Meredith et. al. 1997; Aparicio & Orozco 1998; Røynesdal et. al. 1998; Cranin et. al. 1998; Isidor 1998; Rasmusson et. al. 1999; Verhoeven et. al. 2000; Ramp & Jeffcoat 2001).

A strike on the implant system using the handle of a stainless steel instrument was one of the first manual perturbation methods of measuring implant integrity. The clinician assessed the resulting sound of the vibrating instrument subjectively. If a high frequency sound resulted, the implant was deemed 'healthy'. The result from this method depends both on how the clinician strikes the implant and subjectively perceives the audible response. Consequently, repeatability, resolution, and sensitivity of this method are questionable considering weeks may pass between patient measurements.

A second manual measuring technique is based on physical perturbation of the implant system by hand. In this case, the clinician determines the 'mobility' of the implant based on the displacement resulting from a force applied to the abutment. The ability to measure small changes in implant integrity is not possible using this technique and essentially reports only implant success or failure.

To overcome the lack of resolution in the manual techniques, electronic instruments have been employed to measure the implant system response to controlled, repeatable loading. Two of these instruments that both use mechanical vibration to perturb the implant system include the Periotest®(Niva Inc., Charolette, North Carolina, United States of America) and Osstell®(Integration Diagnostics Inc., Götenburg, Sweden).

The Periotest® was initially developed by Siemens, Germany, to measure natural tooth mobility. To complete a measurement, an accelerometer-equipped rod of known mass is magnetically propelled towards a tooth or implant system and is believed to cause movement as shown in Figure 1-3. The Periotest® rod strikes the implant system with an initial velocity (Figure 1-3a) and causes the implant system to deflect. At some point (Figure 1-3b), the Periotest® rod and implant system reach a maximum deflection. The elastic properties of the implant interface and supporting tissue then cause the implant system to return to its original position (Figure 1-3c) and at this point the Periotest® rod is reset by the instrument for the next strike (Figure 1-3d). The response of the accelerometer while in contact with the tooth (Figure 1-3a through c) is recorded and processed. This four-second measurement involves 16 contacts of the Periotest® rod with the tooth. The response of the accelerometer for a single measurement is shown in Figure 1-4. Figure 1-5 shows a single response of the Periotest® accelerometer while the rod is in contact with the implant system. The main goal of this instrument was to increase the repeatability of measuring the mobility of teeth and develop a scale that correlated with the Miller Mobility Index (Truhlar et. al. 1994). The chosen Periotest® scale was called the **P**erio**T**est **V**alue (PTV) and is calculated using Equation 1-1 for PTVs in the range of –8 to +13.

$$PTV = 50ct - 21.3 \qquad \text{Equation 1-1}$$

where ct is contact time in milliseconds

The PTV corresponds approximately to the Miller Mobility Index (Lukas et. al. 1990, Truhlar et. al. 1994). The PTV-Miller Mobility Index Correlation is shown in Table 1-1 and indicates larger PTV values correspond to decreasing stiffness of the implant interface. The Periotest® offers a non-invasive and easily administered technique for measuring tooth mobility.

Table 1-1: Correlation of PTV to Miller Mobility Index

Miller Mobility Index	PTV Range (Integer Values)	Physical Interpretation
0	-8 to +9	No discernible movement
1	10 to 19	Just discernible movement
2	20 to 29	Obvious visible movement
3	30 to 50	Mobile pressure

From Truhlar, Morris, Ochi, Winkler (1994)

While developed for natural teeth, application of the Periotest® in measuring implant integrity has been actively investigated over several years. The range of PTV that occurs for implants is very limited (approximately –8 to 0, in integer increments) compared to those values for teeth as a result of a stiffer supporting implant-bone interface. In addition, the resolution of the Periotest® instrument is too large to detect small changes in mobility that could clinically indicate a failing implant. Furthermore, clinical variables associated with using the Periotest®, such as striking height and handpiece angulation as shown in Figure 1-6, can cause relatively large variations in the PTV and mask any changes that occur at the implant interface (Giannitsios et. al. 2001).

Unlike the Periotest®, the Osstell® instrument was specifically designed to measure implant integrity. The Osstell® unit also perturbs the implant system using mechanical vibration. The main feature of the Osstell® instrument is a cantilever beam that is either attached to the top of the abutment or directly to the implant. This beam has two piezoelectric crystals – one mounted on either side of the beam, as shown in Figure 1-7. Operation of the unit causes one of the crystals to be excited at a certain frequency while the amplitude of the second crystal is recorded.

The excitation crystal is stepped through a frequency range of 2500 to 9000 Hz in increments of 200 Hz. The signal from the response crystal is processed to find the maximum amplitude and the corresponding frequency that approximates the natural frequency of the implant system with attached transducer lead. Different conditions at the implant interface will lead to different resonant frequencies and allows an opportunity for changes in implant integrity to be monitored (Meredith et. al. 1996). To make the instrument user-friendly, a unique measurement scale called the **I**mplant **S**tability **Q**uotient (ISQ) was created to convert the resonant frequency values into an integer measurement scale between 0 and 100. The ISQ is proportional to the resonant frequency, as shown in Equation 1-2.

$$ISQ = c_1*(\text{Abutment Length})+c_2*(\text{Resonant Frequency})+c_3 \qquad \text{Equation 1-2}$$

where c_1, c_2, and c_3 are calibration constants unique to each transducer lead and the abutment length is entered by the instrument operator

Both the Periotest® and Osstell® instruments use response to a mechanical excitation as a means to evaluate the condition of the implant interface. The Periotest® evaluates the interface using an impulsive excitation while measuring a transient response. The Osstell® system uses a continuous excitation and measures a more steady state response of the implant system with attached transducer lead.

To date, investigation of the Periotest® and Osstell® units have involved both in vitro and in vivo studies. Because of the relatively recent development of the Osstell® instrument compared to the Periotest®, there is more literature investigating the Periotest®.

The in vitro studies of the Periotest® have correlated properties of an implant system to the measured PTV. Some of the implant system properties include the type of supporting tissue, striking height, abutment height, engagement length, and implant diameter, as shown in Figure 1-8. It should be noted that most of the investigations of the Periotest® to date have involved correlating the returned integer PTV to physical changes in the implant system. Recently, Giannitsios et. al. (2001) extracted the Periotest® accelerometer signal and compared it to changes in implant variables, such as striking height and engagement length, and to the response of a strain gauged abutment.

Several investigators have concluded that the PTV is sensitive to the supporting tissue properties. For example, the Periotest® could indicate the difference in implant integrity as epoxy resin cured around an implant. In fact, the resulting trend suggested a negative relationship between drying time and PTV (Meredith et. al. 1996). Application of this result to clinical Periotest® measurements suggests the stiffer the implant interface, the lower the PTV. This result corresponds with the Miller Mobility Index – the basis of the Periotest® scale.

The Periotest® values also vary with striking height. In fact, the PTV can change about 2 PTV for every 2 mm change in striking height (Giannitsios et. al. 2001). A change of 2 mm in striking height corresponds to the difference between the top and bottom of the Periotest® rod striking the abutment – a difficult instrument variable to control without the use of handpiece angulation and completing measurements at the crown of the abutment, as shown in Figure 1-6. Comparison of a 2 PTV change to the limited expected range of –8 to 0 PTV for healthy implants suggests control of striking height during a Periotest measurement is essential for meaningful results (Giannitsios et. al. 2001).

The Periotest® response to changes in engagement length has recently been investigated in vitro by Giannitsios et. al. (2001). The results from this investigation suggest an increase in engagement length causes an overall decrease in the PTV. Similar trends in PTV result whether engagement length increases or the stiffness of the supporting tissue increases.

Some investigators have stated effects of implant diameter changes on PTV. A recent two-degree of freedom mathematical model approximating the motion of the implant system suggested an increase in implant diameter results in decreasing PTVs (Giannitsios et. al. 2001). The explanation for this result is given: as the implant diameter increases, the implant is engaged with more supporting tissue, therefore, the PTV decreases.

Clinically, the properties of the implant system that are expected to change over time are the stiffness of supporting tissue, engagement length, and striking height. These three properties vary because of changes in the interface and/or bone loss. The loss of engagement length, usually starts at the surface of the supporting tissue. If the supporting tissue is lost from the surface, the striking height changes as well. Therefore, bone loss changes both the engagement length and striking height, as seen in Figure 1-9 compared to Figure 1-8.

Similar to the Periotest®, the Osstell® response to changes in the implant interface has been investigated both in vitro and in vivo (Meredith et. al. 1996; Meredith et. al. 1997; Rasmusson et. al. 1999). The in vitro measurements show the Osstell® resonant frequency responds differently as the tissue supporting the implant changes properties. In fact, as the stiffness of the implant interface increases, the resonant frequency increases (Meredith et. al. 1996), and it has been shown that an increase in exposed height, as shown in Figure 1-8, causes the resonant frequency to decrease. These two results are in agreement with vibration theory. The in vivo measurements also show distinct differences in the resonant frequencies for healthy implants versus implants near failure (Rasmusson et. al. 1999).

1.2 Problem Statement and Thesis Outline

With two unique instruments commercially available for measuring implant integrity, several questions arise: which instrument has more favorable sensitivity, repeatability, and resolution? In addition, can these instrument characteristics be improved by post-processing the instrument transducer signals differently, or imposing a more stringent measurement protocol? These questions are addressed by comparing the Periotest® and Osstell® responses when evaluating both in vitro and in vivo implant systems. The materials and methods used to address these questions are presented in Chapter 2. Chapter 3 interprets the collected data and discusses the meaning of the data trends. Conclusions, with recommendations, are presented in Chapter 4.

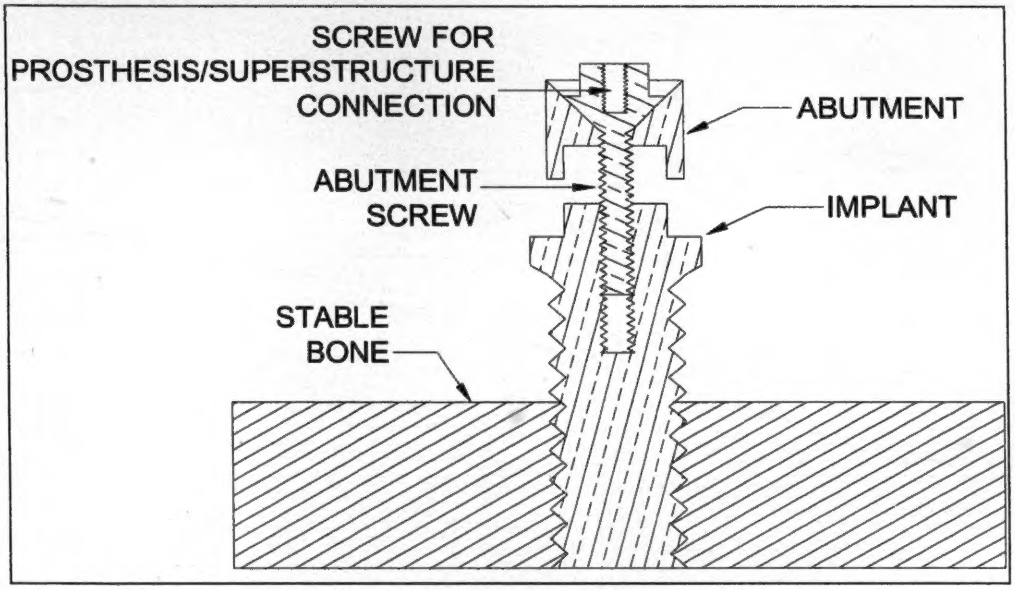
SCREW FOR PROSTHESIS/SUPERSTRUCTURE CONNECTION
ABUTMENT
ABUTMENT SCREW
IMPLANT
STABLE BONE

Figure 1-1: Schematic Cross-Section View of A Two-Piece Implant System

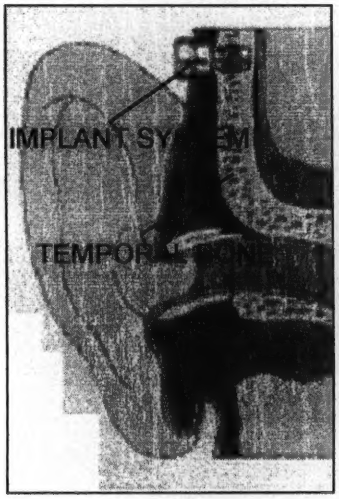
IMPLANT SYSTEM
TEMPORAL BONE

Figure 1-2: Schematic of Implant System for a Bone Anchored Hearing Aid®

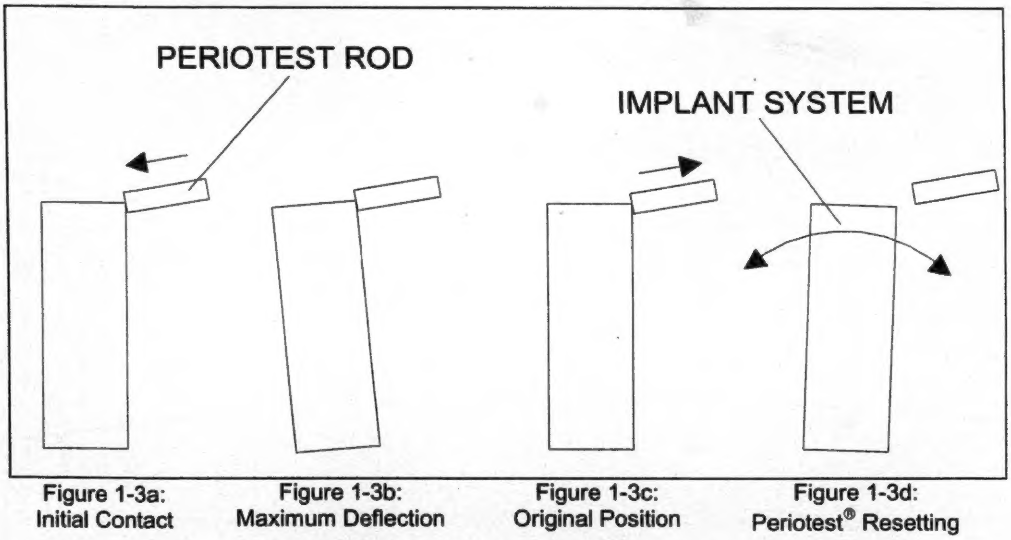

Figure 1-3a: Initial Contact

Figure 1-3b: Maximum Deflection

Figure 1-3c: Original Position

Figure 1-3d: Periotest® Resetting

Figure 1-3: Response of Implant System to Periotest® Rod Strike

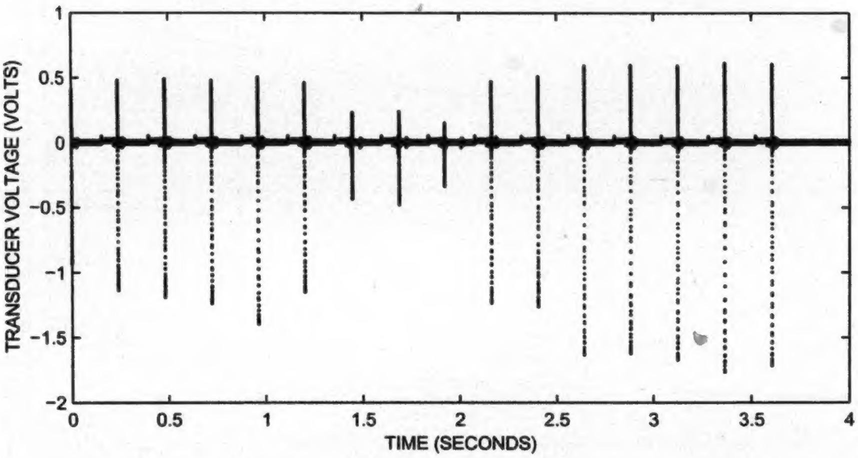

Figure 1-4: Transducer Recording for a Complete Periotest® Measurement Sequence

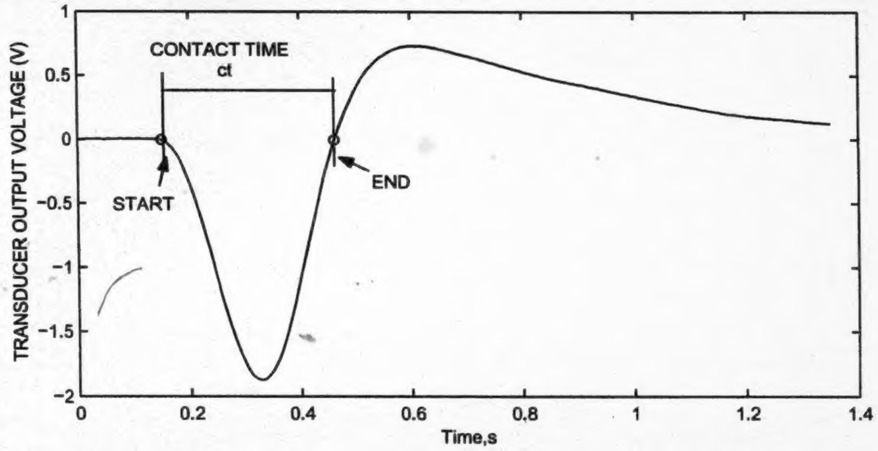

Figure 1-5: Periotest® Accelerometer Response for a Single Strike with Implant System

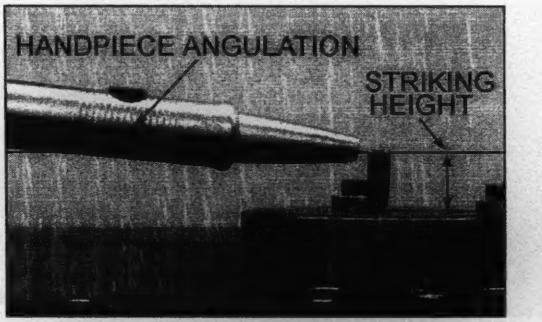
HANDPIECE ANGULATION
STRIKING HEIGHT

Figure 1-6: Periotest® Instrument Variables

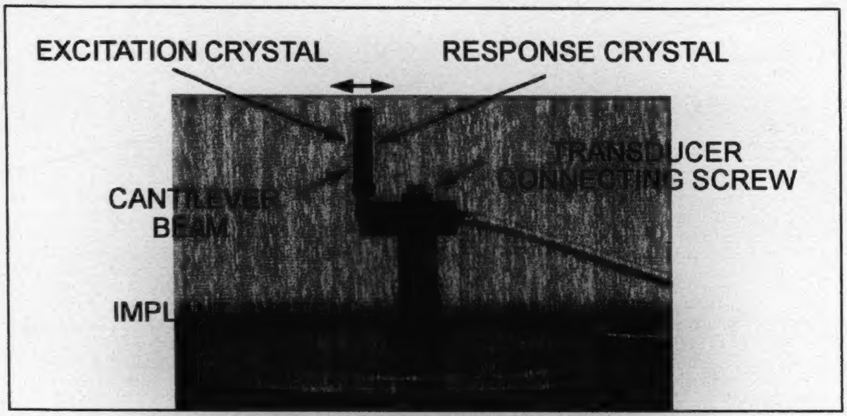
EXCITATION CRYSTAL
RESPONSE CRYSTAL
TRANSDUCER CONNECTING SCREW
CANTILEVER BEAM
IMPL

Figure 1-7: Osstell® Transducer Lead Connected to an Abutment

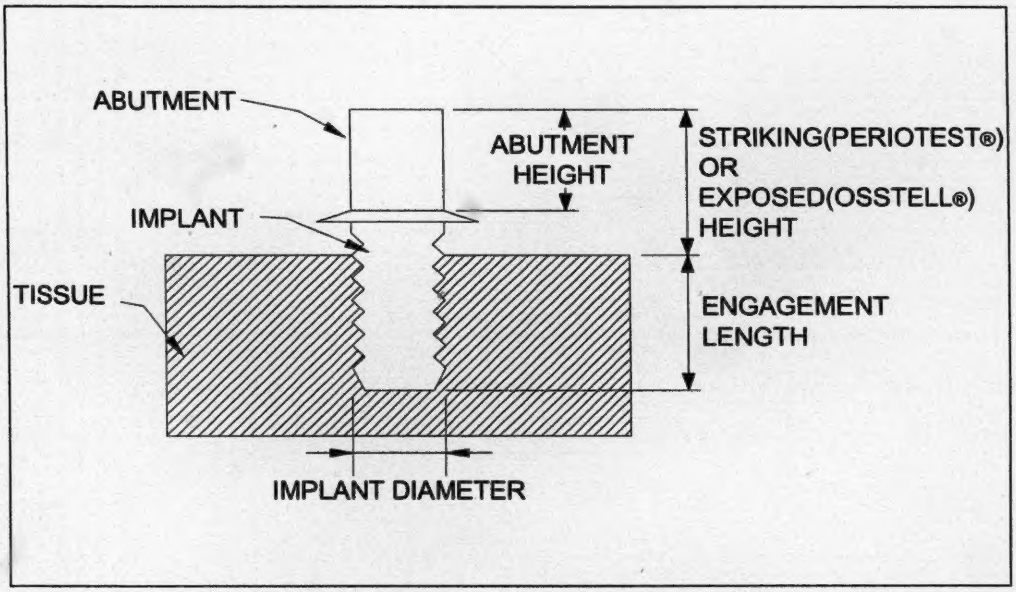
ABUTMENT
ABUTMENT HEIGHT
STRIKING(PERIOTEST®) OR EXPOSED(OSSTELL®) HEIGHT
IMPLANT
TISSUE
ENGAGEMENT LENGTH
IMPLANT DIAMETER

Figure 1-8: Schematic of Implant System Variables

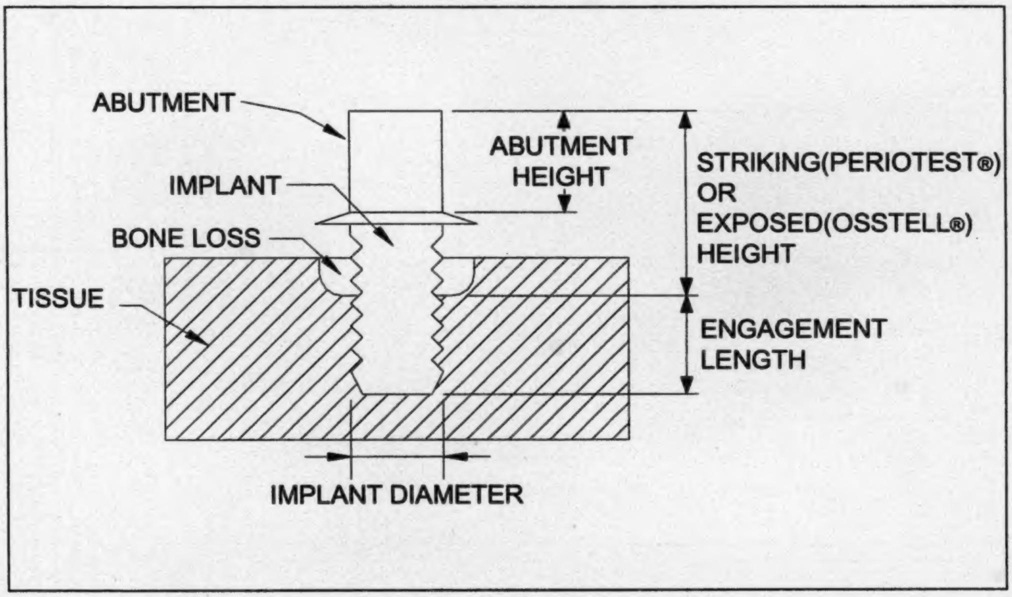
ABUTMENT
ABUTMENT HEIGHT
STRIKING(PERIOTEST®) OR EXPOSED(OSSTELL®) HEIGHT
IMPLANT
BONE LOSS
TISSUE
ENGAGEMENT LENGTH
IMPLANT DIAMETER

Figure 1-9: Schematic of Implant System Variables with Influence of Bone Loss

Chapter 2 - Materials and Methods

2.1 Introduction

The experimental equipment and procedures were designed to better understand and compare the Periotest® and Osstell® instruments for measuring implant integrity. To complete this task, both in vitro and in vivo studies were conducted. The in vitro studies were conducted: 1) to better appreciate how the Periotest® and Osstell® transducer signals were processed to determine the Periotest Values (PTV) and Implant Stability Quotients (ISQ), respectively; 2) to estimate and compare the resolution, repeatability, and sensitivity of the Periotest® and Osstell®; and, 3) to better understand the response of the Periotest® and Osstell® to variations in implant system parameters. The in vivo study investigated practical clinical use of the instruments by tracking PTVs and ISQs of implants placed in 10 adult Bone Anchored Hearing Aid (BAHA) patients from initial installation through routine patient check-ups.

Equipment and procedures common to both the in vitro and in vivo studies are first presented in this chapter. Then specifics are considered for each of the Periotest®

and Osstell® in vitro studies. Finally, the in vivo study, containing both Periotest® and Osstell® procedures, is presented.

2.2 General Equipment and Procedures

2.2.1 Implant Systems

Both the in vitro and in vivo studies used two-piece Brånemark implant/abutment systems, shown schematically in Figure 2-1 The in vitro studies considered both intra-oral and extra-oral implants, whereas, the in vivo study only considered extra-oral implants used specifically for Bone Anchored Hearing Aids (BAHA). The main difference between the intra-oral and extra-oral implants is their length. All abutments attached to the implants were commercially available.

In Vitro Implant Systems

The in vitro implant systems were composed of Brånemark extra-oral and intra-oral implants installed in a modeling material with a stiffness comparable to that of hard tissue found in vivo. Tissue supporting a patient's implant is composed of a combination of cortical and cancelleous bone, with Young's modulus in the range of 5-15GPa. The modeling material, Photoelastic FRB-10 (Measurements Group Inc., P.O. Box 27777, Raleigh North Carolina, USA, 27611), had a modulus of 9.3GPa (Faulkner, Mioduchowski, & Hong 1975).

Implants were installed in 43.7 mm diameter discs of the modeling material in a manner similar to clinical procedures. These procedures included drilling an appropriate diameter hole in the FRB-10 and then cutting threads in the hole using a tap matched to the implant. The implants were threaded into the supporting material to a certain depth, called the engagement length, so that the implant was 0, 1, or 3 mm proud of the supporting material surface, as shown in Figure 2-1. In addition to the above procedures, epoxy was applied to every implant prior to final installation to reduce thread tolerance variations among implants installed in different discs. The above installation procedures differ from the clinical protocol in that the installation torque was not controlled and epoxy is never used to ensure a good bond with the patient's bone. These procedures differ because of mimicking bone loss by leaving the implants proud of the supporting material surface. The diameters of implants were selected to span the typical range available for clinical use. The combinations of implants and engagement lengths evaluated in the in vitro study are shown in Table 2-1.

Table 2-1: Implant/FRB-10 Disc Combinations Considered in the In Vitro Study

Implant Type	Disc Number	Implant Model (Nobel BioCare Inc., Götenburg, Sweden)	Implant Length (mm)	Implant Diameter (mm)	Engagement Length (mm)
Extra-Oral	1	SEC 002	4	3.75	1.87
	2	SEC 002	4	3.75	2.78
	3	SEC 002	4	3.75	3.83
	4	SEC 002	4	3.75	4.16
Intra-Oral	5	MKIII 26979	10	3.3	5.94
	6	MKIII 25977	10	3.75	5.62
	7	MKIII 26967	10	4	5.72
	8	SDCA 146-0	10	5	6.68
	9	MKIII 26979	10	3.3	7.84
	10	MKIII 25977	10	3.75	7.70
	11	MKIII 26967	10	4	7.78
	12	SDCA 146-0	10	5	8.41
	13	MKIII 26979	10	3.3	8.74
	14	MKIII 25977	10	3.75	8.85
	15	MKIII 26967	10	4	8.72
	16	SDCA 146-0	10	5	9.58

Regular platform abutments with lengths of 3, 4, 5.5, 7, 8.5, and 10 mm were attached to the Ø3.75, Ø4.00, and Ø5.00 mm implants. These abutment models are shown in .

Table 2-2: List of Abutments

Type	Abutment Model (Nobel BioCare Inc., Götenburg, Sweden)	Length (mm)
Narrow Platform	SDCA 594-0	3
	SDCA 595-0	4
	SDCA 596-0	5.5
Regular Platform	SDCA 068-0	3
	SDCA 006-0	4
	SDCA 005-0	5.5
	SDCA 004-0	7
	SDCA 041-0	8.5
	SDCA 043-0	10

The connection screws of the abutments were shortened to allow attachment of intra-oral abutments to extra-oral implants. For the so-called narrow platform implants (Ø3.30 mm), abutment lengths of 3, 4, and 5.5 mm were attached because they were the only commercially available lengths for these fixtures and the regular platform abutments could not be connected. In total, 63 combinations of intra-oral and 24 combinations of extra-oral implant systems were measured using both the Periotest® and Osstell® instruments. These combinations were chosen to span the large range of implant system geometric parameters in clinical use today.

In Vivo Implant Systems

Only extra-oral Brånemark Ø3.75 mm flanged implants with 4 mm standard abutments were considered in the in vivo study. The implants were installed in the mastoid region of the temporal bone following clinical protocol for BAHA® procedures. The Osstell® cannot be connected to the BAHA® abutment. Consequently, the BAHA® abutment was removed and a standard 4mm abutment connected for measurements using the Periotest® and Osstell® instruments.

2.2.2 Transducer Signal Recording Apparatus

Apparatus to record the majority of both the Periotest® and Osstell® transducer signals included a multi-channel, analog-to-digital acquisition system (InstruNet Model 100 A/D 8 Bit I/O, GW Instruments Inc., Somerville Massachusetts, USA), and a personal laptop computer, as shown in Figure 2-2. The Periotest® and Osstell® transducer response signals were sampled every 0.006ms using the InstruNet and recorded on a personal laptop computer. The minimum sampling period of 0.006ms was used on the InstruNet to ensure maximum data integrity for post-processing and is considerably faster than required to record the anticipated instrument responses.

To ensure use of the InstruNet acquisition system did not significantly bias the instruments, the instrument measurement values were compared with and without the InstruNet connected. No significant differences were noted in the instrument measurement values.

Samples of the transducer signals obtained from the Periotest® and Osstell® units using the InstruNet are shown in Figure 2-3 and Figure 2-4, respectively. Figure 2-3 displays Periotest® transducer signals sampled before and after an amplifier in the instrument. Note that this figure only shows one of 16 Periotest rod strikes, used to determine a single PTV. The Osstell® transducer signal, shown in Figure 2-4, was recorded after an amplifier in the instrument circuitry and ensured the recorded signal was unbiased by the presence of the recording instrumentation.

In addition to the recorded transducer signals, both the Periotest® and Osstell® instrument measurement values were recorded. Records of both the transducer signal and corresponding instrument measurement values allow PTV and ISQ calculated independently from the transducer signals to be compared to those values returned by the Periotest® and Osstell®.

2.2.3 Development of MATLAB Code to Replicate Periotest® PTV

To better understand how the Periotest® processes the post-amplified accelerometer signal, MATLAB code was developed (Appendix A). This post-processing technique allowed for a comparison of the existing PTVs and MATLAB PTVs.

The MATLAB code searches for a large, negative slope that indicates the initial contact, or starting point, of the Periotest® rod with the abutment. Following the curve from the starting point and searching for a similar voltage value as the start determined the ending point. To increase precision of the MATLAB code, the ending point was calculated using linear interpolation between two voltage data points adjacent to the starting voltage. Figure 1-5 shows a typical post-processed signal using the MATLAB code: the circles identify the start and stop of the contact time interval, *ct*.

Once the contact interval was identified, the MATLAB code calculated the contact time based on a constant time-step of 0.006ms: this time-step corresponds to a sampling frequency of 166,667Hz used with the InstruNet acquisition system. To reduce the file size of the recorded signal, only the voltage data was recorded: even with this reduction, the file sizes remain near 10MB for a single four second Periotest® measurement. As a result, post-processing of the post-amplified signal requires the assumption of a constant time-step.

This assumption was independently verified by simultaneously sampling the Periotest® transducer signal with both the InstruNet and a digital oscilloscope(Tektronix 410AD, Beaverton Oregon, USA) for one in vitro implant system. Figure 2-5 shows the validity of the constant time-step assumption because there is no significant difference between the voltage curve recorded with the InstruNet, assuming a constant time-step, and the time-voltage curve recorded with the digital oscilloscope. As a result, limited error is introduced in making the constant time-step assumption.

The contact times are then converted into PTVs using Equation 1-1 and one decimal place is included in the output. Extension of the PTV to two significant digits is essential to determine if the Periotest® resolution, repeatability, and sensitivity can be improved. For a single Periotest® measurement, there are a maximum of 16 PTVs that can be calculated from each of the Periotest® rod strikes with the abutment. To determine a single Periotest® measurement value, some basic statistical procedures are used on this group of 16 PTVs. Any one of the 16 contact periods a distance greater than one standard deviation from the mean was classified as an outlier and removed from the averaged measurement value. The corresponding variability of the PTVs between the individual Periotest® rod strikes is approximately ±0.1 PTV, with a maximum value of ±0.2 PTV. Without removal of the outlier PTVs, the variability was approximately double those values. This variability is a combination of slight differences in both the initial conditions of the Periotest® rod striking the abutment, and the MATLAB code identifying the contact time of the 16 strikes.

A sample of the PTVs from the Periotest® and MATLAB code are shown in Table 2-3.

Table 2-3: Comparison of PTVs from Periotest® and MATLAB Code

Periotest	MATLAB
-7	-6.8
-6	-6.2
-4	-3.8
-3	-3.0
-2	-2.2
-1	-1.1
0	-0.4
1	0.9
2	2.3
3	3.1
4	4.1

After rounding the MATLAB PTVs in the above table to integer values, the MATLAB and Periotest® PTVs agree. Therefore, the algorithm within the instrument to post-process the conditioned transducer signal seems to be adequately replicated.

2.2.4 Development of MATLAB Code to Replicate Osstell® ISQ

To better understand the algorithm used in the Osstell® instrument to calculate the ISQ, MATLAB code was developed (Appendix B). With reference to literature on the development of the Osstell® instrument, the origin of the ISQ is the resonant frequency determined from the responding piezoelectric crystal on the transducer lead (Meredith 1999). As a result, the main goal of the MATLAB code was to find this resonant frequency and then calculate the ISQ using Equation 1-2, supplied by the manufacturer of the Osstell® instrument.

The response of the Osstell®, identified in Figure 2-6, was decomposed into several thousand complete cycles and the frequency, f, of each cycle calculated based on the corresponding period, T, as

$$f = \frac{1}{T}$$ Equation 2-1

The amplitude associated with this frequency was recorded and the resonant frequency was associated with the maximum amplitude.

Table 2-4 shows the estimated resonant frequency found using the MATLAB code is within 1% of that calculated by the Osstell® instrument over a typical resonant frequency range of 5500 to 7000 Hz.

Table 2-4: Osstell® Instrument and MATLAB Determine Resonant Frequencies

Osstell® Frequency (Hz)	MATLAB Frequency (Hz)
5709	5714
5983	5974
6722	6700

This frequency range corresponds to an ISQ range of approximately 60-80 ISQ. The majority of in vivo ISQ measurements are in this range. Since the MATLAB and Osstell® resonant frequencies are within 1% of one another, the MATLAB code adequately replicates the signal processing within the Osstell®.

The resonant frequency determined by the Osstell® instrument was downloaded from the unit via an infrared port using software specifically modified by Integration Diagnostics Inc. Because the ISQ is directly related to the resonant frequency, determining the resonant frequency using MATLAB and comparing it to the value downloaded from the Osstell® is the same as comparing ISQ values determined by MATLAB and the Osstell®. As a result, only the resonant frequency values are compared.

2.2.5 Instrument Measurement Protocol

In order to obtain the most precise data, measurement of the implant systems followed a stricter protocol than that recommended by either the Periotest® or Osstell® manufacturers. This protocol included control of the Periotest® handpiece angulation and striking position, and increased control of the azimuthal measurement direction for both the Periotest® and Osstell® units. All Periotest® measurements were conducted at the top edge of the abutment with the handpiece angled approximately 5° downwards, as shown in Figure 1-6. To eliminate effects of supporting material nonhomogeniety and ensure the Periotest® and Osstell® measurements for one implant system were comparable, the azimuthal angle of both instruments were chosen to coincide.

The azimuthal angle is defined as the angular direction, about the longitudinal axis of the implant, to the direction of the forces and moments applied by the Periotest® and Osstell® instruments. Forces and moments applied by the instruments were assumed to be in the direction of the Periotest® handpiece and in the plane of the cantilever beam of the Osstell® transducer lead, respectively. For in vitro measurements, the azimuthal direction was chosen perpendicular to labels on the supporting material, as shown in Figure 2-7. For in vivo measurements, the azimuthal direction was chosen parallel to the longitudinal axis of the patient.

In addition to controlling variables associated with the instrument measurement, the torque applied to the abutment connection screw was set using an electronic torque controller (Nobel Biocare, Götenborg, Sweden). The torque applied to the abutment screw was 10Ncm and 20Ncm for the in vitro and in vivo studies, respectively. A lower connection screw torque was used for the in vitro study to reduce the risk associated with multiple attachment-disconnection cycles. The risk associated with a higher torque resulted from an increased chance of stripping the threads or head of this screw. These concerns were reduced for the in vivo study because of fewer attachment-disconnection cycles of the abutment/implant joint.

2.3 In Vitro Periotest® Studies

2.3.1 Investigation of Periotest® Transducer Signal

The origin of the Periotest® transducer signal was investigated to understand how the instrument operated. Because a schematic of the Periotest® circuitry is not readily available, a trial and error approach at finding the transducer signal from the hand piece was employed. From the operating manuals (Siemens, Bensaelu, Germany) and previous investigators, it is generally accepted that the Periotest® derives its measurement value based on the response of an accelerometer attached to the Periotest® rod.

To verify the recorded signal from the Periotest® was from an accelerometer, the tip of the handpiece was disassembled to allow connection of an independent accelerometer to the Periotest® rod. Figure 2-8 shows the Periotest® handpiece located vertically, the Periotest® rod connected to an independent accelerometer (Brüel & Kjær Model 4344, Copenhagen, Denmark) via a connector, and finally the independent accelerometer attached to a shaker table (Brüel & Kjær Model 4809, Copenhagen, Denmark). The shaker table was operated at 5000Hz and with sufficient amplitude to provide noticeable output from the Periotest® accelerometer signal sampled before and after an amplifier (National Semiconductor, LF442 Dual Low Power JFET Input Operational Amplifier, Santa Clara California, USA) in the instrument circuitry. These signals are referred to as pre and post-amplified transducer signals.

Responses of the Periotest® transducer signals, without initiation of a measurement cycle, and the independent accelerometer were recorded simultaneously using an analog-to-digital acquisition system (InstruNet Model 100 A/D 8 bit I/O) sampling at a frequency of 50,000 Hertz. This sampling frequency was chosen because of multiplexing the InstruNet system. Figure 2-9 shows the Periotest® transducer signal sampled after the instrument amplifier compared to the independent accelerometer signal. The Periotest® transducer signal obtained prior the amplifier and the independent accelerometer signal are shown in Figure 2-10. The figures show that the Periotest® signal sampled before the amplifier is in phase with the independent accelerometer response, and the signal collected after the amplifier is out of phase with the independent accelerometer. This difference suggests the Periotest® accelerometer signal has been conditioned during amplification. In addition, the pre and post-amplified transducer signals change very little in magnitude. Therefore, the input operational amplifier in the Periotest® circuitry appears to have a small gain value when a measurement cycle is not initiated.

The Periotest® transducer signal sampled before the amplifier will be considered the actual accelerometer signal, and the post-amplified signal will be considered a conditioned response. The pre-amplified signal will be compared to a strain gauge response of the vibrating abutment and used to further understand the motion of the implant system. The conditioned signal will be used as input for the MATLAB software to replicate instrument PTVs. A similar curve is presented in the operating instructions of the Periotest® and is used as the basis for determining the PTV. Caution should be used when further analyzing the conditioned signal because it is filtered and is not suitable for any curve fitting routine or comparison of accelerations from a mathematical model predicting the motion of the implant system.

2.3.2 Investigation of Periotest® Resolution, Repeatability, and Sensitivity

This in vitro study was designed to determine the resolution, repeatability, and sensitivity of the Periotest® by varying several geometric parameters of the implant system. These geometric parameters included: abutment height, engagement length, and implant diameter, as shown in Figure 1-8. A relationship between the striking height and abutment length exists: an increase in the abutment length causes an increase in striking height. In addition, striking height increases as engagement length decreases for a given implant length because of the choice to fabricate the implant systems with the implants proud of the supporting material surface. Therefore, both engagement and abutment lengths influence striking height.

For each measurement, one FRB-10 disc with an installed implant was mounted in a holding device on a rigid platform, as shown in Figure 2-11. An abutment was connected to the implant and the connection screw tightened to a torque of 10Ncm. The Periotest® handpiece was positioned by adjusting the vertical support to ensure the Periotest® rod was directed radially towards the abutment. The striking height and distances of 1-2 mm from the tip of the Periotest® handpiece to the abutment were adjusted using the 2-axis micrometer. Once the handpiece was positioned, five measurements were recorded for that abutment length. The abutment was then replaced with a different length without removing the FRB-10 disc from the rigid platform and the same measurement set-up was repeated. After measurements had been recorded for all abutment lengths, the FRB-10 disc was removed and the next disc installed. The above procedure was repeated for all 16 FRB-10 discs. A total of 63 intra-oral and 24 extra-oral implant systems were evaluated.

2.3.3 Repeatability of the Periotest® Transducer Signal

The repeatability of the Periotest® was determined by plotting three pre-amplified transducer responses for repeated evaluations of one implant system, as shown in Figure 2-12. Small spread between the recorded transducer signals suggests the Periotest® rod applies repeatable impact forces to the implant system when the measurements are repeated.

2.3.4 Estimation of Clinical Periotest® Repeatability

Periotest® repeatability was estimated by following in vivo protocol to record 30 sequential measurements of in vitro disc number 11, as shown in Table 2-1, with a 7 mm abutment attached. All clinical Periotest® measurements were completed holding the handpiece by hand. However, handpiece angulation, striking height, and azimuthal direction were controlled but not as well as in the in vitro study. These measurement variables have been shown or are believed to influence the Periotest® response and were controlled to limit their effects on the returned measurement value. Because the in vivo study of the Periotest® involved the attachment and detachment of the abutment at each patient check-up, the 7 mm abutment was detached, reattached, and the connection screw tightened to a torque of 20 Ncm between each Periotest® measurement. The transducer signal and PTV were recorded similarly to the methods described above in Section 2.2.2.

2.3.5 Response of Implant System to the Periotest®

This study investigated the response of strain gauges attached to a 10 mm, regular platform abutment connected to each implant installed in 13 FRB-10 discs and impacted by the Periotest® rod. The Ø3.30 mm implant systems could not be measured because the strain gauges were applied to a regular platform abutment only. The two strain gauges were connected into a Wheatstone bridge (Vishay Strain Gage Conditioner 2120, Malvern Pennsylvania, USA) with two active arms. After amplification, one-channel of a two-channel digital oscilloscope (TekTronix TDS 410A, Beaverton Oregon, USA) sampled the strain gauge response, while the other channel simultaneously recorded signals from the Periotest® transducer. The digital oscilloscope was sampling at a rate of one million Hertz.

Similar to Section 2.2.2, two Periotest® transducer signals were considered: one signal was obtained prior the instrument signal conditioning and the other signal after some signal processing. Figure 2-13 shows a sample of the strain gauge and Periotest pre and post-conditioned signals. It is important to note that only two of the three curves shown on this plot were recorded simultaneously because a two-channel oscilloscope was used to record the data. However, all three curves belong to the same implant system.

An example of the strain gauge and pre-amplified transducer signals, shown in Figure 2-14, appear to be in phase as plotted but are approximately 180 degrees out of phase based on the polarity of the two signals. It is important to note that the Periotest® response shown in Figure 2-14 is for an implant/FRB-10 combination that was modified to investigate the effect of changing the supporting disc thickness, as described in

Section 2.3.7. Applying a small, static displacement to the abutment in the outward direction of the Periotest® rod, shown schematically in Figure 2-15, and noting the sign of the recorded voltage obtained the polarity of the strain gauge response. From this investigation, it was determined that displacement increases in the outward direction as the strain gauge output voltage became more negative. In a similar manner, the polarity of the pre-amplified Periotest® transducer signal was determined by applying an acceleration to the Periotest® rod in the outward direction and noting the sign of the recorded voltage. Acceleration increases in the positive direction as the transducer output voltage becomes more positive.

The strain gauge and accelerometer signals agree with the theoretical motion of a single degree of freedom, damped, vibrating system, shown in Figure 2-16, if the strain gauge is considered a measure of the displacement of the Periotest® rod. This model has recently been shown to approximate the motion of the Periotest® rod while contacting the abutment (Giannitsios et. al. 2001), and is useful in describing the phase shift between the strain gauge and accelerometer signals. The displacement, velocity, and acceleration functions describing the motion of the system are given in Equation 2-2.

$$displacement(t) = Ae^{\frac{-ct}{2m}} \sin\left(\frac{\sqrt{4mk - c^2}}{2m}t\right)$$

$$velocity(t) = A\sqrt{\frac{k}{m}}e^{\frac{-ct}{2m}} \cos\left(\frac{\sqrt{4mk - c^2}}{2m}t + \phi\right) \qquad \text{Equation 2-2}$$

$$acceleration(t) = -A\frac{k}{m}e^{\frac{-ct}{2m}} \sin\left(\frac{\sqrt{4mk - c^2}}{2m}t + 2\phi\right)$$

where

A	Amplitude of Motion
k	Spring stiffness
m	mass of system
c	damping coefficient
ϕ	phase shift = $\arcsin\left(\frac{c}{2\sqrt{mk}}\right)$

Explanation of the 180 degree phase shift between the strain gauge and pre-amplified accelerometer signals requires an approximation of the phase shift, ϕ. To estimate ϕ, the strain gauge response after the Periotest® rod had separated from the abutment, as shown in Figure 2-17, was investigated. The slow decay in the amplitude of the strain gauge signal suggests the damping coefficient, *c*, is very small and forces the shift value, ϕ, to be approximately zero. Therefore, the phase shift between the theoretical displacement and acceleration, given in Equation 2-2, is approximately 180 degrees due to the negative sign in the third equation. Comparison of the theoretical and empirical phase shifts of 180 degrees suggests the strain gauge response is related to the Periotest® rod displacement.

2.3.6 Effect of Changing Supporting Material Stiffness on PTV

This study measured two implant systems with similar geometric parameters but different supporting material stiffness. A Ø3.75 mm Brånemark MKIII 25977 intra-oral implant was installed in a disc of modeling material (PhotoElastic FRB-20, Measurements Group Inc., P.O. Box 27777, Raleigh North Carolina, USA, 27611) with a stiffness of 3.3 GPa to the same specifications as in vitro disk number 6, shown in Table 2-1, and following similar installation procedures as mentioned in Section 2.2.1. Regular platform abutments with lengths of 3, 4, 5.5, 7, 8.5, and 10 mm were attached sequentially to the implant, and similar experimental procedures were followed as used in Section 2.2.2 to obtain and record the Periotest® pre and post-amplified transducer signals and the instrument PTV.

2.3.7 Investigation of In Vitro FRB-10 Disc Plate Effects

As there were questions concerning the results for thin discs, testing was done using discs which had their stiffnesses modified. These tests were done to ensure that the stiffness being evaluated was between the supporting material and implant and excluded the stiffness of the disc itself. Periotest® measurements were recorded for two distinct procedures: 1) step-wise removal of FRB-10 material adjacent to the Ø4.00 mm Brånemark implant installed in disc number 11. The modification process is schematically shown in Figure 2-18; and, 2) varying the effective diameter of the FRB-10 disc from 43.7 mm to 12 mm using additional clamping apparatus, as shown in Figure 2-19.

All Periotest® measurements were conducted following a similar protocol as presented in Section 2.2.5. However, only the 10 mm abutment length was attached to the clamped FRB-10 disc because of constraints due to the additional clamping geometry. In addition, PTV values and pre and post-amplified transducer signals were recorded with the Periotest handpiece oriented parallel to the axis of the implant system. These measurements were recorded to compare the response of axial and perpendicular Periotest® measurements.

2.4 In Vitro Osstell® Studies

2.4.1 Investigation of Osstell® Resolution, Repeatability, and Sensitivity

Osstell® measurements were conducted using the 16 in vitro implant systems described above in Section 2.2.1. The measurement procedure for the Osstell® included one additional step beyond the Periotest® protocol. After the abutment was connected to the implant and the connection screw was tightened to a torque of 10Ncm, the Osstell® abutment transducer was attached to the top of the abutment, as shown in Figure 1-7. A careful attachment process ensured the previous Periotest® handpiece direction and Osstell® transducer lead direction, determined by the orientation of the cantilever beam, had similar azimuthal directions. The transducer connecting screw was then tightened to a torque of 10Ncm using an electronic torque controller (Nobel Biocare, Götenborg, Sweden), and a series of five consecutive Osstell® measurements were recorded. The transducer lead and the abutment were then removed, and the same set-up procedure used to attach the next length of abutment and Osstell® transducer lead. After all lengths of abutments had been attached to the implant in the FRB-10 disc, the disc was removed and replaced with another. This process was repeated until measurements were recorded for all 63 intra-oral and 24 extra-oral implant systems.

2.4.2 Estimation of Clinical Osstell® Repeatability

The repeatability of the Osstell® was estimated by recording both the ISQ and transducer signal for 32 measurements using the same in vitro disc and abutment combination presented in Section 2.3.4. The measurement process replicated clinical protocol specific to the Osstell® and included removal and re-attachment of both the abutment and transducer lead between each measurement. A torque of 20Ncm was applied to the abutment connection screw and the connecting Osstell® transducer lead screw was tightened to a torque of 10Ncm.

2.4.3 Response of Implant System to Osstell®

Investigation of the implant system response using the Osstell® instrument followed a similar procedure as presented in Section 2.3.5 for the Periotest®. Again, the procedure was extended one step to ensure the Osstell® transducer lead was attached with the same azimuthal direction as the Periotest® handpiece. In addition, the Osstell® transducer lead connecting screw was tightened to a torque of 10Ncm. Sample strain gauge and Osstell® transducer signals are shown in Figure 2-20A and B.

2.5 In Vivo Study

In vivo testing was completed in conjunction with the Craniofacial Osseointegration and Maxillofacial Prosthetic Rehabilitation Unit (C.O.M.P.R.U.), Misericordia Hospital, Edmonton, Alberta, Canada, and involved measuring the integrity of Bone Anchored Hearing Aid® (BAHA®) implants starting from surgical installation and continuing through 3, 6, and 12 month routine patient visits.

Both the Caritas Health Group and the University of Alberta Health Research Ethics Board approved this two-year study. To date, 10 adult patients have consented to take part in the study. This consent process involves specific education for new BAHA® patients, a statement from the patient saying they understand the procedures and details of the study, and finally, written patient consent.

2.5.1 Periotest® Training Block

The precision of Periotest® measurement values recorded over time is crucial to detect small changes in implant integrity. To aid in precision of Periotest® measurements in the in vivo study, a training block was developed. This training block replicated implant system geometry using four 6061-T6 aluminum cylinders with lengths of 4, 6, 8, and 10 mm threaded 4 mm into a rectangular piece of FRB-10. The FRB-10 was then mounted to a stainless steel base. Epoxy was applied to the aluminum cylinders during final installation to ensure they did not loosen during the anticipated two year study. Figure 2-21 shows the use of the Periotest® training block by the clinician prior to a patient measurement. In addition, the use of the block involves recording at least one Periotest® measurement for each of the four different aluminum post lengths. The recorded measurements were then compared to previous values to determine if significant changes occurred in instrument output.

Development of the training block included investigation of the aluminum cylinder/FRB-10 interface property changes during regular clinical equipment sterilizations. The property changes were monitored using the Periotest® instrument. It was determined the Periotest® training block could not be flash sterilized using an autoclave, but rather had to be gas sterilized at approximately 45°C to ensure negligible changes in the material properties. This method of sterilizing the Periotest® training block was adopted for the duration of the study.

Although the Periotest® training block was originally designed to be used as a calibration tool for monitoring longitudinal drift in the Periotest®, its material properties changed as the study progressed and could not be used for this purpose. It was suspected the training block was accidentally sterilized using the autoclave. Therefore, the regular machine calibration cap was used solely to monitor instrument drift. However, the training block served a very useful purposeful: to focus the operator on the proper measuring technique and allow the Periotest® instrument to reach a steady state of operation prior to evaluating a patient's implant system.

2.5.2 Measurement Protocol

The in vivo study made use of equipment and procedures stated in Section 2.2.5, as well as specific clinical protocol. To reduce inter-operator variability, one clinician conducted all Periotest® and Osstell® measurements. In addition, correct instrument operation was confirmed prior to any patient measurements. Correct operation of the

Periotest® was monitored by following both the manufacturer's instructions and using the Periotest® training block. Correct Osstell® instrument operation was confirmed by connecting the transducer lead to an implant installed in a block of aluminum. The use of these procedures ensured precision in the longitudinal measurements.

In addition to monitoring the precision of the instruments throughout the study, all in vivo measurements were conducted in a specified order. After a 4 mm abutment was connected to the patient's implant, Periotest® measurements were recorded. Because of time limitations in the operating room, only three Periotest® measurements were recorded for each of two directions. These directions included the handpiece oriented parallel to the longitudinal axis of the patient, and directed along the implant axis. Upon completion of the Periotest® measurements, the Osstell® transducer lead was attached to the top of the abutment so that it had the same azimuthal direction as the Periotest®, and the connecting screw was tightened to a torque of 10Ncm. Again, time constraints allowed only three Osstell® measurements. The above protocol is shown in Figure 2-22.

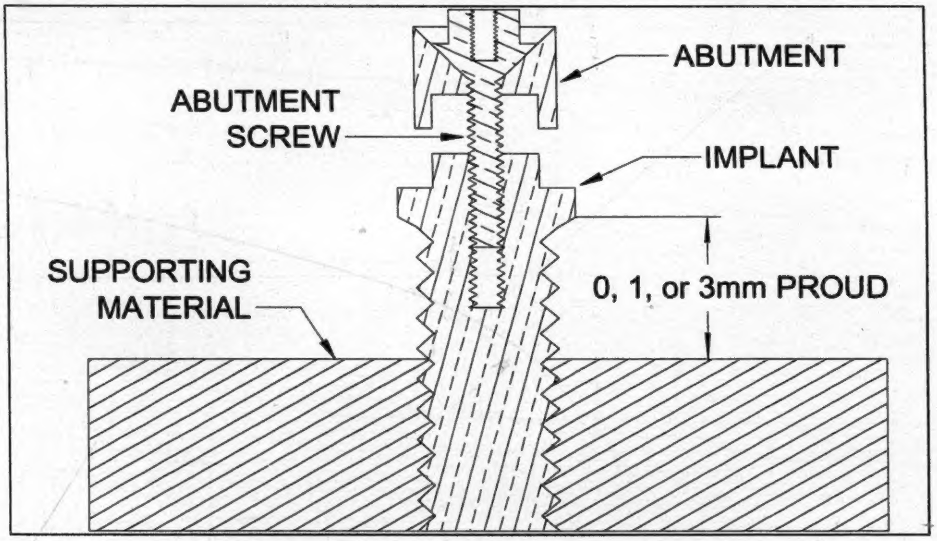
ABUTMENT
ABUTMENT SCREW
IMPLANT
SUPPORTING MATERIAL
0, 1, or 3mm PROUD

Figure 2-1: Schematic of Two-Piece Brånemark Implant System

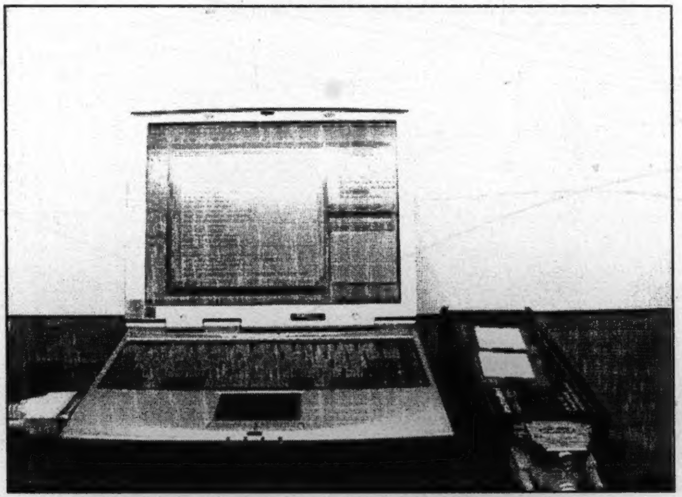

Figure 2-2: Digital Acquisition System

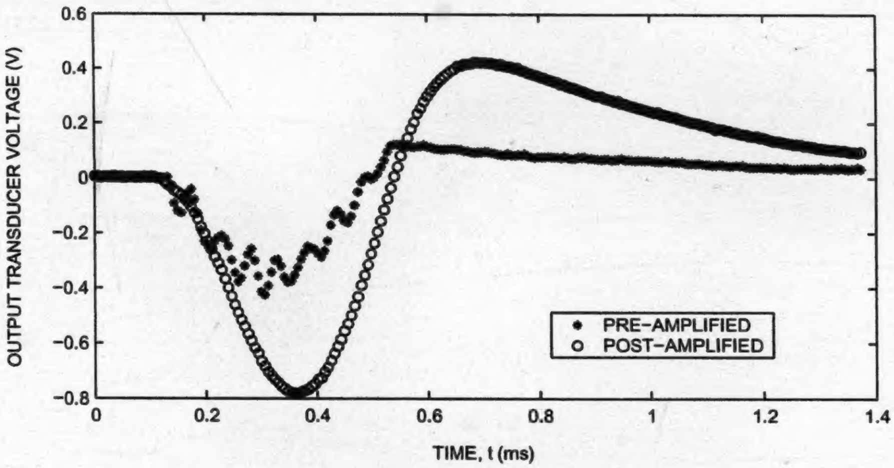

Figure 2-3: Sample of Periotest® Transducer Signals

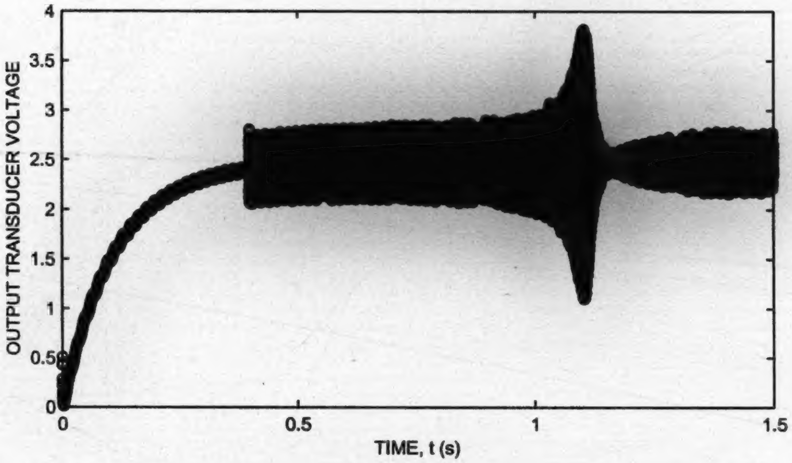

Figure 2-4: Sample Osstell® Transducer Signal

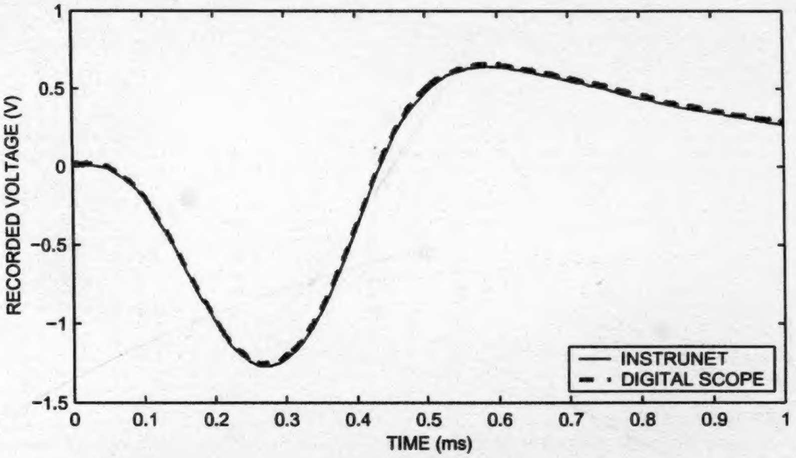

Figure 2-5: Verification of Constant Time-Step Approximation in MATLAB Code

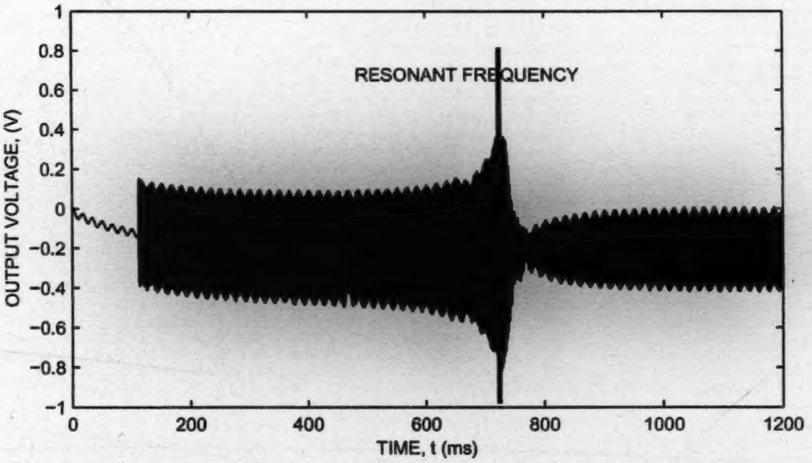

Figure 2-6: Sample Osstell® Signal – Showing Resonant Frequency

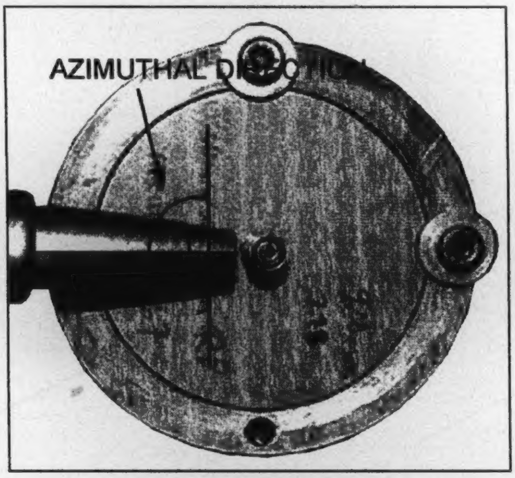
AZIMUTHAL DIRECTION

Figure 2-7: Control of Azimuthal Direction for In Vitro Measurements

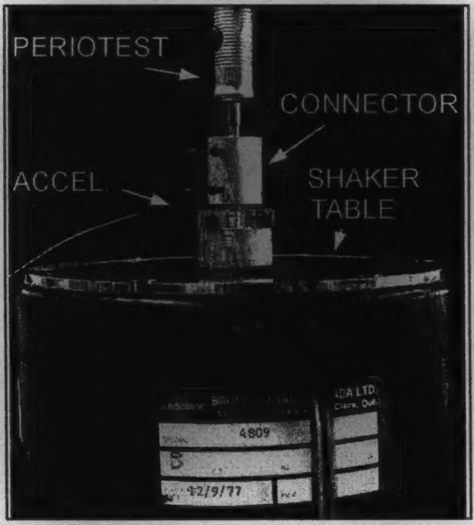
PERIOTEST
CONNECTOR
ACCEL.
SHAKER TABLE

Figure 2-8: Periotest® Accelerometer Verification using Independent Accelerometer Mounted to a Shaker Table

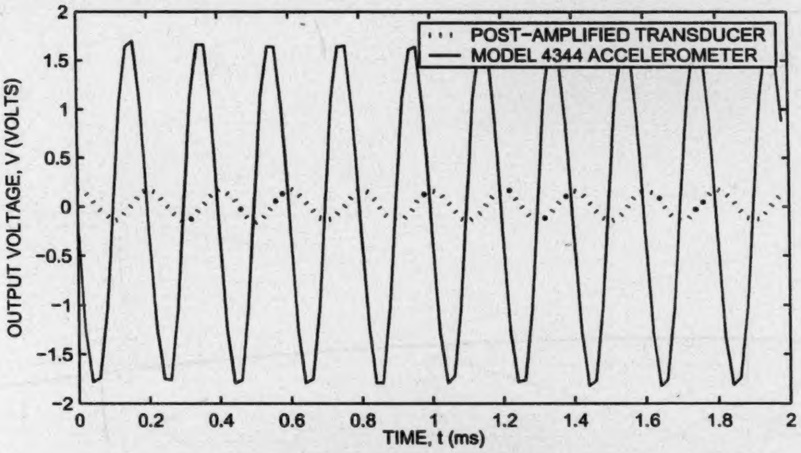

Figure 2-9: Comparison of Periotest® Accelerometer Signal Sampled After an Input Amplifier to an Independent Accelerometer

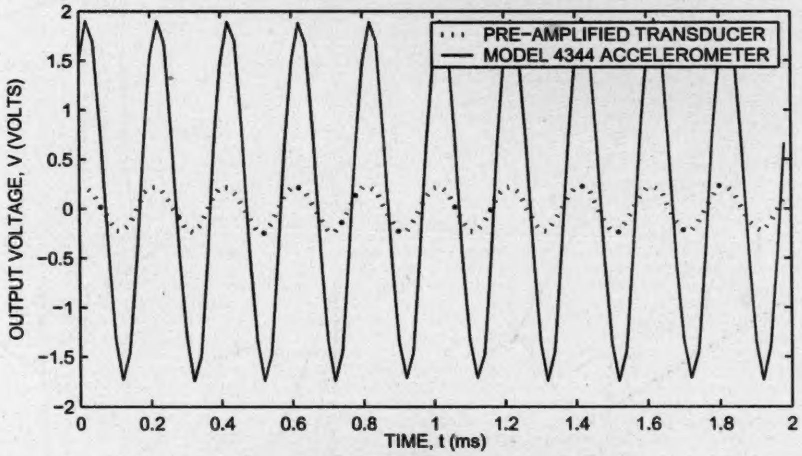

Figure 2-10: Comparison of Periotest® Accelerometer Signal Sampled Before an Input Amplifier to an Independent Accelerometer Signal

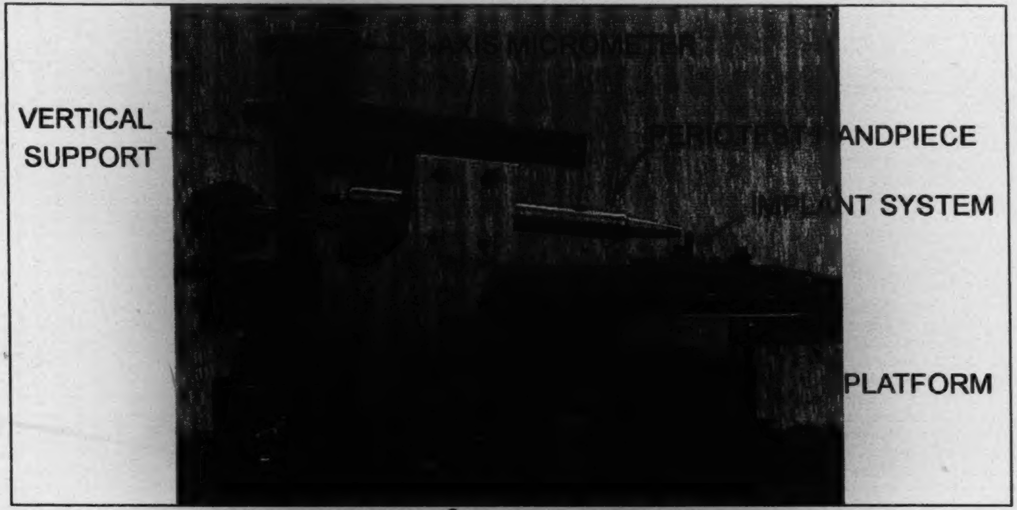
2-AXIS MICROMETER
VERTICAL SUPPORT
PERIOTEST HANDPIECE
IMPLANT SYSTEM
PLATFORM

Figure 2-11: Periotest® In Vitro Experimental Apparatus

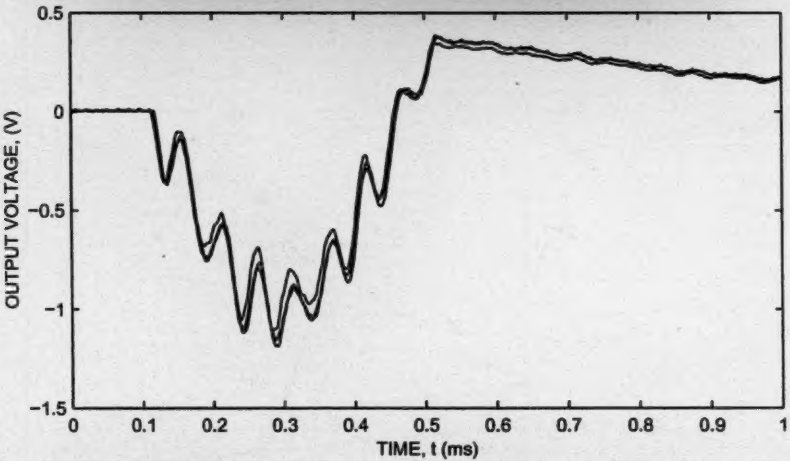

Figure 2-12: Multiple Responses of the Periotest® Transducer when Evaluating a Ø4mm Intra-Oral Brånemark Implant in FRB-10 to an Engagement length of 8.72mm

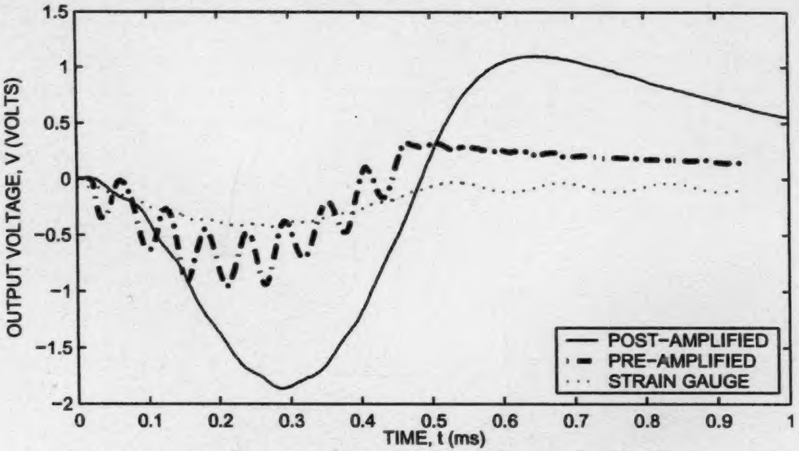

Figure 2-13: Sample of Strain Gauge and Periotest® Signals

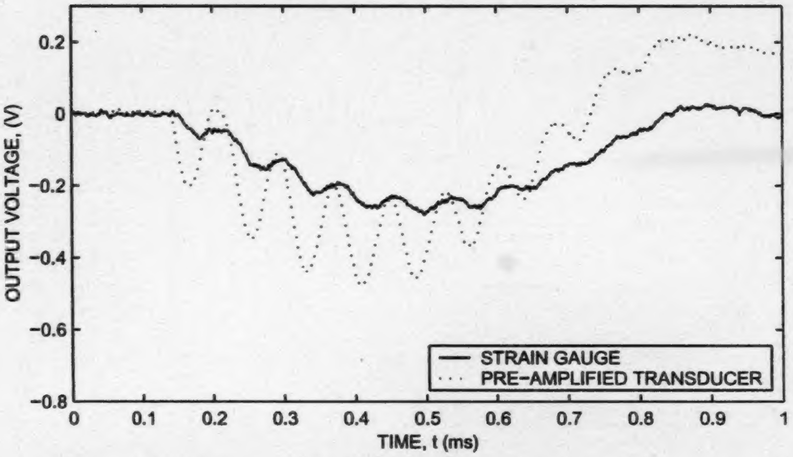

Figure 2-14: Periotest® and Strain Gauge Response of a Ø4mm Intra-Oral Brånemark Implant Mounted in FRB-10 to an Engagement Length of 1.68mm

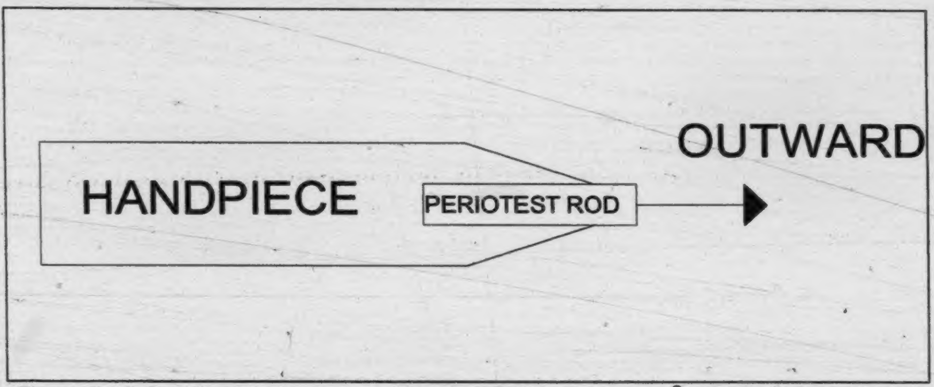
OUTWARD
HANDPIECE
PERIOTEST ROD

Figure 2-15: Positive Displacement of Abutment When Periotest® Rod moving Outwards

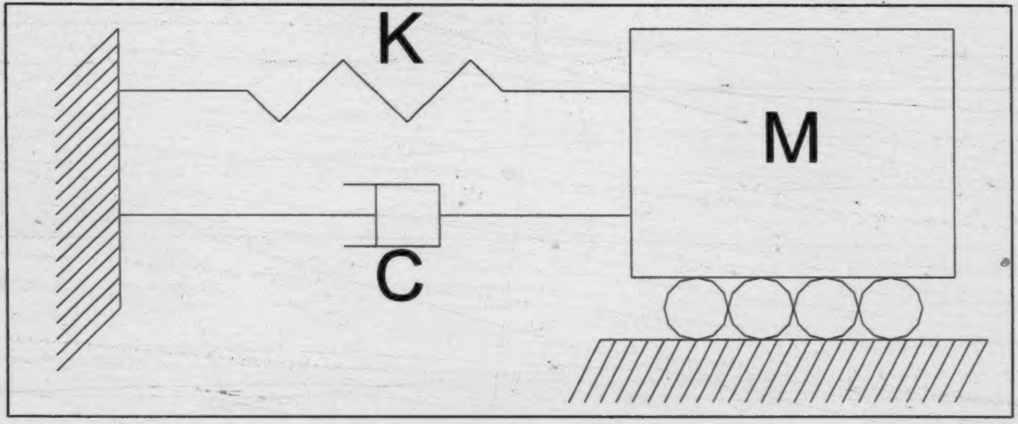

Figure 2-16: Single Degree of Freedom System

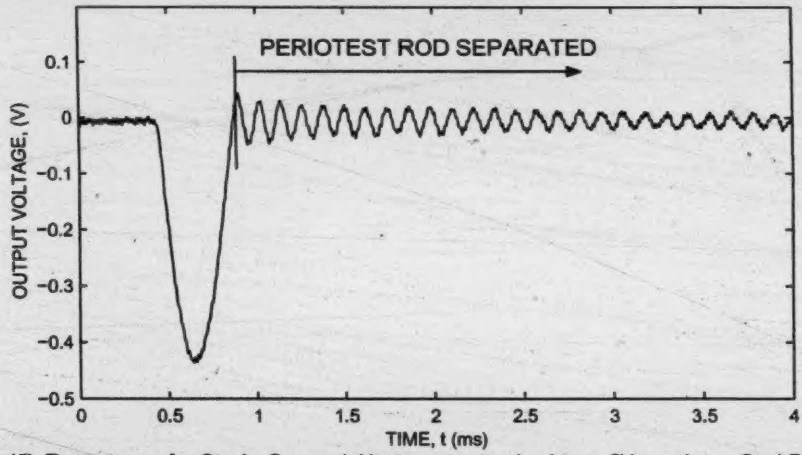

Figure 2-17: Response of a Strain Gauged Abutment, attached to a Ø4mm Intra-Oral Brånemark Implant Installed in FRB-10 to an Engagement Length of 8.72mm, to the Periotest®

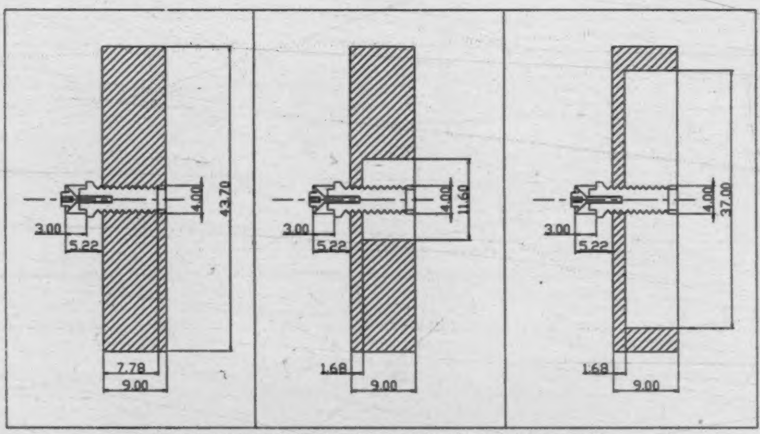
3.00
5.22
4.00
43.70
7.78
9.00
3.00
5.22
4.00
11.60
1.68
9.00
3.00
5.22
4.00
37.00
1.68
9.00

ALL MEASUREMENTS IN MILLIMETERS

Figure 2-18a: Original Figure 2-18b: First Cut Figure 2-18c: Final Cut

Figure 2-18: Modification Process of In Vitro Disc Number 11

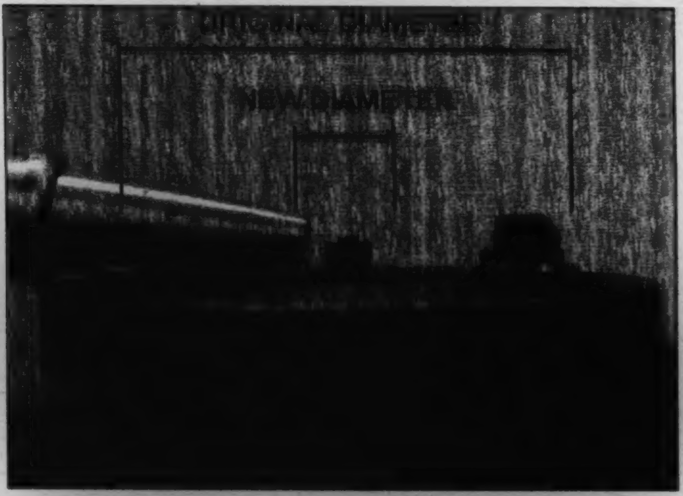
ORIGINAL DIAMETER
NEW DIAMETER

Figure 2-19: Additional Clamping Apparatūs

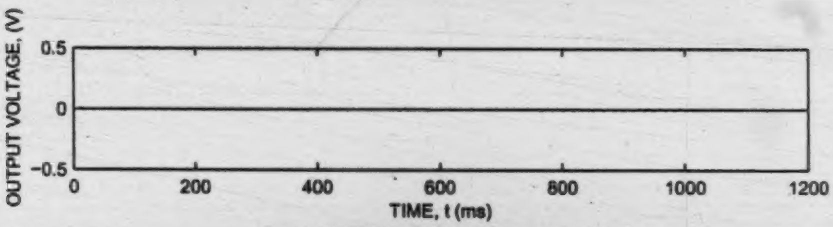

(A) STRAIN GAUGE RESPONSE

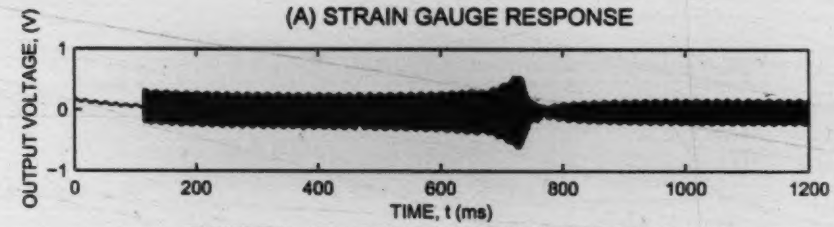

FIGURE 2−17b: OSSTELL TRANSDUCER SIGNAL

Figure 2-20: Strain Gauged Abutment Response to Osstell® Measurement

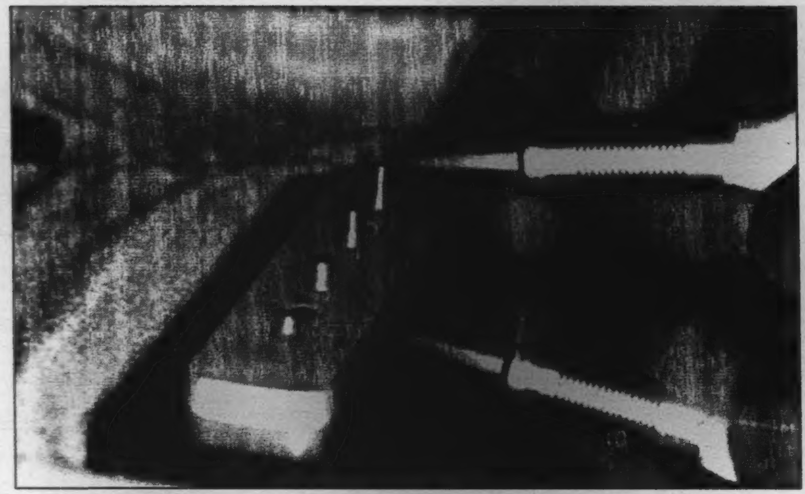

Figure 2-21: Use of Periotest® Training Block During In Vivo Study

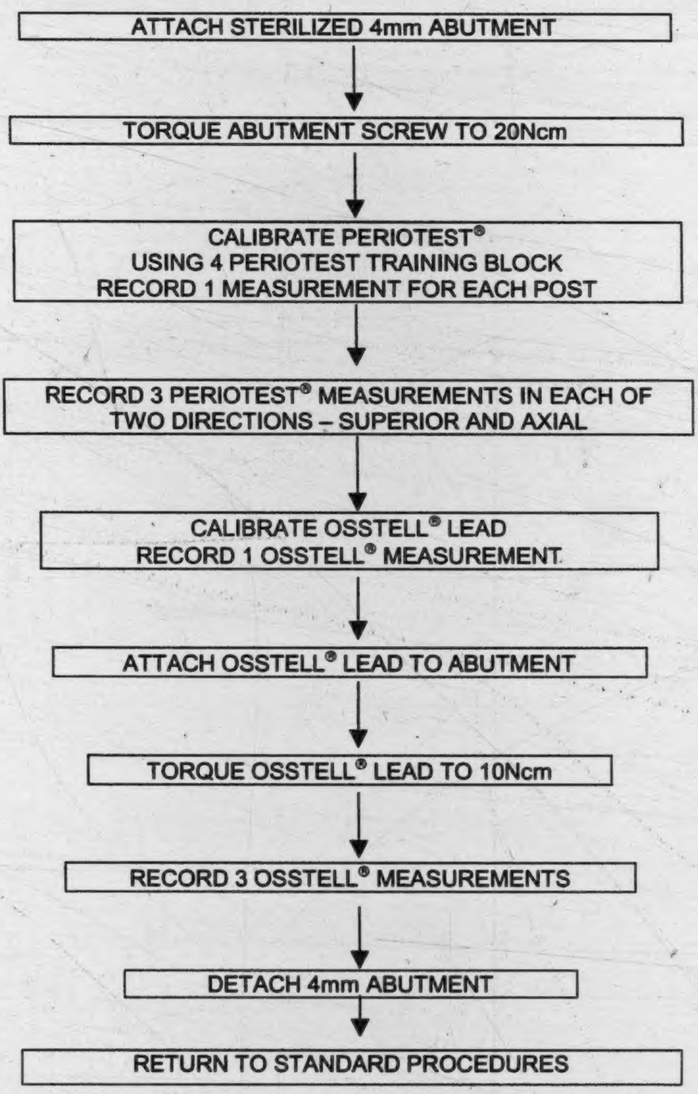
ATTACH STERILIZED 4mm ABUTMENT
TORQUE ABUTMENT SCREW TO 20Ncm
CALIBRATE PERIOTEST®
USING 4 PERIOTEST TRAINING BLOCK
RECORD 1 MEASUREMENT FOR EACH POST
RECORD 3 PERIOTEST® MEASUREMENTS IN EACH OF
TWO DIRECTIONS – SUPERIOR AND AXIAL
CALIBRATE OSSTELL® LEAD
RECORD 1 OSSTELL® MEASUREMENT
ATTACH OSSTELL® LEAD TO ABUTMENT
TORQUE OSSTELL® LEAD TO 10Ncm
RECORD 3 OSSTELL® MEASUREMENTS
DETACH 4mm ABUTMENT
RETURN TO STANDARD PROCEDURES

Figure 2-22: Flow Chart of In Vivo Protocol

Chapter 3 – **Results and Discussion**

3.1 Introduction

This chapter presents the results from experiments described in Chapter 2 and discusses their significance in comparing the Periotest® and Osstell® instruments for measuring implant integrity. Instrument operation is better understood using the response from a strain-gauged abutment prior to comparing the response of the instruments to changes in geometric implant system parameters. This comparison includes discussion on the repeatability, resolution, and sensitivity of the instruments. After the comparison is complete, a model of the implant system's motion and the relationship of representative mechanical and geometrical properties of the implant-supporting material interface to the Periotest® measurement values will be discussed. The Osstell® instrument is not considered using this model at this time because of the complexity of analytically modeling the vibratory motion of the Osstell® transducer lead attached to the implant system.

This chapter will conclude with initial results from the in vivo study. Discussion of the in vivo results will focus on the precision of the recorded Periotest® and Osstell® clinical measurements.

3.2 Understanding Instrument Operation

By examining their respective transducer signals and then comparing the response of a strain-gauged, 10mm abutment to the transducer signal, a better understanding of the operation of the Periotest® and Osstell® instruments is obtained.

3.2.1 Periotest® Measurements

Figure 3-1 shows that both the pre-amplified Periotest® transducer and strain-gauged abutment signals are a combination of at least two relatively distinct frequency components. This result suggests the second frequency is not strictly a phenomenon of how the instrument completes a measurement. The lowest frequency component has a half cycle period, or contact time, of approximately 0.7ms. The superimposed component appears to have a frequency between 12-14 kHz. A likely source of this frequency will be explored in Section 3.6. Appendix C shows the presence of more than one frequency component in the pre-amplified Periotest® transducer signal for all of the in vitro implant systems evaluated. It is important to note that the post-amplified Periotest® accelerometer signal does not contain this second frequency component – again confirming the filtering of the accelerometer signal by the operational amplifier.

The collected data suggests the pre-amplified transducer and strain gauge signal amplitudes decrease as the engagement length decreases and striking height increases (bone loss). An example of this magnitude decrease in collected signals for Ø4 mm intra-oral implants is shown in Figure 3-2, Figure 3-3, and Figure 3-4. In addition, as the engagement length decreases and striking height increases, the amplitude of the higher frequency increases relative to that of the primary frequency amplitude. The contact time of the Periotest® rod with the abutment also increases. Similar trends exist for the Ø3.3, Ø4, and Ø5 mm intra-oral implants and can be seen in Appendix C.

The response of Ø3.75 mm extra-oral implants, shown in Figures 3.5, 3.6, 3.7, and 3.8, display an inconsistent trend with engagement length compared to the intra-oral implants of Figures 3.2, 3.3, and 3.4. These figures show the amplitude of the pre-amplified transducer signal remains relatively constant as engagement length decreases and striking height increases. This inconsistency may be a result of the thinner FRB-10 discs deforming as a thin plate and as a result the Periotest® is evaluating a combination of both the implant interface and disc stiffnesses. The larger disc thicknesses, used to support the intra-oral implants, probably result in the Periotest® measurement being more strongly related to the implant interface stiffness than the FRB-10 disc stiffness and is discussed in more detail in Section 3.6.1. In addition, the changes in engagement length between Figures 3.5 to 3.8 are much smaller than the changes in engagement length between Figures 3.2 to 3.4. Therefore, the changes in magnitude would probably be more minute than those seen in Figures 3.2 to 3.4.

Although the amplitude trend of the Periotest® pre-amplified signal for the Ø3.75mm extra-oral implants is different than seen in the intra-oral implants, the contact time increases as the engagement length decreases and striking height increases. Therefore, the contact time may be the most sensitive to the combined changes in engagement length and striking height. It is important to note that previous research by Giannitsios et. al. (2001) suggested the independent effects of engagement length and striking height on the Periotest® response were the following: a decrease in engagement length caused the PTV to increase, and an increase in striking height resulted in an increase in PTV. As a result, bone loss would cause the Periotest® PTV to increase because of a combined influence of both a reduction in engagement length and an increase in striking height.

The influence of changes in supporting material stiffness on the strain gauge and pre-amplified transducer signals is shown in Figure 3-9 and Figure 3-10. The geometric parameters of the implant system are the same for both but the stiffness of FRB-20 is approximately a third of the stiffness of FRB-10. This reduction in the stiffness influences the pre-amplified transducer and strain gauge signals by reducing their amplitudes. In addition, the contact time increases with a decrease in supporting material stiffness. It should also be noted that the magnitude and frequency of the secondary component in the accelerometer signal appears relatively unaffected by the change in material stiffness compared to the lowest frequency.

The natural frequency of the implant system, without the Periotest® rod in contact, can be estimated by analyzing the strain gauge signal after separation of the Periotest® rod. The natural frequencies of the 13 implant systems, shown in Table 3-1, were estimated by measuring the period of oscillation of the strain gauge response after the Periotest® rod separated from the abutment, as shown in Figure 2-17.

Table 3-1: Natural Frequencies of the Implant System Measured Using A Strain Gauged Abutment

Implant Type	Implant Type (Nobel Biocare)	Implant Diameter (mm)	Engagement Length, L (mm)	Natural Frequency (Hz)
Extra-Oral	SEC-002	3.75	1.87	6400
Extra-Oral	SEC-002	3.75	2.78	7619
Extra-Oral	SEC-002	3.75	3.83	8889
Extra-Oral	SEC-002	3.75	4.16	10000
Intra-Oral	MKIII 25977	3.75	5.62	6667
Intra-Oral	MKIII 25977	3.75	7.70	8000
Intra-Oral	MKIII 25977	3.75	8.85	10667
Intra-Oral	MKIII 26967	4	5.72	6667
Intra-Oral	MKIII 26967	4	7.78	8889
Intra-Oral	MKIII 26967	4	8.72	**8421**
Intra-Oral	SDCA 146-0	5	6.68	**11429**
Intra-Oral	SDCA 146-0	5	8.41	10000
Intra-Oral	SDCA 146-0	5	9.58	13333

Similar natural frequencies can be obtained for the other 12 in vitro discs from the plots shown in Appendix D. Note that all plots in Appendix D have five strain gauge and post-amplified curves shown, reconfirming the high repeatability of the Periotest® instrument. In addition, the Periotest® measurement was conducted in a fixed azimuthal direction relative to the position of the strain gauges on the abutment.

In most cases, the natural frequency of the implant system increases as the engagement length increases and striking height decreases. This increase in natural frequency suggests the effective stiffness of the implant system increases as the engagement length increases and striking height decreases. The inconsistencies to this trend, shown in bold type face for the Ø4 and Ø5 mm intra-oral implants, may result because of air pockets trapped in the FRB-10 supporting material. While constructing the supporting material discs, it was noted several times that voids occurred in the resin-aluminum mixture. In addition, small variations in the torque applied to screw connecting the abutment to the implant may cause changes in the natural frequency. However, only one torque controller was used to complete all of the in vitro measurements.

3.2.2 Osstell® Measurements

An example of the strain gauge and Osstell® output transducer signals is shown in Figure 3-11 and indicates that strains applied to the abutment by the Osstell® transducer are undetectable using the strain gauged abutment and associated recording equipment. The frequency shown in the strain gauge response is 60Hz - most likely noise - and remains constant whether or not an Osstell® measurement is conducted. Similar trends exist between the Osstell® signal and the strain gauged abutment for other in vitro discs and can be seen in Appendix E.

The inability of the strain gauges to detect the vibration of the abutment when the Osstell® transducer was used but able to detect a Periotest® rod strike, suggests the Osstell® applies significantly smaller forces to the abutment than the Periotest®.

3.3 Estimate of Periotest® Repeatability and Resolution

Four distinct estimations of Periotest® repeatability and resolution are possible from the data collected. These estimations correspond to Periotest® measurement values presented by the instrument and calculated from the MATLAB code. Each of the Periotest® and MATLAB PTV repeatability and resolution can also be split into two categories: in vivo and in vitro.

Both the repeatability and resolution are based on measurement values recorded using one Periotest® instrument with one operator.

3.3.1 Existing Periotest® PTV

Repeatability of the existing Periotest® instrument was determined by calculating the standard deviation of 30 Periotest® measurements recorded following methods described in Section 2.3.4. The standard deviation of these 30 Periotest® measurements, was calculated to be ±0.5 PTV. Multiplication of this value by two, yields an estimated Periotest® repeatability uncertainty of ±1.0 PTV and corresponds to a 95% confidence interval. Since the Periotest® output resolution is integer values, the repeatability is rounded to an integer. Therefore, the best estimate of the repeatability for the existing Periotest® instrument is ±1 PTV.

Initial results from the in vivo study suggest the repeatability uncertainty of the Periotest® is approximately ±1 PTV.

3.3.2 MATLAB PTV

The repeatability uncertainty of the MATLAB PTV was estimated using the same experimental set-up and in a similar manner as described in Section 3.3.1. In this case, the repeatability uncertainty was determined to be ±0.2 PTV. This uncertainty includes three components: 1) variation of the Periotest® rod interaction with the abutment; 2) error of the MATLAB code in determining the contact time; and, 3) variation of the measurement method.

MATLAB PTV repeatability can also be estimated from in vivo measurement data and may yield a more realistic clinical uncertainty of the Periotest®. The in vivo repeatability uncertainty is estimated to be ±0.4 PTV. This repeatability uncertainty is based on only three repeated measurements of one implant system.

One method of determining the MATLAB PTV resolution is to consider the change in PTV resulting from the resolution of the time-voltage data, with emphasis on the time data. The change in PTV is based on a time-step of 0.006 ms and is calculated to be ±0.3 PTV. This value becomes the estimate of the MATLAB PTV resolution and could be modified by changing the sampling rate.

The repeatability and resolution of the existing Periotest® PTV and MATLAB PTV, for both in vitro and in vivo measurements, are shown in Table 3-2.

Table 3-2: Properties of Existing Periotest® and MATLAB Measurement Values

	Existing Periotest® PTV		MATLAB PTV	
	In vivo	In vitro*	In vivo	In vitro*
Repeatability	±1	±1	±0.4	±0.2
Resolution	±1	±1	±0.3**	±0.3**

* Estimated clinical repeatability based on repeated in vitro measurements
** Based on a sampling frequency of 166, 667 Hz and can vary with sampling frequency

The repeatability and resolution of the Periotest® improve when using the MATLAB code to post-process the conditioned transducer signal. Therefore, the best estimate of the Periotest® repeatability and resolution for clinical use would be ±0.4 PTV and ±0.3 PTV, respectively, and is based on the MATLAB PTV. The remaining portions of this chapter will make use of the MATLAB PTV exclusively.

The repeatability and resolution of the MATLAB PTV measurements are not integer values and suggests extending the Periotest® instrument to include one decimal place in its measurement scale. Extension of the PTV in this manner will enable more minute changes of the implant system to be detected. For example, extension of the Periotest® to include one decimal place in the PTV shows a difference between in vitro disc number 6 with abutment lengths of 3 and 4 mm attached. Table 3-3 shows that integer PTVs for both abutment lengths are within the existing instrument repeatability, whereas, the MATLAB PTV suggests two unique PTVs exist.

Table 3-3: PTVs from Periotest® and MATLAB Code for In Vitro Disk Number 6

Abutment Length (mm)	Periotest PTV ±1 PTV	MATLAB PTV ±0.4 PTV
3	-4	-3.8
4	-3	-2.7

3.4 Estimate of Osstell® Repeatability and Resolution

Estimation of the Osstell® repeatability and resolution follows a similar method as used for the Periotest®, described in Section 3.3. All Osstell® measurements used to determine the repeatability and resolution were recorded using the same Osstell® central processing unit. Again, repeatability and resolution estimates can be determined for the existing Osstell® ISQ and MATLAB ISQ for two categories: in vitro and in vivo.

An estimate of the existing Osstell® repeatability was determined by analyzing data collected following methods described in Section 2.4.1. The standard deviation of 32 recorded measurements was calculated to be ±1 ISQ. Therefore, an estimated Osstell® repeatability is ±2 ISQ. The resolution of the existing Osstell is ±1 ISQ.

The initial in vivo data suggests the maximum repeatability uncertainty value of the Osstell® instrument is ±2 ISQ. This repeatability uncertainty value is based on the repetition of three Osstell® measurements for a given implant system. Similar to the Periotest®, the presence of only three measurements is a very small sample size to calculate a precise repeatability value. However, agreement of the in vitro and in vivo estimated repeatability values gives confidence that the estimate is applicable.

The repeatability of the Osstell® instrument based on post-processing of the transducer signal using MATLAB was determined using data recorded following a similar procedure as used in Section 3.3. In this case, the variation of the resonant frequency determined by the MATLAB code and the existing Osstell® instrument were compared. Table 3-4 shows that the variability of the resonant frequencies determined by the MATLAB code and the Osstell® instrument are the same for the recorded 32 measurements.

Table 3-4: MATLAB and Osstell® Resonant Frequency Standard Deviations

Osstell® (Hz)	MATLAB (Hz)
23	23

Because the ISQ value is linearly related to the resonant frequency and the variability is the same for both the Osstell® and MATLAB frequencies, the repeatability of the MATLAB ISQ is the same as the existing Osstell ISQ: ±2 ISQ. Therefore, no improvement in the precision of the Osstell® instrument is noticed using the developed MATLAB algorithm. However, other methods of post-processing the Osstell® transducer signal may improve the instrument. Therefore, for this study the repeatability of the Osstell® instrument based on signal post-processing using MATLAB will be taken as ±2 ISQ.

Since there appears to be no improvement in the repeatability of the Osstell® instrument using the MATLAB code and the resolution is less than the repeatability of the existing instrument, an estimated value of the MATLAB code resolution was not completed.

The effective repeatability and resolution of the Osstell® instrument will be taken as ±2 ISQ and ±1 ISQ, respectively. All future references to the Osstell® measurements will be based on ISQ values returned by the existing unit.

3.5 Effect of Geometric Implant System Variables

Meaningful comparison of the Periotest® and Osstell® instruments requires converting the ISQ and PTV values to a common scale. This common scale could be taken as dimensional changes in abutment length, implant radius, and implant engagement length. The most important of these three implant system geometric parameters is engagement length because both abutment length and implant diameter remain constant after installation but engagement length can change because of bone loss.

The following sections consider the effects of varying abutment length, implant diameter, and implant engagement on Periotest® and Osstell® measurements. At the end of each section the minimum detectable change that can be measured by the Periotest® or Osstell® instruments is presented.

3.5.1 Effect of Abutment Length on Periotest®

An example of the Periotest® response to changes in abutment length of the in vitro implant systems is shown in Figure 3-12, while all of the data for the in vitro implant systems evaluated are shown in Appendix F. The error bars shown on these plots correspond to repeatability values of ±0.4 PTV. In addition, these figures include the fit of a recently proposed model to predict the Periotest® value based on implant geometric and mechanical properties. The details of this model and fitted curve are discussed below in Section 3.6.

Certain general trends can be seen in the Periotest® plots:1) an increase in the abutment length causes the PTV to increase; 2) over the range of abutment lengths considered, the PTV increases approximately in a linear fashion with abutment length; and 3) the PTVs for the 3 mm abutment deviate from the linear trend. The first trend agrees with previous studies and gives confidence in the correct operation of both the Periotest® instrument and the measurement method. The second trend suggests the sensitivity of the Periotest® to changes in abutment length could be determined by a linear regression analysis. Finally, the third trend suggests a possible difference between the 3 mm abutment and the 4, 5.5, 7, 8.5 and 10 mm abutments.

A linear regression analysis was completed for each of the 16 PTV-abutment length curves shown in Appendix G. Table 3-5 shows the approximate slopes and uncertainty associated with each curve. It is important to note the slope uncertainties correspond to twice the standard deviation of the slope: a 95% confidence interval for the normally distributed MATLAB PTV values.

Table 3-5: Linear Regression Results for MATLAB PTV/Abutment Length Plots

Implant Type	Implant Diameter (mm)	Engagement Length, L (mm)	Slope, m (PTV/mm)	Slope Uncertainty (±PTV/mm)	R^2 (%)
Extra-Oral	3.75 (SEC-002)	1.87	1.47	0.08	99.7
		2.78	0.96	0.17	97.1
		3.83	0.89	0.22	94.3
		4.16	0.76	0.14	96.7
Intra-Oral	3.3 (MKIII 25979)	5.94	1.25	0.13	99.7
		7.84	**1.23**	**0.55**	**95.3**
		8.74	0.76	0.05	99.9
	3.75 (MKIII 25977)	5.62	1.09	0.08	99.4
		7.70	0.83	0.09	98.8
		8.85	0.77	0.21	93.3
	4 (MKIII 25967)	5.72	1.04	0.11	98.9
		7.78	0.85	0.07	99.3
		8.72	0.65	0.07	98.8
	5 (SDCA 146-0)	6.68	0.64	0.20	91.4
		8.41	**0.67**	**0.26**	**86.6**
		9.58	0.65	0.19	92.2

In the majority of the linear regression fits shown above, the coefficient of determination, R^2, is 90% or greater. This relatively high value for R^2 suggests at least 90% of the variation shown in the MATLAB PTV can be explained by a linear relationship with abutment length. Therefore, the use of linear regression to calculate the sensitivity of the Periotest® to changes in abutment length is appropriate. However, a few results of the linear regression are considered outliers because of a R^2 value lower than 90% or a slope uncertainty greater than a third of the calculated slope value and are shown in bold type in the above table. These rather poor linear fits may be a result of variability in the installation of the implants in the discs of FRB-10 and will be confirmed if the Osstell® instrument returns similar results.

Figure 3-12 also shows the MATLAB PTV for the 3 mm abutment are slightly more positive than an extrapolation of the trend based on the other abutment lengths and indicates a slightly less stiff implant system. This trend of a higher MATLAB PTV for the 3 mm abutment than the other abutment lengths is representative of the plots shown in Appendix G. The reason for this deviation could be explained by the change in dimensions of the 3 mm abutment compared to the 4, 5.5, 7, 8.5, or 10 mm abutments. The 3 mm abutment has a reduced wall thickness compared to the other abutment lengths which could influence the effective stiffness of the implant system and, therefore, the Periotest® and Osstell® measurements.

To explain the deviation of the 3 mm abutment from the linear trend, composition of the effective stiffness of the implant system is considered. The effective stiffness of the implant system is some combination of the effective supporting material stiffness, the implant interface stiffness, the stiffness of the connection between the implant and abutment, and the stiffness of the attached abutment. The supporting material stiffness and stiffness of the implant connection remain constant when only the abutment lengths are changed because the engagement length is constant and a repeatable torque value is applied to the connecting screw. However, the stiffness of the abutment changes because of variations in length and wall thickness. If the abutment is treated as a cantilever beam, its stiffness for a point load applied perpendicular to the neutral axis at the end of the beam is proportional to the area moment of inertia and inversely proportional to the cube of its length. Therefore, as the abutment length decreases the effective stiffness of the implant increases. A decrease in the area moment of inertia – corresponding to a reduction in wall thickness – decreases the effective stiffness of the implant system. These changes in effective stiffness influence the Periotest® response.

Figure 3-12 shows the Periotest® response is proportional to changes in abutment length. Since increases in abutment length decrease the effective stiffness of the implant system, the Periotest® response must be inversely proportional to the effective stiffness of the system. Therefore, a reduced wall thickness of the 3 mm abutment would cause the Periotest® measurement to increase because of a reduced effective stiffness. This increase in the Periotest® measurement is not seen between the other lengths of abutments because their wall thicknesses remain relatively constant.

3.5.2 Osstell® Sensitivity to Changes in Abutment Length

The sensitivity of the Osstell® instrument to changes in abutment length was determined in a similar method as the Periotest®. All Osstell® measurements were recorded with the Osstell® internal value for the abutment length set at 3 mm.

Figure 3-13 shows a representative response of the Osstell® ISQ to changes in abutment length while Appendix H contains the entire set of plots for all implant systems considered. In all of these figures, the ISQ decreases as the abutment length increases. In addition, the response of the Osstell® to changes in abutment length appears to be relatively linear. Linearity in the measurements again suggests the use of linear regression to determine the sensitivity of the Osstell® instrument to changes in abutment length.

Results from the linear regression of the Osstell® measurements, shown in Table 3-6, indicates that at least 90% of the variation in the Osstell® ISQ values is linearly related to changes in abutment length.

Table 3-6: Linear Regression Results for Osstell® ISQ/Abutment Length Plots

Implant Type	Implant Diameter (mm)	Engagement Length, L (mm)	Slope, m (ISQ/mm)	Slope Uncertainty (±ISQ/mm)	R^2 (%)
Extra-Oral	3.75 (SEC-002)	1.87	-2.70	0.24	96.8
		2.78	-2.79	0.24	97.1
		3.83	-4.13	0.34	97.3
		4.16	-2.28	0.32	92.7
Intra-Oral	3.3 (MKIII 25979)	**5.94**	**-0.79**	**0.09**	**98.7**
		7.84	-3.63	0.27	99.4
		8.74	**-2.89**	**0.82**	**92.6**
	3.75 (MKIII 25977)	5.62	-2.58	0.19	98.0
		7.70	-2.96	0.17	98.7
		8.85	-3.67	0.20	98.9
	4 (MKIII 25967)	5.72	-2.51	0.12	99.1
		7.78	-3.31	0.21	98.5
		8.72	-3.46	0.13	99.4
	5 (SDCA 146-0)	6.68	-3.44	0.17	99.1
		8.41	-4.00	0.17	99.3
		9.58	-3.99	0.26	98.3

It is important to note that linear regression analysis of the Osstell® measurements shows similar unexpected results for the Ø3.3 mm intra-oral implant as did the Periotest®. Therefore, the Ø3.3 mm implant systems evaluated may have significant variations in the installation of the implant in the FRB-10 discs causing changes in effective implant system stiffness. As a result, the validity of further analyzing the instrument measurements for the Ø3.3 mm in vitro implant systems is questionable.

3.5.3 Minimum Measurable Change of Abutment Length

The Osstell® and Periotest® instruments are compared to a common scale by estimating the minimum measurable change of abutment length, Δ_{min}, using

$$\frac{repeatability}{sensitivity + error} \leq \Delta_{min} \leq \frac{repeatability}{sensitivity - error} \qquad \text{Equation 3-1}$$

The minimum changes in abutment length that can be detected by the Periotest® and Osstell® instruments are shown in Table 3-7 for all of the in vitro implant systems.

Table 3-7: Minimum Detectable Abutment Length using the Periotest® or Osstell®

Implant Type	Implant Diameter (mm)	Engagement Length, L (mm)	Δ_{min} Periotest® (mm Abut.)	Δ_{min} Osstell® (mm. Abut)
Extra-Oral	3.75 (SEC-002)	1.87	0.3-0.3	0.7-0.8
		2.78	0.4-0.5	0.7-0.8
		3.83	0.4-0.6	0.4-0.5
		4.16	0.4-0.6	0.8-1.0
Intra-Oral	3.3 (MKIII 25979)	**5.94**	**0.3-0.4**	**2.3-2.9**
		7.84	**0.2-0.6**	**0.5-0.6**
		8.74	**0.5-0.6**	**0.5-1.0**
	3.75 (MKIII 25977)	5.62	0.3-0.4	0.7-0.8
		7.70	0.4-0.5	0.6-0.7
		8.85	0.4-0.7	0.5-0.6
	4 (MKIII 25967)	5.72	0.3-0.4	0.8-0.8
		7.78	0.4-0.5	0.6-0.6
		8.72	0.6-0.7	0.6-0.6
	5 (SDCA 146-0)	6.68	0.5-0.9	0.6-0.6
		8.41	**0.4-1.0**	**0.5-0.5**
		9.58	0.5-0.9	0.5-0.5
		Average	**0.4-0.6**	**0.6-0.7**

Neither the Periotest® nor the Osstell® instrument shows any consistent significant advantage in detecting a smaller change in abutment length. It is important to note that this conclusion is based on the improved Periotest® PTV calculated by the MATLAB code and the response of the existing Osstell® instrument. Consequently, the existing Osstell® instrument would be able to detect smaller changes in abutment length than the **existing** Periotest®.

It is important to note that the minimum detectable changes in abutment length shown in bold type in the above table were considered outliers because they correspond to outliers identified in Tables 3-5 and 3-6. To estimate an overall average minimum detectable change in abutment length for both the Periotest® and Osstell® instruments outliers in the data were removed. An estimated value of an average detectable change in abutment length is approximately 0.6 mm for both the Periotest® and Osstell® instruments.

3.5.4 Effect of Engagement Length on Periotest® and Osstell®

Figure 3-14 shows representative MATLAB PTVs as engagement length is varied while holding both implant diameter and abutment length constant. It is important to note that as engagement length is decreased, striking height increases since implant length is constant. Refer to Appendix I for complete plots of the Periotest® response to changes in engagement length.

The Periotest® response to changes in engagement length and striking height appears to have linear relationship. Therefore, a linear regression analysis was completed. The results from this analysis are shown in Table 3-8. However, the following results should be used with reservations because the results are only based on three data pairs. To have greater confidence in the returned sensitivities of the MATLAB PTV to changes in engagement length, more data points should be included.

Table 3-8: Linear Regression Results for MATLAB PTV/Engagement Length/Striking Height Plots

Implant Type	Implant Diameter (mm)	Abutment Length (mm)	Slope, m (PTV/mm)	Slope Uncertainty (±PTV/mm)	R^2 (%)
Extra-Oral	3.75 (SEC-002)	**3.00**	**-0.70**	**0.18**	**88.8**
		4.00	**-1.21**	**0.39**	**83.0**
		5.50	**-1.66**	**0.47**	**86.0**
		7.00	**-2.09**	**0.57**	**87.2**
		8.50	**-2.27**	**0.67**	**85.1**
		10.00	**-2.80**	**0.73**	**88.0**
Intra-Oral	3.3 (MKIII 25979)	3.00	-0.93	0.16	97.1
		4.00	-1.09	0.25	95.0
		5.50	-1.30	0.12	99.1
	3.75 (MKIII 25977)	3.00	-0.69	0.03	99.8
		4.00	-0.89	0.06	99.6
		5.50	-1.07	0.25	94.9
		7.00	-1.32	0.09	99.5
		8.50	-1.18	0.22	96.8
		10.00	-1.49	0.00	100.0
	4 (MKIII 25967)	**3.00**	**-0.68**	**0.36**	**78.4**
		4.00	**-0.65**	**0.24**	**87.7**
		5.50	-0.91	0.19	95.8
		7.00	-1.00	0.29	92.4
		8.50	-1.29	0.11	99.3
		10.00	-1.52	0.11	99.4
	5 (SDCA 146-0)	3.00	-0.34	0.08	95.0
		4.00	-0.31	0.01	99.8
		5.50	-0.29	0.09	91.4
		7.00	-0.31	0.01	99.8
		8.50	**-0.25**	**0.23**	**54.9**
		10.00	-0.35	0.00	100.0

This analysis shows that in most cases at least 90% of the variation in the Periotest® measurement for the intra-oral implant systems can be explained by a linear relationship with changes in engagement length. Outlier values are considered those that have a R^2 value of 90% or less and are shown in bold type in the above table. The results for the extra-oral implant systems show about a 10% decrease in the R^2 value. This reduction can be explained by the extra-oral implants having small engagement lengths and the Periotest measurement being influenced by the stiffness of the thin FRB-10 disc. Section 3.6.1 will explain in more detail the effect of the thin FRB-10 discs on the Periotest® measurements compared to the thicker discs used to support the intra-oral implants.

A representative response of the Osstell® to changes in engagement length is shown in Figure 3-15. As the engagement length increases and exposed height decreases, the Osstell® ISQ increases in value. Appendix J contains the results from all in vitro implant systems evaluated using the Osstell® instrument. Similar to the Periotest® response, the Osstell® response appears to be relatively linear. Consequently, a linear regression analysis was completed and the results are shown in Table 3-9. However, the linear regression is only based on three data points.

Table 3-9: Linear Regression Results for Osstell® ISQ/Engagement Length/Striking Height Plots

Implant Type	Implant Diameter (mm)	Abutment Length (mm)	Slope, m (ISQ/mm)	Slope Uncertainty (±ISQ/mm)	R^2 (%)
Extra-Oral	3.75 (SEC-002)	**3.00**	**1.37**	**3.93**	**5.7**
		4.00	**2.45**	**3.06**	**24.3**
		5.50	2.01	0.37	93.8
		7.00	**1.94**	**1.60**	**42.1**
		8.50	**1.65**	**0.77**	**70.0**
		10.00	**0.42**	**0.47**	**29.2**
Intra-Oral	3.3 (MKIII 25979)	**3.00**	**3.92**	**1.67**	**84.7**
		4.00	3.75	0.88	94.8
		5.50	1.84	0.24	98.3
	3.75 (MKIII 25977)	3.00	4.88	0.45	99.1
		4.00	4.70	1.50	90.8
		5.50	4.22	0.70	97.3
		7.00	3.95	0.48	98.6
		8.50	3.07	0.15	99.8
		10.00	2.74	0.28	99.0
	4 (MKIII 25967)	3.00	3.78	0.53	98.1
		4.00	3.78	0.53	98.1
		5.50	3.62	0.20	99.7
		7.00	2.83	0.80	92.6
		8.50	2.07	0.32	97.6
		10.00	1.71	0.21	98.5
	5 (SDCA 146-0)	**3.00**	**2.54**	**1.11**	**83.9**
		4.00	3.49	0.41	98.7
		5.50	2.77	0.09	99.9
		7.00	3.13	0.25	99.4
		8.50	2.09	0.17	99.4
		10.00	1.41	0.24	97.1

This analysis shows that about 90% of the variation in the Osstell® measurements can be explained linearly with changes in engagement length, if the results from the extra-oral implants are ignored. Outlier values are considered those that have a R^2 value less than 90% and are shown in bold type in the above table. The Osstell® measurements from the extra-oral implants are uniquely different because of the thin engagement lengths and FRB-10 disc thicknesses. As will be shown in Section 3.6.1, evaluation of implant integrity for thin engagement lengths leads to measurements influenced by the local implant/supporting material interface, as well as disc stiffness far away from the interface. However, the slopes returned by the linear regression fit for the intra-oral implants are good estimates of the Osstell® sensitivity to changes in engagement length, as evidence by the high R^2 values.

A second trend is also visible: as the abutment length increases, the sensitivity of the Osstell® to changes in engagement length decreases.

The minimum detectable change in the combined effects of engagement length and striking can be calculated in a similar manner as in Section 3.5.3 to determine the minimum measurable change in abutment length. These values are shown in Table 3-10 for both the Periotest® and Osstell® instruments. A range of values was not completed in this case because of the small sample size used to determine the sensitivity of the instruments to changes in engagement length caused by bone loss.

Table 3-10: Minimum Detectable Engagement Length* Changes

Implant Type	Implant Diameter (mm)	Abutment Length (mm)	Periotest Minimum (mm)	Osstell Minimum (mm)
Extra-Oral	3.75 (SEC-002)	**3.00**	**0.6**	**1.5**
		4.00	**0.3**	**0.8**
		5.50	**0.2**	**1.0**
		7.00	**0.2**	**1.0**
		8.50	**0.2**	**1.2**
		10.00	**0.1**	**4.7**
Intra-Oral	3.3 (MKIII 25979)	**3.00**	**0.4**	**0.5**
		4.00	0.4	0.5
		5.50	0.3	1.1
	3.75 (MKIII 25977)	3.00	0.6	0.4
		4.00	0.5	0.4
		5.50	0.4	0.5
		7.00	0.3	0.5
		8.50	0.3	0.7
		10.00	0.3	0.7
	4 (MKIII 25967)	**3.00**	**0.6**	**0.5**
		4.00	**0.6**	**0.5**
		5.50	0.4	0.6
		7.00	0.4	0.7
		8.50	0.3	1.0
		10.00	0.3	1.2
	5 (SDCA 146-0)	**3.00**	**1.2**	**0.8**
		4.00	1.3	0.6
		5.50	1.4	0.7
		7.00	1.3	0.6
		8.50	**1.6**	**1.0**
		10.00	1.2	1.4
		Average	**0.6**	**0.7**

*** In this case, the change in engagement length is caused by bone loss.**

It appears from this table that there are no significant differences between the Periotest® and Osstell®. Both of the instruments show large variations in the minimum detectable changes in engagement length depending on the implant system being evaluated. However, if the outliers, shown in bold, are extracted from the calculated values based on a R^2 value less than 90%, both instruments have an averaged ability to detect changes in engagement length, caused by bone loss, of approximately 0.6mm.

Table 3-10 also shows that as the abutment length increases, the Periotest® can detect more minute changes as a result of bone loss, whereas, the Osstell® instrument cannot detect as small of changes. Therefore, when using these instruments it is important to realize that one instrument may be more sensitive to changes in implant integrity than the other for a given abutment length. For example, the Periotest® appears to have a higher sensitivity to changes in implant system geometry when the abutment length is longer. In contrast, the Osstell® instrument appears to have a higher sensitivity when the abutment lengths are shorter.

3.5.5 Effect of Implant Diameter on Periotest® and Osstell®

The response of the Periotest® and Osstell® instruments to varying implant diameter was also compared. In order to complete this comparison, all other implant geometric properties had to be held constant. The in vitro implant systems were built by ensuring the implants were 0, 1, or 3 mm proud of the supporting material surface. Since the apparatus was constructed with this objective slight variations in engagement length and striking heights required normalizing of the data to isolate the effects of varying implant diameter. Fortunately, the linear regression analysis completed on the response of instrument changes to engagement length and striking height could be used to remove their effects from changing implant diameters.

To accomplish this task, the sensitivity of the Osstell® and Periotest® instruments to changes in engagement length, and corresponding striking height, were first considered. These sensitivities provided equations to normalize the MATLAB PTV and Osstell® ISQ for each given implant diameter to the mean engagement length value. By completing this small shift in the values, the independent effect of the implant diameter on the Osstell® ISQ and MATLAB PTV can be determined. Representative MATLAB PTV and Osstell® ISQ changes to implant diameter are shown in Figure 3-16 and Figure 3-17 for an effective engagement length of 5.72 mm. Similar trends for engagement lengths of 7.78 and 8.74 mm are shown in Appendix K. It is important to note that normalizing the engagement length to the mean value also resulted in the removal of any variations caused by striking height because all plots and linear regression analysis in Section 3.5.4 combine the effects of engagement length and striking height.

Implants with Ø5.00 mm diameters are not included in these figures because the engagement lengths are about 0.6-1.0 mm larger than implants with diameters of 3.3, 3.75, or 4 mm and it was deemed that this large change in engagement length could not be confidently normalized. It is important to note that the engagement lengths for the Ø3.3, 3.75, or 4 mm implants varied by approximately 0.3 mm. The main difference in the implants is the absence of a flange on the Ø5.00 mm compared to the other implant diameters. This flange is approximately 0.5 mm thick.

A similar linear regression analysis used to determine the sensitivity of the Periotest® and Osstell® to changes in abutment length is desired, however, the three data points do not appear to have a strong linear relationship. Therefore, a linear regression analysis was not performed. Consequently, the smallest detectable changes was not calculated.

However, a general trend of the response of the Periotest® and Osstell® instruments to changes in implant diameter appears to exist: as the implant diameter increases, the Periotest® and Osstell® measurements decrease and increase, respectively. Again, it is observed when the Periotest® measurement increases in value, the Osstell® ISQ decreases.

3.6 Mathematical Model of Implant System Motion

To better understand the response of an implant system to a Periotest® measurement, a theoretical model of the implant system is useful. The deflection of an implant system to a force and/or moment applied at the top of the abutment is dependent on mechanical properties of

- the supporting material,
- the interface between the implant and supporting material,
- the connection between the abutment and implant, and
- the abutment and implant. The implant and abutment are assumed rigid.

For a statically applied force and/or moment, these four mechanical properties can be represented as stiffnesses. A dynamic response of the implant system includes both stiffnesses and damping properties of each component.

These individual stiffnesses could be combined to form an equivalent stiffness to describe the motion of the implant system. Previous investigators have shown that a change in each one of these four components can influence the response of the implant system measured using the Periotest® or Osstell® instruments (Derhami et. al. 1995, Meredith et. al. 1996, Giannitsios et. al. 2001). Therefore, an equivalent stiffness to represent the vibrating implant system is possible.

The main objective of modeling the motion of the implant system using an equivalent stiffness is to correlate the mechanical properties of the implant interface to the measurement returned by the Periotest® or Osstell®. This correlation aids in understanding what physical properties the Periotest® and Osstell® instruments measure. A recently proposed analytical model to better understand and predict the Periotest® measurement has attempted to correlate the geometric parameters of an implant to the PTV (Giannitsios et. al. 2001). The brief derivation, including arbitrary forcing functions, and fit of this model to the collected Periotest® data is discussed below. It is important to note that the Osstell® data cannot be approximated using this model because of the complexity of the Osstell® transducer lead, which includes an additional stiffness within the transducer lead.

The Giannitsios et. al. (2001) model of a vibrating implant system is based on the implant supported with springs and viscous dampers, as shown in Figure 3-18. The corresponding free body diagram (FBD) and mass acceleration diagram (MAD) is shown in Figure 3-19. Table 3-11 indicates the various variable definitions used in deriving this model.

Table 3-11: Variable Definitions for Giannitsios et. al. (2001) Model

Variable Name	Meaning
k	constant radial horizontal stiffness coefficient of the supporting tissue per unit length of engagement ($\left(N/m\right)/m$)
k^*	constant vertical stiffness coefficient of the supporting tissue per unit length of engagement ($\left(N/m\right)/m$)
c	constant radial horizontal viscous damping coefficient of the supporting tissue per unit length of engagement ($\left(N/(m/s)\right)/m$)
c^*	constant vertical viscous-damping coefficient of the supporting tissue per unit length of engagement ($\left(N/(m/s)\right)/m$)
E	engagement length – length of implant engaged with supporting tissue (m)
Q	distance to center of mass of system from bottom of implant system (m)
L	distance from bottom of implant to location of applied force and moment (m)
O	point of application of external force and moment
$\varnothing$	diameter of implant (m)
$f(t)$	applied forcing function at top of abutment (N)
$M(t)$	applied moment function at top of abutment (Nm)
$x(t)$	translation movement of the implant's center of mass (m)
$\vartheta(t)$	rotational movement of implant about center of mass (rad)
J	rotational mass moment of inertia for the implant system (kgm^2)
m	mass of the implant system (kg)

Several assumptions are included in this model to simplify the derivation. These assumptions include: 1) the implant system acts as a rigid body; 2) the implant abutment system can only translate in the *x* direction and rotate in the plane of the forces; and, 3) the implant undergoes small translational and rotational displacements. The assumption of rigid body motion forces the stiffnesses of the implant connection and the implant/abutment to be infinite. As a result, the effective stiffness of the system reduces to the stiffness of the implant interface and supporting material only (see pg.73).

The assumption of small translational and rotational displacements is based on an analysis which estimated the displacement of the abutment, when forced by the Periotest® rod, to be on the order of 10-100 μm (Lukas et. al. 1992). In comparison to a Ø4 mm implant with a length of 10 mm and attached to a 10 mm abutment, these displacements and corresponding rotations are small.

The equations of motion describing the movement of the implant system can be written using Newton's laws and the FBD/MAD shown in Figure 3-19. A matrix representation of these equations is (for a brief derivation, see Appendix L).

$$\left[\begin{gathered}\begin{bmatrix} m & 0 \\ 0 & J \end{bmatrix}\begin{Bmatrix} \ddot{x} \\ \ddot{\vartheta} \end{Bmatrix} + E\begin{bmatrix} c & c\left(E/2 - Q\right) \\ c\left(E/2 - Q\right) & \begin{bmatrix} c\left(Q^2 - QE + E^2/3\right) \\ + c^{*}\left(\phi/2\right)^2 \end{bmatrix} \end{bmatrix}\begin{Bmatrix} \dot{x} \\ \dot{\vartheta} \end{Bmatrix} \\ + E\begin{bmatrix} k & k\left(E/2 - Q\right) \\ k\left(E/2 - Q\right) & \begin{bmatrix} k\left(Q^2 - QE + E^2/3\right) \\ + k^{*}\left(\phi/2\right)^2 \end{bmatrix} \end{bmatrix}\begin{Bmatrix} x \\ \vartheta \end{Bmatrix}\end{gathered}\right] = \begin{Bmatrix} f(t) \\ f(t)(L - Q) + M(t) \end{Bmatrix} \qquad \text{Equation 3-2}$$

These equations are independent of the Periotest® instrument, but written for general forcing, *f(t)*, and moment, *M(t)*, functions. To apply Equation 3-2 to the Periotest® instrument specifically, requires *f(t)* and *M(t)* for the Periotest® rod interaction with the abutment. If this interaction is assumed perfectly inelastic – for example, no relative motion between the Periotest® rod and the abutment – then the forcing function, *f(t)*, and assumed moment function, *M(t)*, are given as Equation 3-3.

$$\begin{aligned} f(t) &= -m_{Periotest}\left(\ddot{x}(t) + (L - Q)\ddot{\vartheta}\right) \\ M(t) &= 0 \end{aligned} \qquad \text{Equation 3-3}$$

Use of Equation 3-3 in Equation 3-2 yields

$$\left[\begin{bmatrix} m+m_p & (L-Q)m_p \\ (L-Q)m_p & J+(L-Q)^2 m_p \end{bmatrix}\begin{Bmatrix} \ddot{x} \\ \ddot{\vartheta} \end{Bmatrix} + E\begin{bmatrix} k & k\left(E/_2-Q\right) \\ k\left(E/_2-Q\right) & \begin{bmatrix} k\left(Q^2-QE+E^2/_3\right) \\ +k^*\left(\phi/_2\right)^2 \end{bmatrix} \end{bmatrix}\begin{Bmatrix} x \\ \vartheta \end{Bmatrix}\right]=\begin{Bmatrix} 0 \\ 0 \end{Bmatrix} \qquad \text{Equation 3-4}$$

The free-vibration response of the implant system, as recorded by strain gauges fixed to a 10 mm abutment, shows the vibrating implant system to have little damping. Therefore, the theoretical response of the system will only consider stiffness components. It should be noted the effects of damping have been previously shown to be small and therefore, the damping terms in Equation 3-2 have been removed.

This equation can be further simplified by writing the mass of the Periotest® rod, m_p, in terms of the implant mass, m. An equation that relates these two masses is given in Equation 3-5 and is derived from the sum of the forces in the horizontal direction.

$$m\ddot{x}+kEx+kE\left(E/_2-Q\right)\vartheta=-m_p\left(\ddot{x}+(L-Q)\ddot{\vartheta}\right) \qquad \text{Equation 3-5}$$

Substitution of Equation 3-5 into 3-4 yields equations of motion based on a mass matrix with the second row based only on the mass properties of the implant and abutment, as shown in Equation 3-6. This step is required in order to further simplify the two coupled equations.

$$\left[\begin{bmatrix} m+m_p & m_p(L-Q) \\ m(L-Q) & -J \end{bmatrix}\begin{Bmatrix} \ddot{x} \\ \ddot{\vartheta} \end{Bmatrix} + \begin{bmatrix} kE & kE\left(E/2-Q\right) \\ kE\left(L-E/2\right) & \begin{bmatrix} -k^{*}\left(\phi/2\right)^{2}E \\ +kE\left(L\left(E/2-Q\right)+E\left(Q/2-E/3\right)\right) \end{bmatrix} \end{bmatrix}\begin{Bmatrix} x \\ \vartheta \end{Bmatrix}\right] = \begin{Bmatrix} 0 \\ 0 \end{Bmatrix} \qquad \text{Equation 3-6}$$

With the assumption of negligible implant system mass compared to the mass of the Periotest® rod and a shift in the coordinate system, given by $x_D = x + (L-Q)\vartheta$ shown on Figure 3-19, the two coupled equations, shown above, reduce to a single degree of freedom system with an equation of motion given below.

$$\left[m_p\ddot{x}_D + \left[kE - \left(k/2\right)\left((L-E)^2 - L^2\right)\left(\frac{\left[\left(k/2\right)\left((L-E)^2 - L^2\right)\right]}{\begin{bmatrix}\left(k/3\right)\left((L-E)^3 - L^3\right) \\ +k^{*}\left(\phi/2\right)^{2}E\end{bmatrix}}\right)\right]x_D\right] = 0 \qquad \text{Equation 3-7}$$

Therefore, the equivalent stiffness at the striking point of the Periotest® rod that describes the stiffness of the implant interface is

$$K_I = \left[kE - \left(k/2\right)\left((L-E)^2 - L^2\right)\left(\frac{\left[\left(k/2\right)\left((L-E)^2 - L^2\right)\right]}{\begin{bmatrix}\left(k/3\right)\left((L-E)^3 - L^3\right) \\ +k^{*}\left(\phi/2\right)^{2}E\end{bmatrix}}\right)\right] \qquad \text{Equation 3-8}$$

3.6.1 Correlation of Model and Experiments

To fit the above model to the Periotest® data, the PTV must be calculated using the interface stiffness, K_I. Because this model simplifies to a single degree of freedom system, the contact time of the Periotest® rod with the abutment is theoretically determined by calculating the natural frequency of the system, ω, and calculating the half period of oscillation.

$$ct = \frac{\pi}{\omega} = \frac{\pi}{\sqrt{\frac{K_I}{m_p}}} = \pi\sqrt{\frac{m_p}{K_I}} \qquad \text{Equation 3-9}$$

To determine the values of k^* and k, a least squares curve-fitting routine utilizing Equations 3-8 and 3-9, was employed using MATLAB, as shown in Appendix M. MATLAB PTV data corresponding to changes in abutment length were used as the input because the implant interface stiffness remains constant. Results from the curve fit are shown in Table 3-12 and graphically displayed in Appendix F.

Table 3-12: Least Squares Results for In Vitro Implant Systems

Implant Type	Implant Diameter (mm)	Engagement Length, L (mm)	k^* – Vertical Stiffness (x.xxe9 N/m^2)	k – Horizontal Stiffness (x.xxe8 N/m^2)	$\frac{k^*}{k}$
Extra-Oral	3.75 (SEC-002)	1.87	7.41±0.64	5.32±0.63	11-17
		2.78	9.50±0.59	4.07±0.43	20-28
		3.83	8.17±0.42	3.22±0.33	22-30
		4.16	9.33±0.46	2.87±0.28	28-38
Intra-Oral	3.3 (MKIII 25979)	5.94	5.43±0.19	3.57±0.54	13-19
		7.84	3.95±0.11	3.79±0.70	9-13
		8.74	6.36±0.24	1.70±0.18	33-43
	3.75 (MKIII 25977)	5.62	5.90±0.22	3.28±0.45	15-22
		7.70	5.83±0.21	1.93±0.21	26-35
		8.85	5.56±0.20	1.86±0.21	26-35
	4 (MKIII 25967)	5.72	5.46±0.21	3.21±0.44	14-20
		7.78	5.13±0.18	2.35±0.29	19-26
		8.72	6.03±0.22	1.52±0.15	35-46
	5 (SDCA 146-0)	6.68	5.56±0.22	2.12±0.22	23-30
		8.41	4.02±0.15	1.76±0.19	20-27
		9.58	3.51±0.13	1.57±0.17	19-26

The error in determining the k^* and k values was computed numerically by assuming errors of ±0.1mm, ±0.1mm, and ±0.4 PTV, in engagement length, abutment height, and calculated MATLAB PTV, respectively. These groups of stiffness values were then averaged and the standard deviation calculated. The stiffness errors shown in Table 3-12 correspond to two standard deviations, or a 95% confidence interval. An estimated range of the k^*:k ratio was determined using

$$\frac{\left(k^* - k^*_{error}\right)}{\left(k + k_{error}\right)} \le \left(\frac{k^*}{k}\right) \le \frac{\left(k^* + k^*_{error}\right)}{\left(k - k_{error}\right)} \qquad \text{Equation 3-10}$$

Table 3-12 illustrates that the fitted stiffness parameters, k^* and k, vary substantially for the in vitro implant systems evaluated using the Periotest®. This variance may be a result of supporting material inhomogeneities due to encapsulated air pockets, inconsistent implant integrity caused by the method of fabrication, and/or the basic assumptions in the derivation of the Giannitsios et. al. model (2001). Several times during the process of manufacturing FRB-10 discs to support the implants, encapsulated air pockets were noted. The chances of identifying a disc with an air pocket would be greater for thin discs compared to thicker discs used to support the intra-oral implants.

Inconsistencies in the method of installing the implant in the FRB-10 disc may influence the integrity of the implant interface. For example, if the self-threading implant was installed in a manner that resulted in new threads being cut, implant integrity may be different than if the implant exactly followed the tapped threads. This inconsistency was addressed with the application of epoxy prior final installation of the implant, however, it may still be partially responsible for the variations seen in k^* and k.

A third reason for the variations in the k^* and k values could be caused by the assumptions of negligible implant mass and an infinitely stiff implant/abutment. Verification of this assumption has not been completed to date, therefore, it's validity may be questionable and responsible for variations in k^* and k.

Another reason for the variance in the stiffnesses of Giannitsios et. al.'s model (2001) may be a result of the thinner supporting structure incorporating the stiffness of the supporting disc, as well as the implant interface. To explain this tendency, the ability of the Periotest® to detect changes in the stiffness of the FRB-10 disc thickness was investigated as described in Section 2.3.7.

The response of the Periotest® pre-amplified transducer signal to the first and final cuts of disc number 11, corresponding to effective FRB-10 disc diameters of 11.60 and 37 mm, respectively, are plotted in Figure 3-20. The Periotest® responses shown in

Figure 3-20 are from the handpiece oriented, as shown in Figure 1-6. The amplitude of the transducer signal is slightly less for the 37 mm effective disc diameter than the 11.6 mm diameter. In addition, the contact time is greater for the larger effective disc diameter. Since the engagement length and striking height remain the same for the 11.6 and 37 mm effective disc diameters, the reason for the change in the Periotest® pre-amplified transducer signal is because of the Periotest® measuring both the stiffness of the thin disc and the implant interface. Therefore, Periotest® measurements for thin discs, such as for in vitro discs 1 through 4, may be evaluating both the implant interface and the stiffness of the thin plate.

As a result, the motion of the extra-oral implant systems with the Periotest® rod in contact cannot be reliably curve fit using Giannitsios et. al.'s model (2001). The reason the model cannot be used is that its derivation is based on local implant interface stiffnesses only and assumes the supporting material is rigid.

Similar results from the pre-amplified transducer signal for Periotest® measurements completed with the handpiece oriented along the implant axis and are shown in Figure 3-21. Noticeable changes in both the amplitude and duration of the signals occur when the effective thin disc diameter increases. The amplitude halves and the contact time increases by about 50%.

The above results led to more testing to ensure the thicker FRB-10 discs, with thicknesses greater than 5 mm and used to support the intra-oral implants, were independent of the disc diameter. To complete this evaluation, in vitro disc number 6 was held with additional clamping apparatus, as shown in Figure 2-19, to reduce the effective disc diameter. This disc was chosen because it is the thinnest disc supporting the intra-oral implants, with a disc thickness of 5.62 mm, and would be most prone to thin plate effects. The results with and without the additional clamping are shown in Figure 3-22.

These results show the amplitude and duration of the pre-amplified Periotest® transducer signal remain effectively the same for changes in effective disc diameter. This result suggests that thin plate effects are not seen in the thicker FRB-10 discs used to mount the intra-oral implants. Therefore, it seems more valid to fit the intra-oral Periotest® data to the Giannitsios et. al. model (2001).

3.6.2 Possible Second Mode of Vibration

The superimposed frequency in the pre-amplified Periotest® transducer signal may be a result of the implant system having two-degrees of freedom. So far, the Giannitsios et. al. model (2001) was simplified to a one degree of freedom system by assuming the mass of the Periotest® rod was much greater than the mass of the implant/abutment. This assumption has the model return only one frequency of vibration. To compare the two distinct frequencies in the pre-amplified transducer signal to this model requires a two-degree of freedom system. By estimating the mass properties of the implant and abutment, the Giannitsios et. al. model (2001) remains a two-degree of freedom system and returns two natural frequencies.

To complete this investigation, the mass of implant and abutment were measured to be 0.35g and 0.65g, respectively. From these masses, and the geometric properties of the implant system, the moment of inertia of a Ø3.75 mm Intra-Oral Brånemark Implant with a 10 mm regular platform abutment was determined to be about 31 g*mm^2 about the center of gravity of the combined implant and abutment. These mass values, along with the geometric parameters and stiffness values shown in Table 3-12 for a Ø3.75 mm implant with engagement length of 5.62 mm, were used to calculate the mass and stiffness matrices. The mode shapes, shown in Figure 3-23, and the corresponding theoretical frequencies, shown in Table 3-13, were then determined following methods described in Appendix N.

Table 3-13: Natural Frequencies of Implant System

Mode	Theoretical Frequency (Hz)	Empirical Frequency (Hz)
1	1000	~1070
2	14000	~17000

Initial investigation of the pre-amplified Periotest® transducer signal showed a similar ratio. Decomposition of this signal, by removing the first mode of vibration from the signal, shows the presence of another mode of vibration. The signal shown in Figure 3-24 was decomposed by first fitting a damped sinusoidal curve to the pre-amplified transducer signal, and then subtracting this least squares fitted curve from the original signal to produce a plot of the higher frequency component, shown in Figure 3-25. A damped sinusoidal curve was selected because it is a solution of the equation of motion for a vibrating system with both stiffness and damping. The empirical frequencies were then estimated by converting the radian frequency, ω=6700 rad/s, shown in Figure 3-24, to a frequency in Hertz. This conversion returned a first mode frequency of approximately 1070Hz. The second mode of vibration was estimated by determining the ratio of frequencies of the second to first mode of vibrations to be approximately 16. Because the magnitudes of the theoretical and empirical frequencies of vibration for the first two modes are similar, as shown in Table 3-13, this suggests that the higher frequency component seen in the pre-amplified Periotest® transducer signal could be a result of the second mode of vibration.

3.7 *In Vivo Results*

Representative Periotest® and Osstell® results for the in vivo study are shown in Figure 3-26 and Figure 3-27, and plots of the complete data are shown in Appendix O. All of the Periotest® and Osstell® data were recorded using one operator and a stricter protocol, as discussed in Section 2.5.2.

Similar measurement trends exist in the in vivo as in the in vitro evaluations: as the Periotest® value increases, the Osstell® ISQ decreases. This trend is seen in Figure 3-26 and Figure 3-27 for the Periotest® measurement recorded in the axial and superior directions and the Osstell® measurement recorded in the superior direction using the fixture and abutment leads. As a result of this trend, the precision of the Periotest® appears to be sufficient when used under the stricter protocol and post-processed using the MATLAB developed code. In addition, similar trends in the Periotest® in vivo and in vitro data suggests the new protocol controls the important measurement variables of the Periotest® sufficiently to mimic the in vitro measurement protocol.

It is important to note that clinical sterilization protocol resulted in different Periotest® instruments and Osstell® transducer leads being used to complete the longitudinal measurements for a given patient. As a result, inter-instrument measurement comparisons were completed following the procedure outlined in Appendix O to remove inter-instrument variation from the patient data. Consequently, Figure 3-26 and Figure 3-27 show an estimated measurement value for the Periotest®

instruments and one of the Osstell® leads. In addition, each data point shown on the figures is based on three repeated measurements.

In addition, Figures 3.26 and 3.27 show that the interface between the implant and the supporting bone tends to decrease in stiffness at the three month visit and then become stiffer by the six month visit. This trend is generally explained by the remodeling of the bone surrounding the implant from initial installation during the first bone healing cycle. This is also consistent with the initial period of cellular mineralization of the osseous matrix that is followed by the longer period of cellular mineralization. Therefore, the results from this in vivo study agree with the current understanding of bone remodeling and mineralization.

Further work on the in vivo study will assist in determining the relative value of the Periotest® and Osstell® instruments for measuring implant integrity in the clinic.

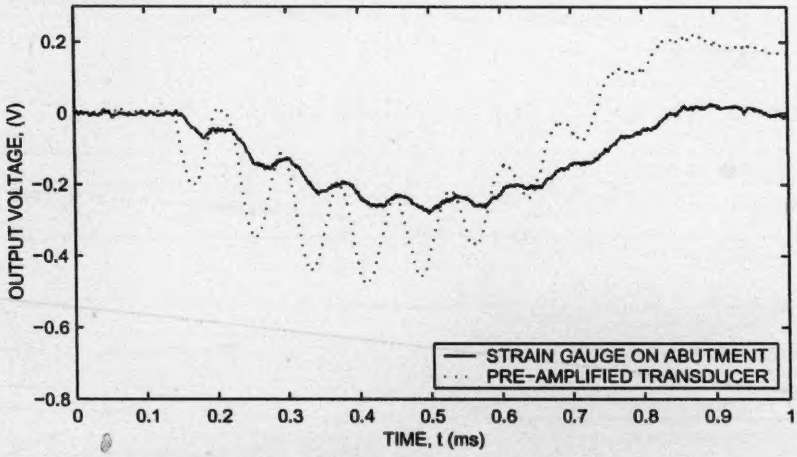

Figure 3-1: Periotest® and Strain Gauge Response of a Ø4mm Intra-Oral Brånemark Implant Mounted in FRB-10 to an Engagement Length of 1.68mm

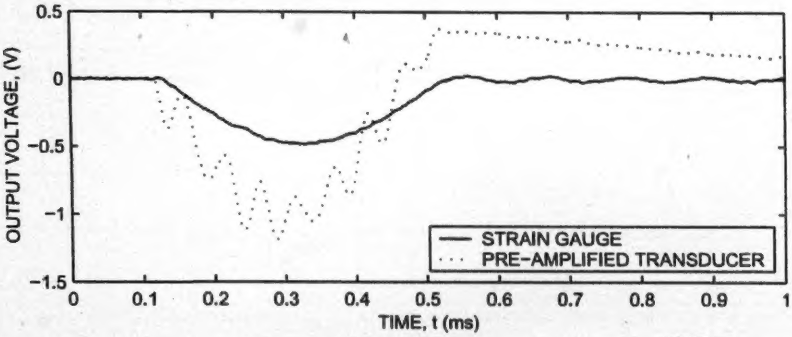

Figure 3-2: Response of Ø4mm Intra-Oral Brånemark Implant in FRB-10 to an Engagement Length of 8.72mm

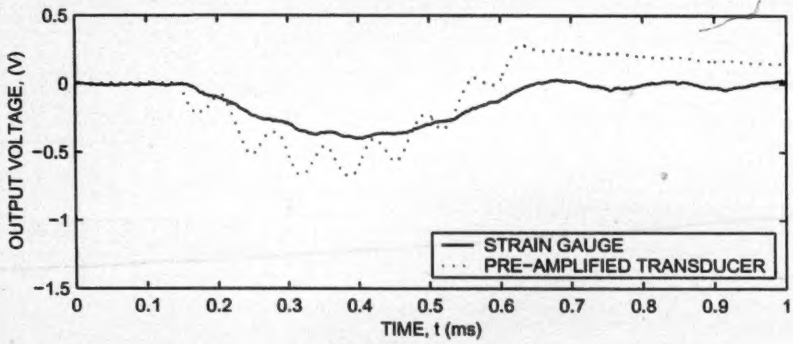

Figure 3-3: Response of Ø4mm Intra-Oral Brånemark Implant in FRB-10 to an Engagement Length of 5.72mm

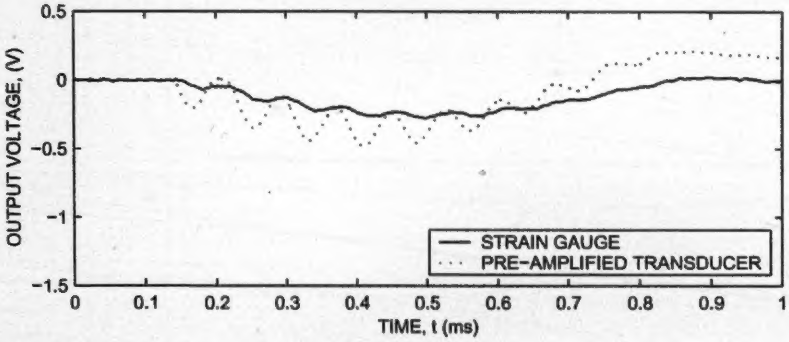

Figure 3-4: Response of Ø4mm Intra-Oral Brånemark Implant in FRB-10 to an Engagement Length of 1.68mm

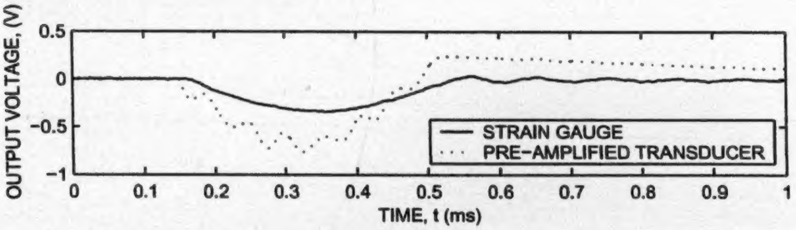

Figure 3-5: Response of Ø3.75mm Extra-Oral Brånemark Implant in FRB-10 to an Engagement length of 4.78mm

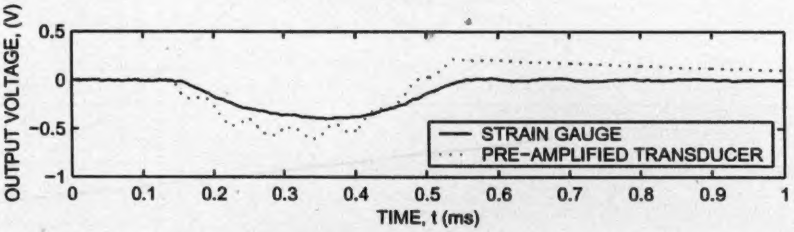

Figure 3-6: Response of Ø3.75mm Extra-Oral Brånemark Implant in FRB-10 to an Engagement length of 3.83mm

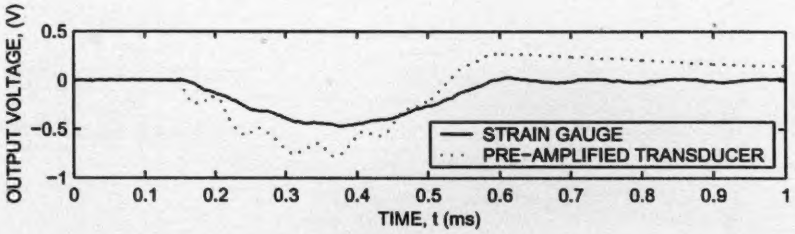

Figure 3-7: Response of Ø3.75mm Extra-Oral Brånemark Implant in FRB-10 to an Engagement length of 2.78mm

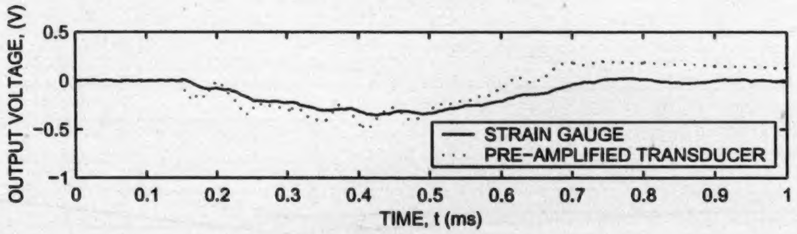

Figure 3-8: Response of Ø3.75mm Extra-Oral Brånemark Implant in FRB-10 to an Engagement length of 1.87mm

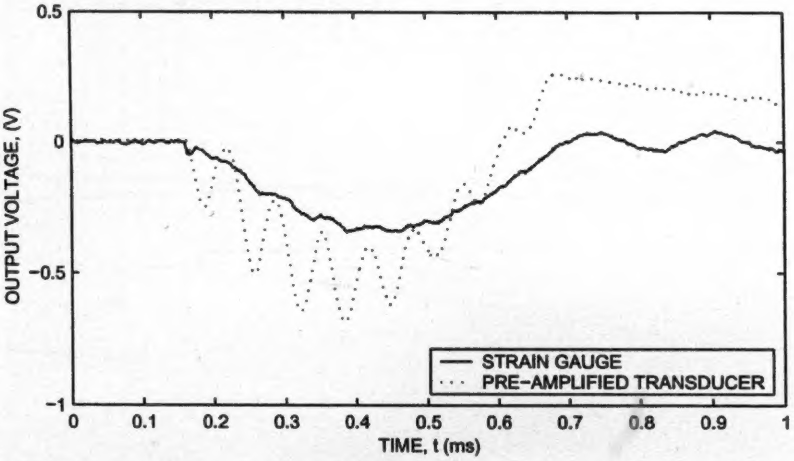

Figure 3-9: Response of Ø3.75mm Intra-Oral Brånemark Implant in FRB-10 to an Engagement length of 5.62mm

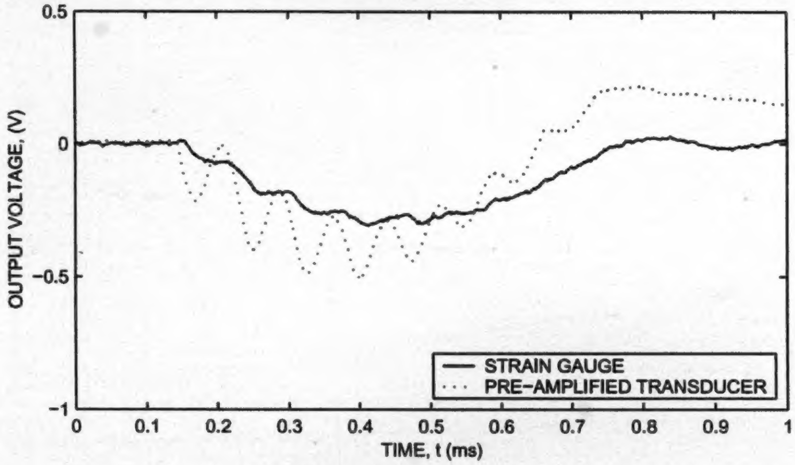

Figure 3-10: Response of Ø3.75mm Intra-Oral Brånemark Implant in FRB-20 to an Engagement length of 5.62mm

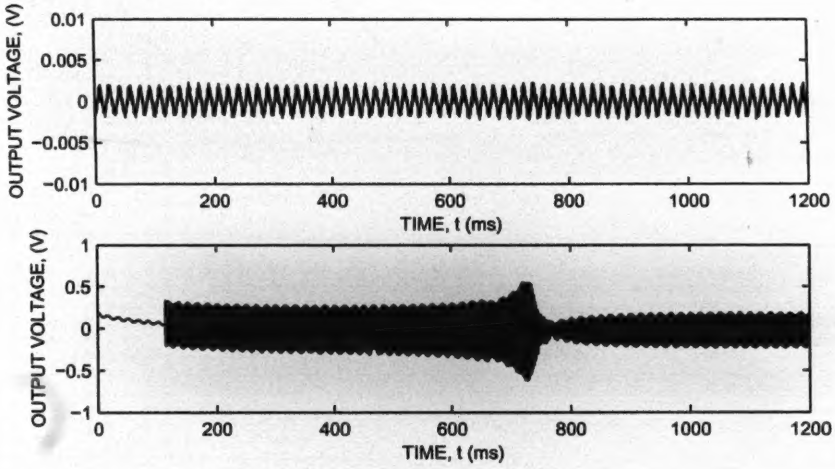

Figure 3-11: Strain Gauge and Osstell® Recording Transducer Simultaneous Responses (shown on top and bottom, respectively)

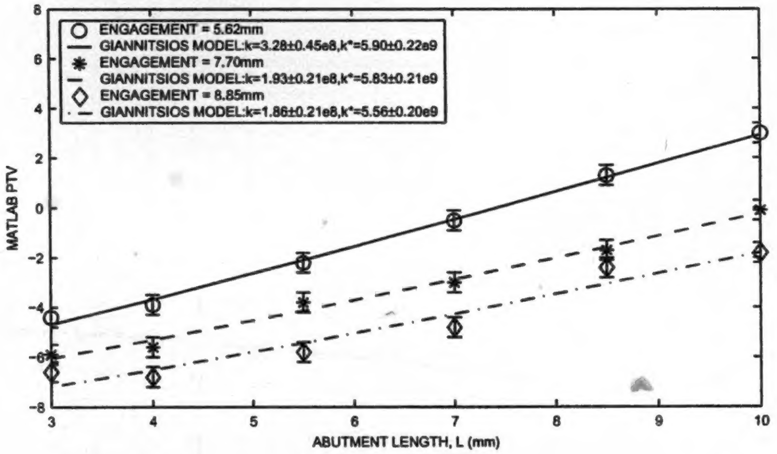

Figure 3-12: Representative Periotest® Response to Changes in Abutment Length for Ø3.75mm Brånemark Intra-Oral Implants installed in FRB-10

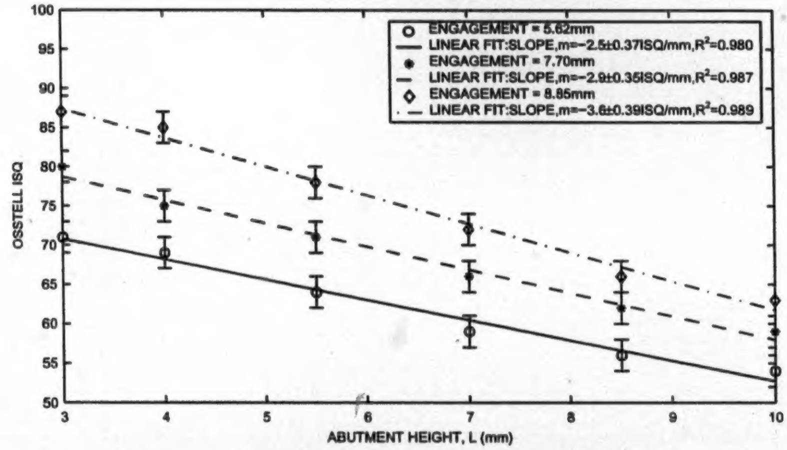

Figure 3-13: Representative Osstell® Response to Changes in Abutment Length for Ø3.75mm Brånemark Intra-Oral Implants installed in FRB-10

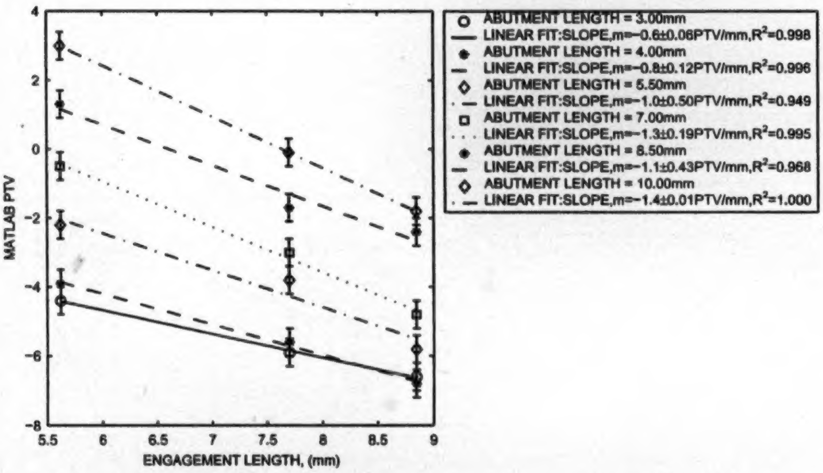

Figure 3-14: Periotest® Response to Changes in Engagement Length and Striking Height for Ø3.75mm Brånemark Intra-Oral Implants installed in FRB-10

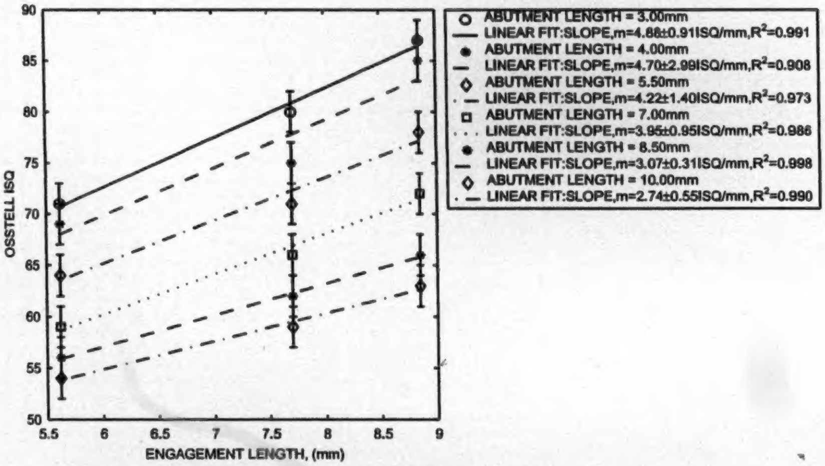

Figure 3-15: Osstell® Response to Changes in Engagement Length and Striking Height for Ø3.75mm Brånemark Intra-Oral Implants installed in FRB-10

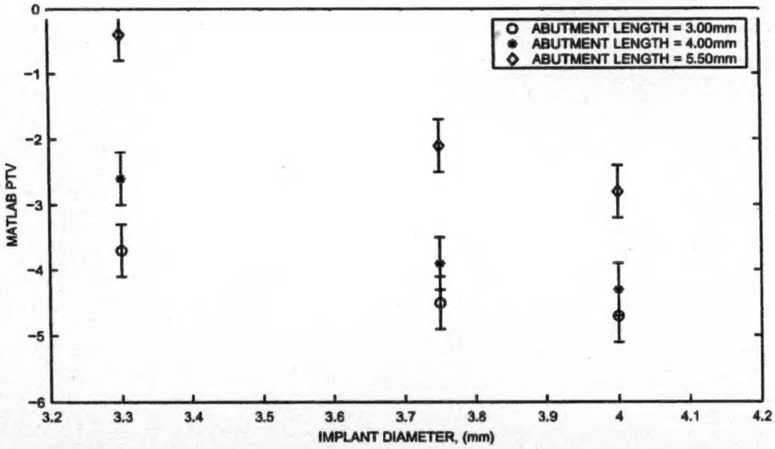

Figure 3-16: Representative Periotest® Response to Changes in Implant Diameter for Brånemark Intra-Oral Implants installed in FRB-10 to an Effective Engagement Length of 5.72mm

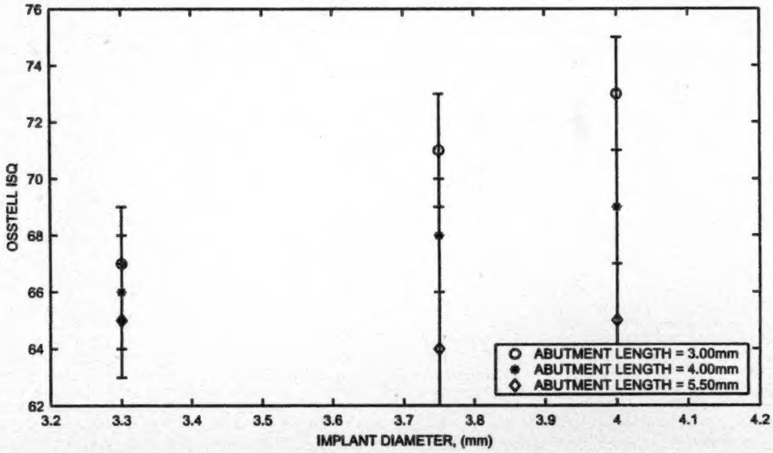

Figure 3-17: Representative Osstell® Response to Changes in Implant Diameter for Brånemark Intra-Oral Implants installed in FRB-10 to an Effective Engagement Length of 5.72mm

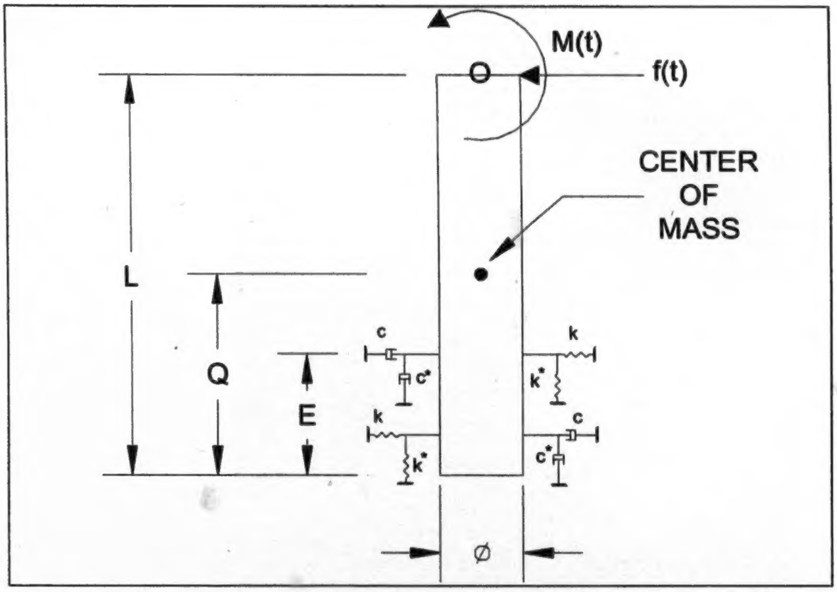
M(t)
O
f(t)
CENTER OF MASS
L
Q
E
c
c*
k
k*
k
k*
c
c*
Ø

Figure 3-18: Giannitsios et. al.(2001) Model of Vibrating Implant System

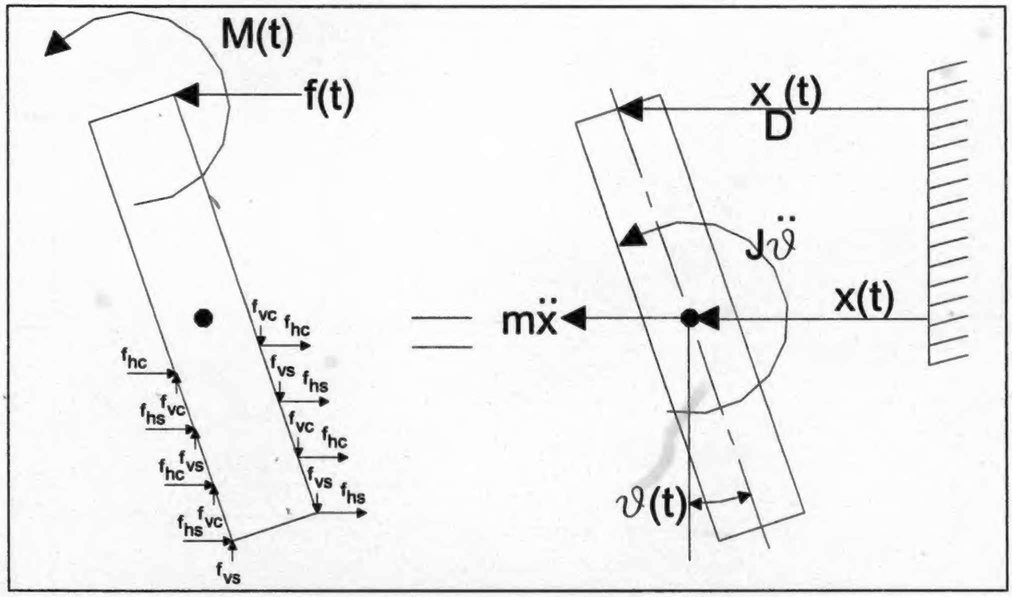
M(t)
f(t)
f_hc
f_vc
f_hs
f_vs
=
mẍ
x_D(t)
Jϑ̈
x(t)
ϑ(t)

Figure 3-19: FBD/MAD of Implant Model Proposed by Giannitsios et. al.(2001)

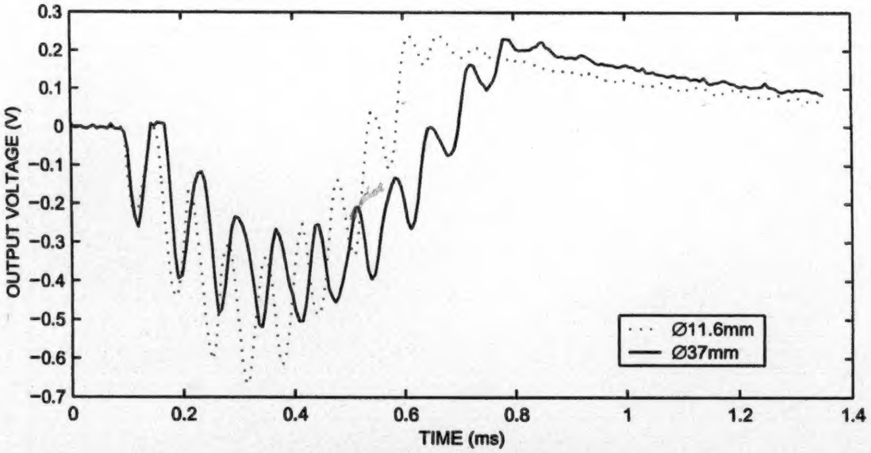

Figure 3-20: Response of Periotest® Pre-Amplified Transducer Signal to Changes in Effective FRB-10 Disc Diameter – Thin Plate Study

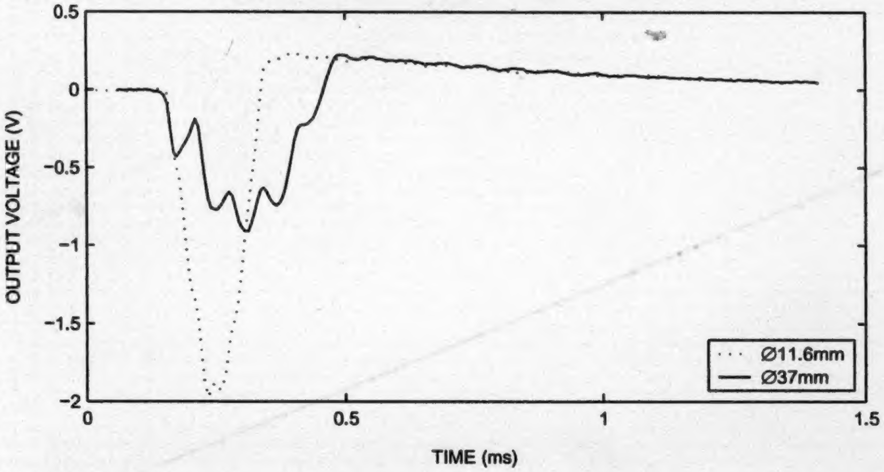

Figure 3-21: Response of Periotest® to Axial Evaluation of Implant System – Thin Plate Study

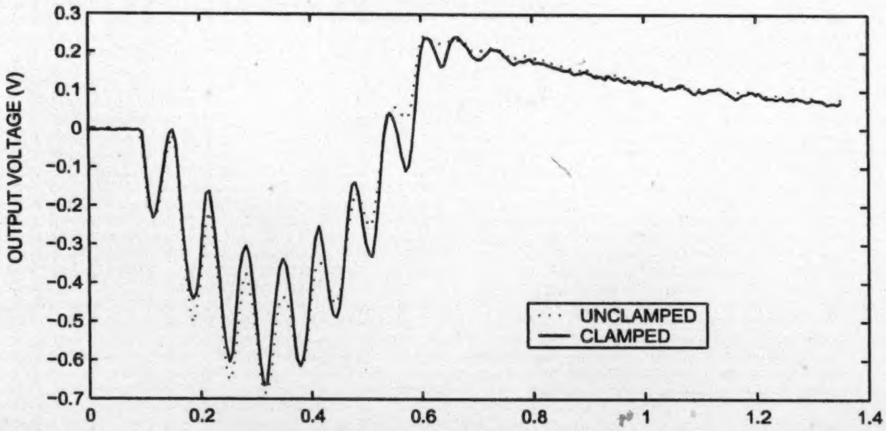

Figure 3-22: Response of Perpendicular Periotest® Evaluation of In Vitro Disc Number 6 with and without Additional Clamping – Thin Plate Study

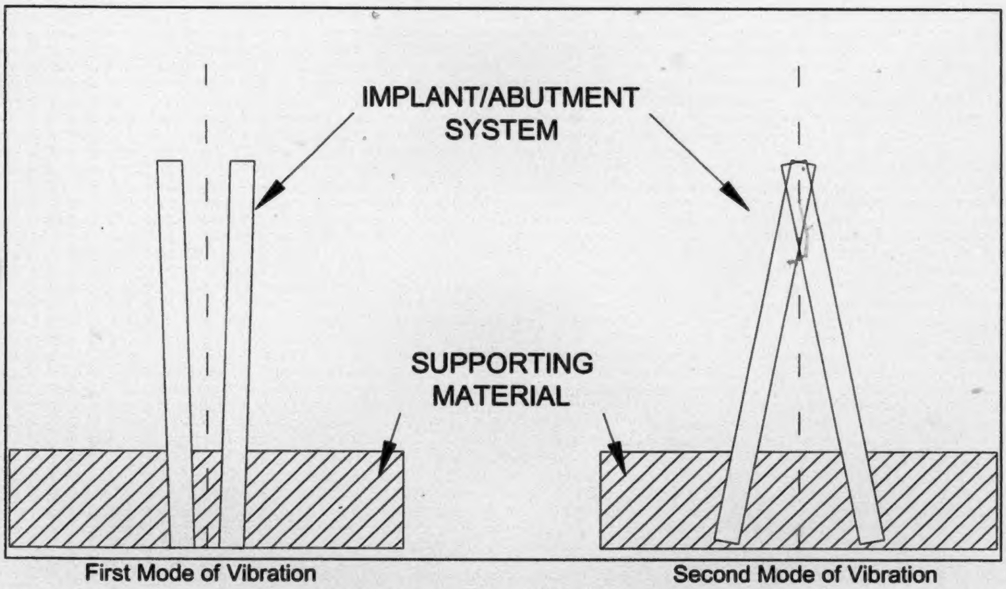
IMPLANT/ABUTMENT SYSTEM
SUPPORTING MATERIAL
First Mode of Vibration
Second Mode of Vibration

Figure 3-23: Mode Shapes for Ø3.75mm Intra-Oral Brånemark Implant Installed in FRB-10 to an Engagement Length of 5.62mm (Not drawn to scale)

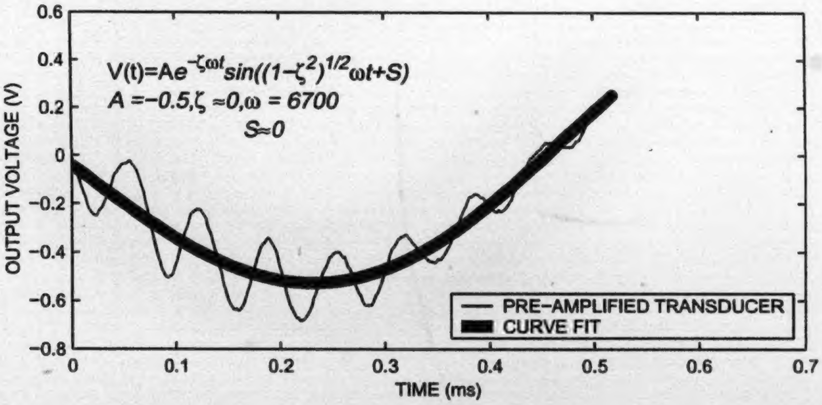

Figure 3-24: Pre-Amplified Periotest® Response for Ø3.75mm Intra-Oral Brånemark Implant, with 10mm Abutment, and Installed in FRB-10 to an Engagement Length of 5.62mm – Curve Fit Using A Damped Sine

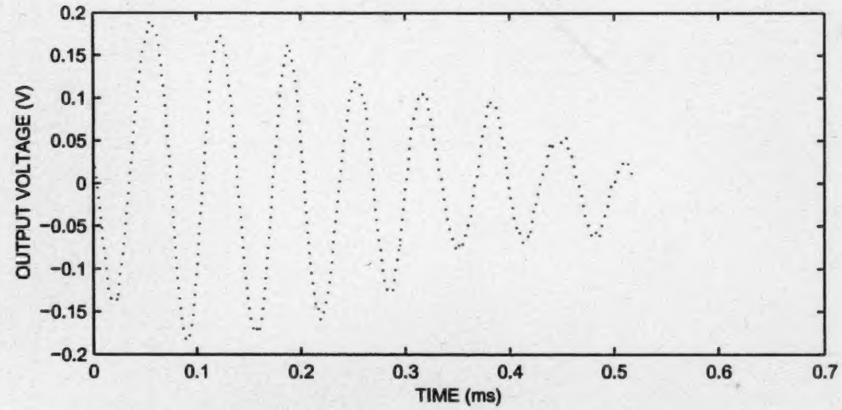

Figure 3-25: Second Frequency Component for Figure 3-24

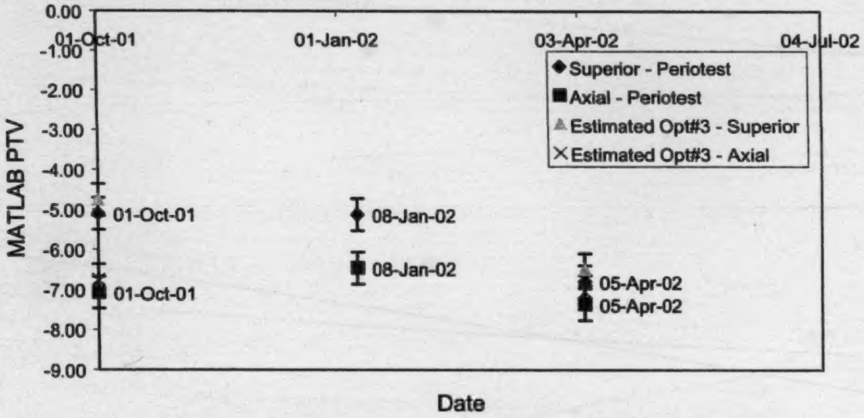

Figure 3-26: Representative Periotest® In Vivo Measurements

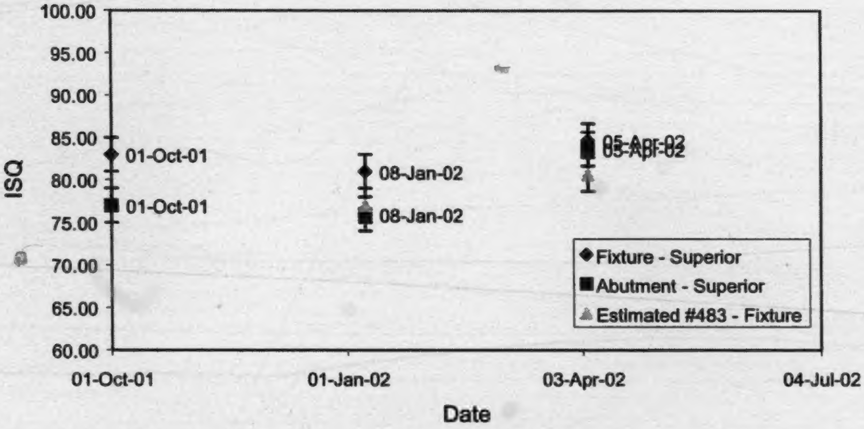

Figure 3-27: Representative Osstell® In Vivo Measurements

Chapter 4 – Conclusions and Recommendations

4.1 Conclusions

The comparison of the Periotest® and Osstell® instruments for measuring implant integrity has resulted in several conclusions, as well as an improved understanding of instrument operation.

It is possible to replicate the measurement values for both the Periotest® and Osstell® instruments using a collected transducer signal. In this comparison, the transducer signals were post-processed using MATLAB code developed specifically for each instrument. The measurement value returned by the independent post-processing agree closely with the instrument returned values. Therefore, a better understanding of the instrument operation is achieved and allows a starting point for future enhancements in the instruments.

With the aid of the independent processing of the Periotest® transducer signal, the Periotest® instrument resolution and repeatability were increased and allowed more minute changes in implant integrity to be measured. This enhancement to the Periotest® allows it to measure similar changes in implant integrity as the existing Osstell®

instrument. For example, both the enhanced Periotest® and the existing Osstell® instruments can measure engagement length changes of approximately 0.6 mm. In addition, it is predicted that both instruments can detect a change of 0.6 mm in abutment length. Therefore, the enhanced Periotest® and existing Osstell® instruments exhibit the same abilities to measure changes in implant geometric parameters. It should be noted that the resolution of the improved Periotest® is estimated to be ±0.3 PTV and the existing Osstell® has a resolution of ±1 ISQ. The repeatability of the Periotest and Osstell are estimated to be ±0.4 PTV and ±2 ISQ, respectively.

The pre-amplified transducer signal from the Periotest® instrument contains at least two distinct frequency components. These components appear to be related to two unique modes of vibration as predicted by the two-degree of freedom vibratory model for implant system suggested by Giannitsios et. al. (2001). The presence of this higher frequency mode may allow the Periotest® value calculation to be modified to increase the instrument's sensitivity to changes in implant system geometric parameters.

The in vivo results suggests the new instrument protocol, including the use of the Periotest® training block prior patient measurements, ensures the precision of the instrument measurements collected. As a result of the changes in the protocol and enhancement of the Periotest® instrument, the changes in the Periotest® values are anticipated to be a result of changes in the implant interface properties and not the measuring technique.

4.2 Recommendations

Recommendations for future research on the application of the Periotest® and Osstell® instruments for measuring implant integrity include:

Other methods of post-processing the transducer signals from both instruments should be investigated to determine if the sensitivity could be improved. This investigation may involve redefining how the PTV and ISQ are calculated. Possible redefinitions of the PTV may include basing the measurement on the second frequency component, the area under the accelerometer response, or the initial slope of the accelerometer response.

A Periotest® calibration block, capable of withstanding autoclave sterilizations should be developed to reliably monitor the precision of the Periotest® instrument. This calibration may include a hands-free function so that operator influence on the Periotest® measurement is minimized.

The influence of nonhomogenieties in implant interface properties should be investigated to determine the importance of controlling the azimuthal direction of either the Periotest® or Osstell® instruments. In addition, this investigation could include optimization of the position of the Periotest® handpiece during a measurement to ensure the best sensitivity to changes in implant integrity. More than one Periotest® handpiece direction may be required to provide adequate information for a clinician to determine if an implant is about to fail.

Investigation of how the instrument measurements relate to the mechanical properties of the implant interface and surrounding supporting material may provide a more accurate relation to the stiffness of the interface. This relation may lead to a more sensitive instrument scale, composed of stiffness units. To accomplish this task, modifications of existing mathematical models may be possible to predict the motion of the implant system resulting from both Periotest® and Osstell® instrument measurements.

To gain an appreciation of the damping in the in vivo implant system, an pilot study should be initiated in which the response from a strain-gauged abutment is recorded during and after completion of a Periotest® rod strike. The response of the strain gauges after the Periotest® rod separated from the abutment would give a good indication of the damping present. The correlation between the damping shown in the strain gauge response and the Periotest® pre-amplified signal may be possible.

List of References

Aparicio C. (1997). The use of the periotest value as the initial success criteria of an implant: 8-year report. International Journal of Periodontal Restorative Dentistry, 17, 151-161.

Aparicio C., & Orozco P. (1998). Use of 5-mm-diameter implants: periotest values related to a clinical and radiographic evaluation. Clinical Oral Implant Research, 9, 398-406.

Carr A.B., Papazoglou E., & Larsen P.E. (1995). The relationship of periotest values, biomaterial, and torque to failure in adult baboons. International Journal of Prosthodontics, 8, 15-20.

Chavez H., Ortman L.F., DeFranco R.L., & Medige J. (1993). Assessment of oral implant mobility. Journal Prosthetic Dentistry, 70, 412-426.

Cranin A.N., DeGrado J., Kaufman M., Baraoidan M., DiGregorio R., Batgitis G., & Lee Z. (1998). Evaluation of the periotest as a diagnostic tool for dental implants. Journal of Oral Implantology, 24(3), 139-146.

Derhami K., Wolfaardt J.F., Faulkner G., & Grace M. (1995). Assessment of the periotest device in baseline mobility measurements of craniofacial implants. International Journal of Oral and Maxillofacial Implants, 10, 221-229.

Drago C.J. (2000). A prospective study to assess osseointegration of dental indosseous implants with the periotest instrument. International Journal of Oral and Maxillofacial Implants, 15, 389-395.

Elias J.J., Brunski J.B., & Scarton H.A. (1996). A dynamic modal testing technique for noninvasive assessment of bone-dental implant interfaces. International Journal of Oral and Maxillofacial Implants, 11, 728-734.

Faulkner M.G., Mioduchowski A., & Hong D.P. (1975) Determining the Torsional Rigidity of Square Bars with Jump Nonhomogeneities. Department of Mechanical Engineering, University of Alberta.

Faulkner M.G., Giannitsios D., Lipsett A.W., & Wolfaardt J.J. (2001). The use and abuse of the periotest for 2-piece implant/abutment systems. International Journal of Oral and Maxillofacial Implants, 16, 486-494.

Faulkner M.G., Wolfaardt J.F., & Chan A. (1999). Measuring abutment/implant joint integrity with the periotest instrument. International Journal of Oral and Maxillofacial Implants, 14, 681-688.

Haas R., Bernhart T., Dörtbudak O., & Mailath G. (1999). Experiment study of the damping behaviour of IMZ implants. Journal of Oral Rehabilitation, 26, 19-24.

Haas R., Saba M., Mensdorff-Pouilly N., & Mailath G. (1995). Examination of the damping behaviour of IMZ implants. International Journal of Oral and Maxillofacial Implants, 10, 410-414.

Huang H., Pan L., Lee. S., Chiu C., Fan K., & Ho K. (2000). Assessing the implant/bone interface by using natural frequency analysis. Oral Surgery Oral Medicine Oral Pathology, 90, 285-291.

Ichikawa T., Miyamoto M., Horisaka Y., & Matsumoto N. (1994). Clinical evaluation of periotest for two-piece apatite implants. International Journal of Oral and Maxillofacial Implants, 9, 461-467.

Isidor F. (1998). Mobility assessment with the periotest system in relation to histologic findings of oral implants. International Journal of Oral and Maxillofacial Implants, 13, 377-383.

Kaneko T.M. (1993). Dynamics of the periotest method of diagnosing the dental implant-bone interface. Journal of Materials Science: Materials in Medicine, 4, 256-259.

Kaneko T.M. (1994). Relationship between the stiffness of the dental implant-bone system and the duration of the implant-tapping rod contact. Medical Engineering Physics, 16, 310-315.

Kaneko T. (1998). Theoretical percussion force of the periotest diagnosis. International Journal of Oral and Maxillofacial Implants, 13, 97-101.

Lukas D., Schulte W., König M., & Reim M. (1992). High-speed filming of the periotest measurement. Journal of Clinical Periodontal, 19, 388-391.

Lukas D., & Schulte W. (1990). Periotest – a dynamic procedure for the diagnosis of the human periodontium. Clinical Physical Physiological Measurements, 11, 65-75.

Meredith N., Friberg B., Sennerby L., & Aparicio C. (1998). Relationship between contact time measurments and PTV values when using the periotest to measure implant stability. International Journal of Prosthodontics, 11, 269-275.

Meredith N. (1999) Resonant frequency – what does it measure?. Talk of the Times, 4, 25-31.

Meredith N., Book K., Friberg B., Jemt T., & Sennerby L. (1997). Resonance frequency measurements of implant stability in vivo. Clinical Oral Implants Research, 8, 226-233.

Meredith N., Shagaldi F., Alleyne D., Sennerby L., & Cawley P. (1997). The application of resonance frequency measurements to study the stability of tianium implants during healing in the rabbit tibia. Clinical Oral Implants Research, 8, 234-243.

Meredith N., Alleyne D., & Cawley P. (1996). Quantitative determination of the stability of the implant-tissue interface using resonance frequency analysis. Clinical Oral Implants Research, 7, 261-267.

Ochi S., Morris H.F., & Winkler S. (1994). The influence of implant type, material, coating, diameter, and length of periotest balues at second-stage surgery: DICRG interim report no.4. Implant Dentistry, 3, 159-162.

Olivè J., & Aparicio C. (1990). The periotest method as a measure of osseointegrated oral implant stability. International Journal of Oral and Maxillofacial Implants, 5, 390-400.

Ramp L.C., & Jeffcoat R.L. (2001). Dynamic behaviour of implants as a measure of osseointegration. International Journal of Oral and Maxillofacial Implants, 16, 637-645.

Ramp L.C., Reddy M.S., & Jeffcoat R.L. (2000). Assessment of osseointegration by nonlinear dynamic response. International Journal of Oral and Maxillofacial Implants, 15, 197-208.

Rasmusson L., Stegersjö G., Kahnberg K., & Sennerby L. (1999). Implant stability measurment using resonance frequency analysis in the grafted maxilla: a cross-sectional pilot study. Clinical Implant Dentistry Research, 1, 70-74.

Røynesdal A.K., Ambjørnsen E., Støvne S., & Haanæs H.R. (1998). A comparative clinical study of three different endosseous implants in edentulous mandibles. International Journal of Oral and Maxillofacial Implants, 13, 500-505.

Salonen M.A.M., Oikarinen K., Virtanen K., & Pernu H. (1993). Failures in the osseointegration of endosseous implants. International Journal of Oral and Maxillofacial Implants, 8, 92-97.

Salonen M.A.M., Raustia A.M., Kainulainen V., & Oikarinen K.S. (1997). Factors related to periotest values in endosseal implants: a 9-year follow-up. Journal of Clinical Periodontol, 24, 272-277.

Schulte W., & Lukas D. (1992). The periotest method. International Dental Journal, 42, 433-440.

Truhlar R.S., Morris H.F., Ochi S., & Winkler S. (1994). Assessment of ipmlant mobility at second-stage surgery with the periotest: DICRG interim report no.3. Implant Dentistry, 3, 153-156.

Verhoeven J.W., Cune M.S., & de Putter C. (2000). Reliability of some clinical parameters of evaluation in implant dentistry. Journal of Oral Rehabilitation, 27, 211-216.

Walker L., Morris H.F., & Ochi S. (1997). Periotest values of dental implants in the first 2 years after second-stage surgery: DICRG interim report no.8. Implant Dentistry, 6, 207-212.

Wolfaardt J., Tjellström A., Parel S.M., & Wilkes G.H. International perspective of treatment outcomes.

Appendix A – MATLAB Code for Periotest®

This appendix contains MATLAB code that calculates the Periotest® Value from the post-amplified transducer signal.

%patientperioanalysis.m

```
samplerate=166666;
sampleduration=4;
j=1;
z=1;
startingpointfound=0;
displayed=0;
while j<samplerate*sampleduration
%starting point criteria
if (((volt(j+1)-volt(j))<=...
       (-1e-2))&(volt(j)<(1e-2)))&(startingpointfound==0)
    if startingpointfound==0
        jstart(z)=j;%save a potential starting point
        startingpointfound=1;
    end
%ending point criteria
elseif ((startingpointfound==1)&(volt(j)>volt(jstart(z))))
    goodstartingpt=0;
    for w=jstart(z):j
        if volt(w)<-0.5
            goodstartingpt=1;
        end
    end
    if goodstartingpt==1
        jend(z)=(j-1)+((volt(jstart(z))-volt(j-1))/...
             (volt(j-1)-volt(j)))*((j-1)-j);
        startingpointfound=0;
        ctt(z)=(jend(z)-jstart(z))/samplerate;
        fprintf('\n%3i  The contact time = %10.10f seconds',z,ctt(z));
        j=j+35000;%skip these data points
        z=z+1;
    elseif goodstartingpt==0
        startingpointfound=0;
    end
%every bad starting point criteria
elseif (((volt(j+1)-volt(j))>(-1e-2))&...
       (volt(j)>(1e-1)))&(startingpointfound==1)
    startingpointfound=0;
elseif ((volt(j+1)-
volt(j)>0)&(startingpointfound==1))&(j<=(jstart(z)+5))
    startingpointfound=0;
end%if
j=j+1;
end %while
%calculate PTV only valid for -8<=ptv<=13
sum=0;
sumptv=0;
for zzz=1:length(ctt)
   sum=sum+ctt(zzz);
   ptv(zzz)=50*ctt(zzz)*1000-21.3;
   sumptv=sumptv+ptv(zzz);
end
cttavg=sum/length(ctt);
ptvavg=sumptv/length(ctt);
num=0;
```

```
for zzz=1:length(ctt)
   num=num+(ptv(zzz)-ptvavg).^2;
end
ptvstd=sqrt(num/(length(ctt)-1));

%check to insure good data points - ie. make sure all of the data points
are within 1 std dev.
%to this comparison once only.
clear goodpt;
countt=1;
for fooo=1:length(ptv)
    if abs(ptv(fooo)-ptvavg)<1*ptvstd %within 1 std deviation
        goodpt(countt)=fooo;
        countt=countt+1;
    end
end
%revise the ctt vector with good data points only.
cntt=1;
clear newctt;
for fooo=1:length(goodpt)
    newctt(cntt)=ctt(goodpt(fooo));
    cntt=cntt+1;
end
clear ctt;
ctt=newctt;
sum=0;
sumptv=0;
clear ptv cttavg ptvavg ptvstd;
for zzz=1:length(ctt)
   sum=sum+ctt(zzz);
   ptv(zzz)=50*ctt(zzz)*1000-21.3;
   sumptv=sumptv+ptv(zzz);
end
cttavg=sum/length(ctt);
ptvavg=sumptv/length(ctt);
num=0;
for zzz=1:length(ctt)
   num=num+(ptv(zzz)-ptvavg).^2;
end
ptvstd=sqrt(num/(length(ctt)-1));
fprintf('\n\nThe average contact time is %10.10f seconds',cttavg);
fprintf('\n\nThe PTV is %10.2f +-%10.2f\n\n',ptvavg,ptvstd);
fprintf('\n Based on points.');
for fo=1:length(goodpt)
    fprintf('%3i',goodpt(fo));
end
fprintf('\n\n');
fid = fopen('d:\patient_data\periodataall_MAR802.txt','a+');
fseek(fid,0,'eof');
fprintf(fid,'%s\n',filename);
fprintf(fid,'These PTV values based on data within 1 std dev!!!\n');
for fo=1:(length(goodpt))
    fprintf(fid,'%4.2f\n',round(ptv(fo)*100)/100);
end
fclose(fid);
fid =
fopen('d:\patient_data\patient10\mar82002_3monthvisit\periodata_MAR802.t
xt','a+');
fseek(fid,0,'eof');
fprintf(fid,'%s %4.2f %3.2f %3i\n',.

filename,round(ptvavg*100)/100,round(ptvstd*100)/100,length(goodpt));
fclose(fid);
```

Appendix B – MATLAB Code for Osstell®

This appendix contains MATLAB code to determine the resonant frequency of the implant system from the response signal of the Osstell® transducer lead.

```
%MATLAB CODE TO ANALYZE OSSTELL TRANSDUCER SIGNAL
clear;
samplerate=166666;
sampleduration=1.5;
filename=input('Please input filename(complete path): ','s');
finput = fopen(filename,'rt');
for n=1:27
    fgetl(finput); %throw away lines
end
clear volt;
volt(1:round(samplerate*sampleduration)) = fscanf(finput, '%f ',
round(samplerate*sampleduration));
fclose(finput);
volt=-volt;
[startpos, startavgvolt]=findrfastartpos(volt);
[endpos, endavgvolt]=findrfaendpos(volt,startpos);
clear data;
data(:,2)=volt(startpos:endpos)';
data(:,1)=(0:1/166666:(endpos-startpos)/166666)';
jstart=1;
endcyclepos=startpos;
numm=1;
maxsavedamplitude=0;
zzz=1;
while jstart<(length(data(:,1))-50)
    clear analdata;
    startcycletime=findstartcycle(data,jstart,startavgvolt);
    [endcycletime, endcyclepos]=findendcycle(data,jstart,startavgvolt);
    if endcyclepos==length(data(:,1))
        fprintf('\nbreaking from routine because
endcycle==length(data(:,1))');
        break
    end
    analdata(1,1)=startcycletime;
    analdata(1,2)=startavgvolt;
    analdata(endcyclepos-jstart+1,1)=endcycletime;
    analdata(endcyclepos-jstart+1,2)=startavgvolt;
    analdata(2:(endcyclepos-jstart),1)=...
      data((jstart+1):(endcyclepos-1),1);
    analdata(2:(endcyclepos-jstart),2)=...
      data((jstart+1):(endcyclepos-1),2);
    freq(numm)=1/(endcycletime-startcycletime);
    maxamplitude(numm)=(max(analdata(:,2))-min(analdata(:,2)))/2;
    fprintf('jstart = %10i, numm = %5i, freq = %5.5f, maxamplitude =
      %5.5f, zzz=%5i\n',jstart,numm,freq(numm),maxamplitude(numm),zzz);
    startavgvolt=sum(analdata(:,2))/length(analdata(:,2));
    jstart=endcyclepos-1;
    if maxamplitude(numm)>maxsavedamplitude
        maxsavedamplitude=maxamplitude(numm);
        savenum=numm;
        zzz=1;
    else
        zzz=zzz+1;%increment counter so that loop can be stopped after a
max of 100 pts beyond max.
    end
    numm=numm+1;
end
fprintf('\n\nThe resonant frequency is calculated to be %4i Hz with
amplitude of %5.5f.',round(freq(savenum)),maxamplitude(savenum));
fid = fopen('d:\patient_data\rfaavg_mar802.txt','a+');
fseek(fid,0,'eof');
fprintf(fid,'%s %4i
%5.5f\n',filename,round(freq(savenum)),maxamplitude(savenum));
fclose(fid);
```

```
%findstartcycle.m
%this code will find one cycle in the signal
function startcycletime=findstartcycle(data,jstart,startavgvolt)
j=jstart;
m=(data(j+1,2)-data(j,2))/(data(j+1,1)-data(j,1));
if m==0
    startcycletime=(data(j+1,1)+data(j,1))/2;%average of the two times.
else
    b=data(j+1,2)-m*data(j+1,1);
    startcycletime=(startavgvolt-b)/m;
end
```

```
%findrfastartpos.m
%this code will find the start of the RFA frequency ramp.
function [startpos, startavgvolt]=findrfastartpos(volt);
%volt = the voltage data
j=10;
k=1;
avgvolt=volt(j);
while volt(j)<(avgvolt+0.012)
    j=j+1;
    if k>10
        k=1;
        avgvolt=volt(j);
    else
       newavgvolt=(avgvolt*k+volt(j))/(k+1);
        k=k+1;
        avgvolt=newavgvolt;
    end
end
startavgvolt=avgvolt;
startpos=j-1;
newvolt=volt(startpos:length(volt));
```

```
%findrfaendpos.m
%this code will find the end of the RFA frequency response.
function [endpos, endavgvolt]=findrfaendpos(volt,startpos);
j=1000;
k=1;
avgvolt=volt(j);
while volt(j)<(avgvolt+0.03)
    j=j-1;
    if k>4
        k=1;
        avgvolt=volt(j);
    else
       newavgvolt=(avgvolt*k+volt(j))/(k+1);
        k=k+1;
        avgvolt=newavgvolt;
    end
end
endavgvolt=avgvolt;
endpos=j+2;
newvolt=volt(startpos:endpos);
```

```
%findendcycle.m
%this code will find one cycle in the signal
function
[endcycletime,endcyclepos]=findendcycle(data,jstart,startavgvolt)
volt=data(:,2);
j=jstart;
while (volt(j+1)-volt(j))==0
    j=j+1;
end
jstart=j;
if (volt(j+1)-volt(j))>0
    slopeup=1;%initial slope is positive
    slopedown=0;
    negslope=0;%cycle must pass through negative slope
elseif (volt(j+1)-volt(j))<0
    slopedown=1;%initial slope is negative
    slopeup=0;
    posslope=0;%cycle must pass through positive slope
end
foundpt=0;
if slopeup==1
    j=jstart+2;
    while (foundpt==0)&(j<length(volt))
        if ((volt(j+1)-volt(j))<0)&(volt(j+1)<startavgvolt)
            negslope=1;
        end
        if (volt(j+1)>startavgvolt)&...
            ((volt(j+1)-volt(j))>0)&(negslope==1)
            foundpt=1;
        end
        j=j+1;
    end
elseif slopedown==1
    j=jstart+2;
    while (foundpt==0)&(j<length(volt))
        if ((volt(j+1)-volt(j))>0)&(volt(j+1)>startavgvolt)
            posslope=1;
        end
        if (volt(j+1)<startavgvolt)&...
            ((volt(j+1)-volt(j))<0)&(posslope==1)
            foundpt=1;
        end
        j=j+1;
    end
end
if j<length(volt)
    endcyclepos=j;
    j=j-1;
    m=(data(j+1,2)-data(j,2))/(data(j+1,1)-data(j,1));
    b=data(j+1,2)-m*data(j+1,1);
    endcycletime=(startavgvolt-b)/m;
else
    endcycletime=data(length(data(:,1)),1);
    endcyclepos=length(data(:,1));
end
```

Appendix C – Pre-Amplified Periotest® Transducer

This appendix contains the strain gauge and pre-amplified Periotest® transducer signal for all of the in vitro implant systems evaluated (Abut. = 10mm).

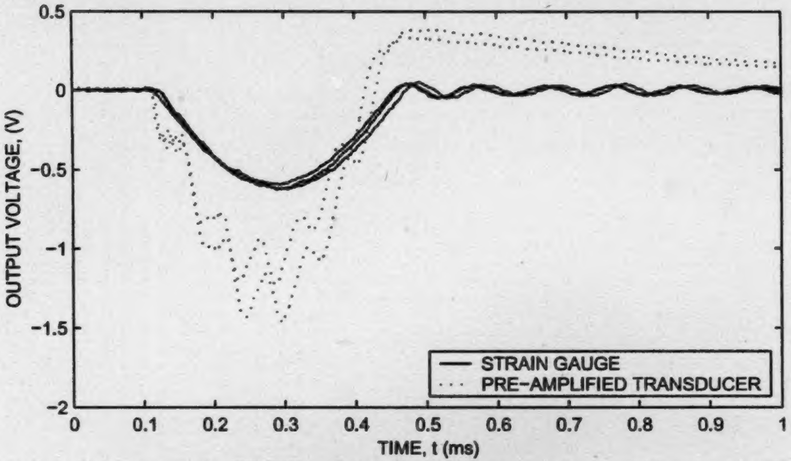

Figure C-1: Response of a Ø3.75mm Intra-Oral Brånemark Implant Mounted in FRB-10 to an Engagement Length of 8.85mm

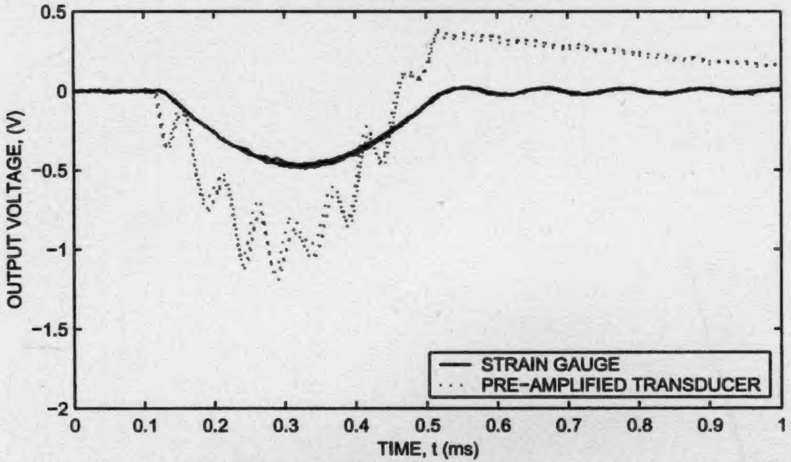

Figure C-2: Response of a Ø4mm Intra-Oral Brånemark Implant Mounted in FRB-10 to an Engagement Length of 8.72mm

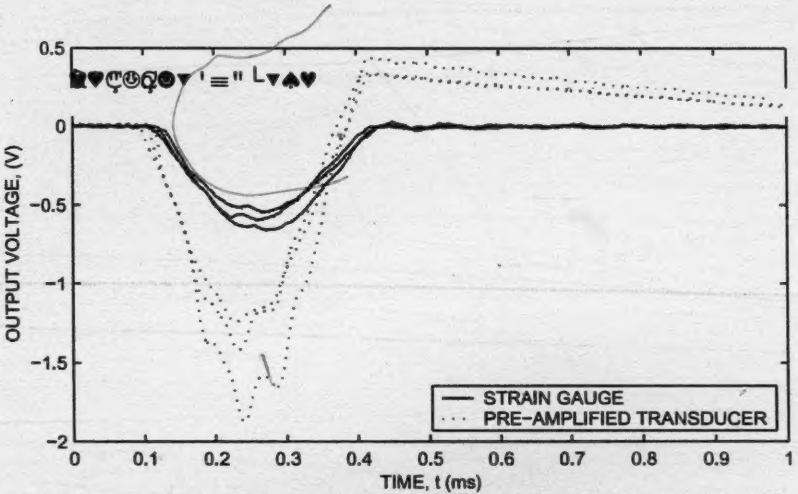

Figure C-3: Response of a Ø5mm Intra-Oral Brånemark Implant Mounted in FRB-10 to an Engagement Length of 9.58mm

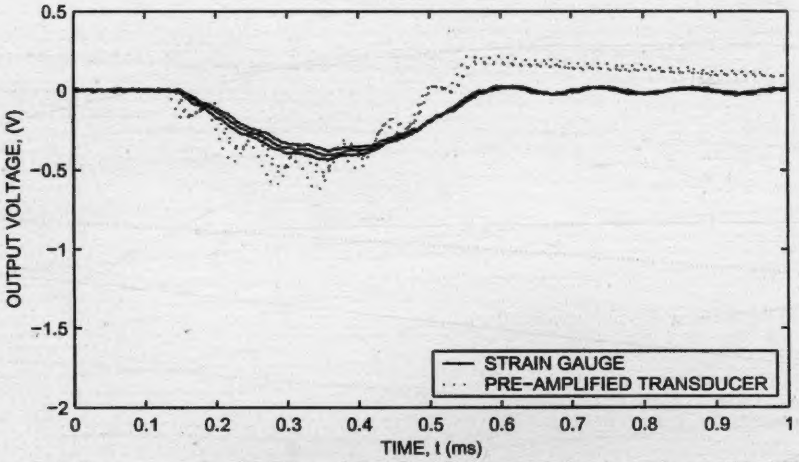

Figure C-4: Response of a Ø3.75mm Intra-Oral Brånemark Implant Mounted in FRB-10 to an Engagement Length of 7.70mm

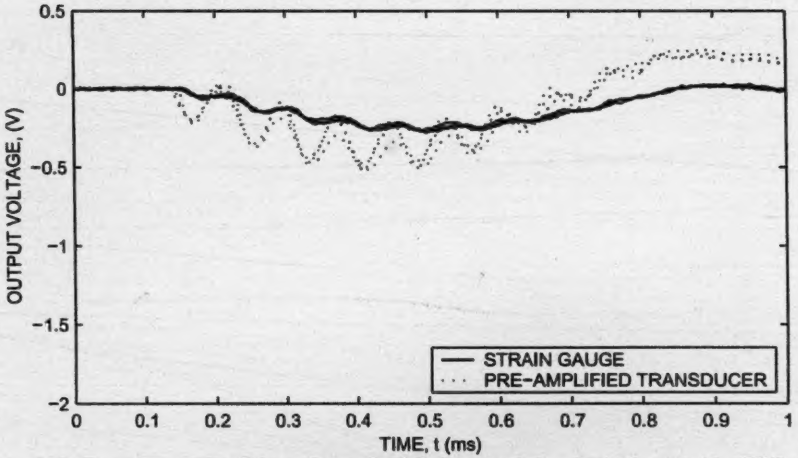

Figure C-5: Response of a Ø4mm Intra-Oral Brånemark Implant Mounted in FRB-10 to an Engagement Length of 1.68mm

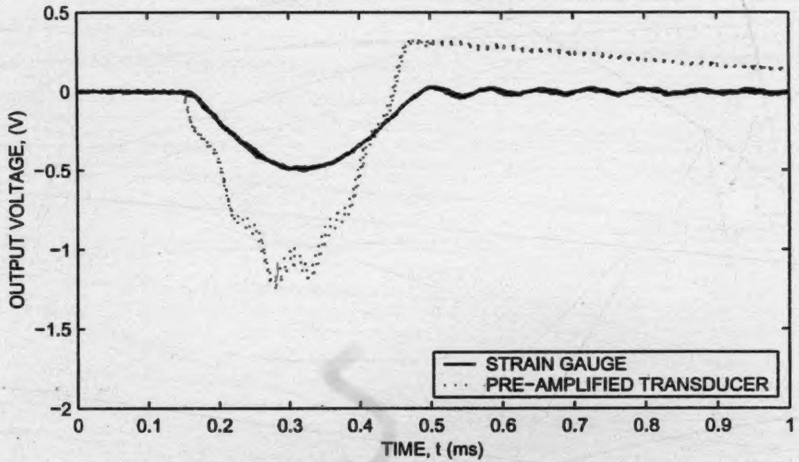

Figure C-6: Response of a Ø5mm Intra-Oral Brånemark Implant Mounted in FRB-10 to an Engagement Length of 8.41mm

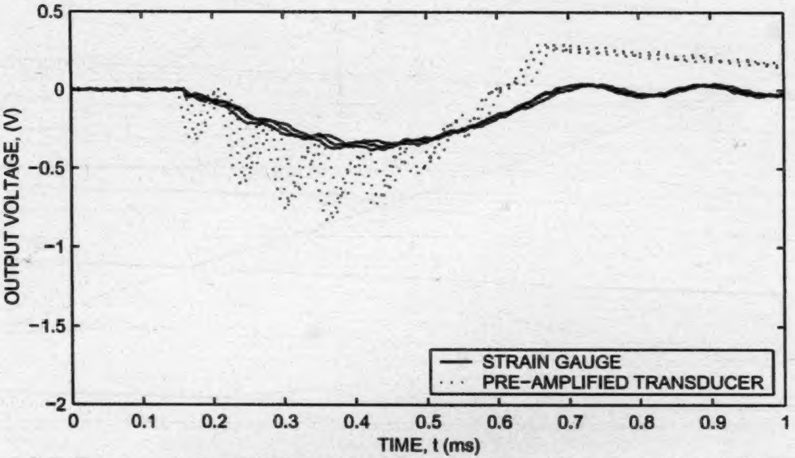

Figure C-7: Response of a Ø3.75mm Intra-Oral Brånemark Implant Mounted in FRB-10 to an Engagement Length of 5.62mm

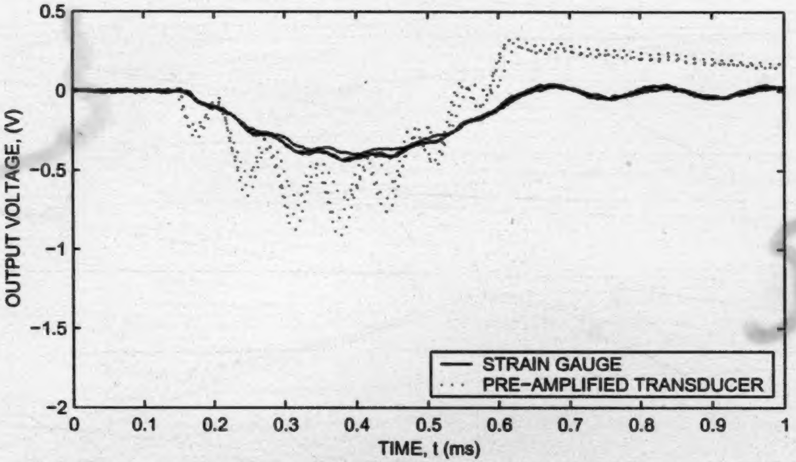

Figure C-8: Response of a Ø4mm Intra-Oral Brånemark Implant Mounted in FRB-10 to an Engagement Length of 5.72mm

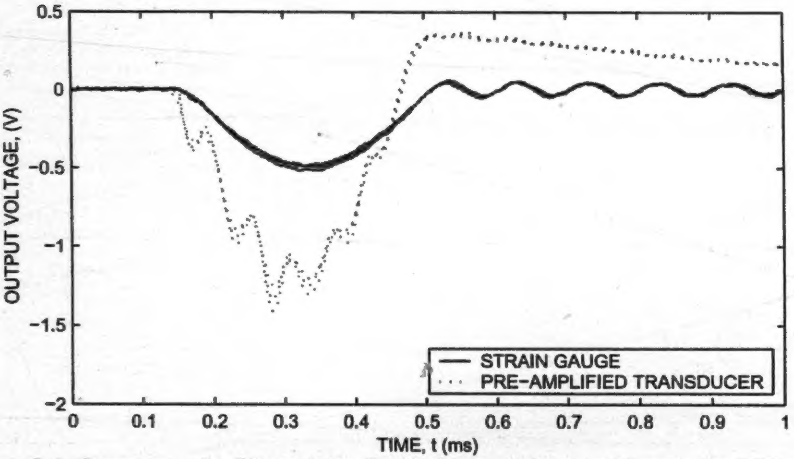

Figure C-9: Response of a Ø5mm Intra-Oral Brånemark Implant Mounted in FRB-10 to an Engagement Length of 6.68mm

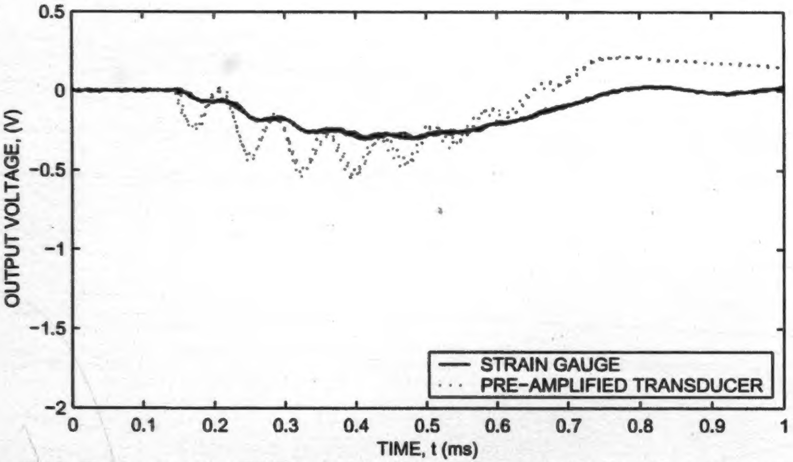

Figure C-10: Response of a Ø3.75mm Intra-Oral Brånemark Implant Mounted in FRB-20 to an Engagement Length of 5.62mm

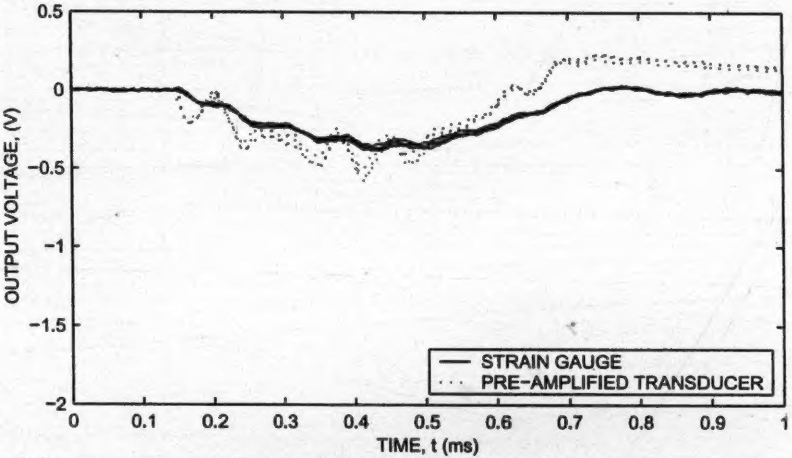

Figure C-11: Response of a Ø3.75mm Extra-Oral Brånemark Implant Mounted in FRB-10 to an Engagement Length of 1.87mm

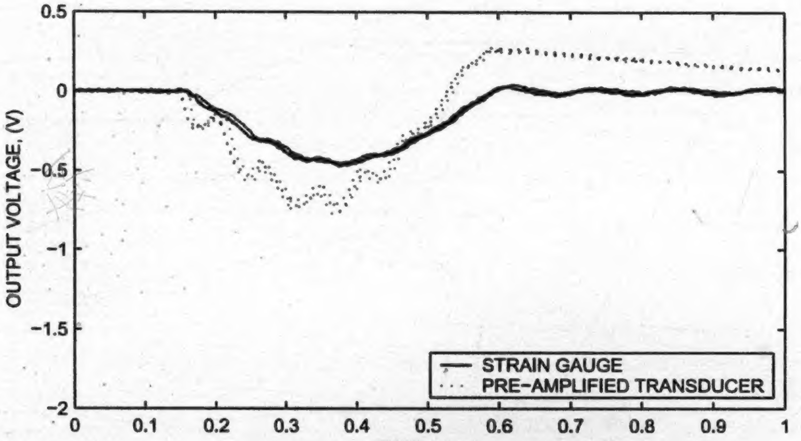

Figure C-12: Response of a Ø3.75mm Extra-Oral Brånemark Implant Mounted in FRB-10 to an Engagement Length of 2.78mm

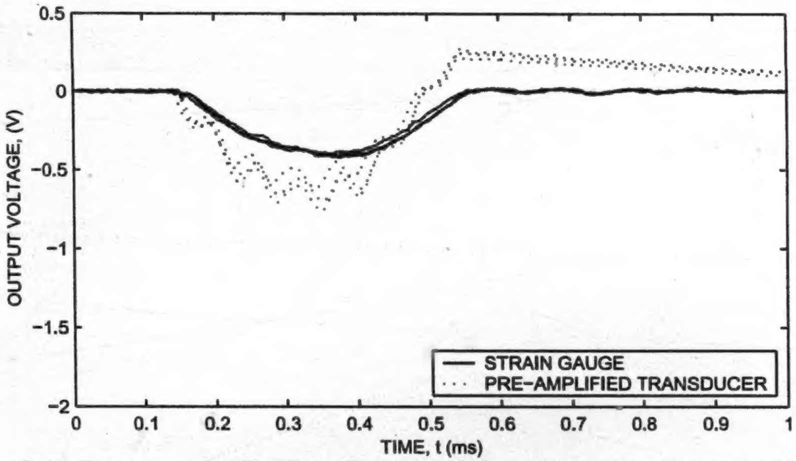

Figure C-13: Response of a Ø3.75mm Extra-Oral Brånemark Implant Mounted in FRB-10 to an Engagement Length of 3.83mm

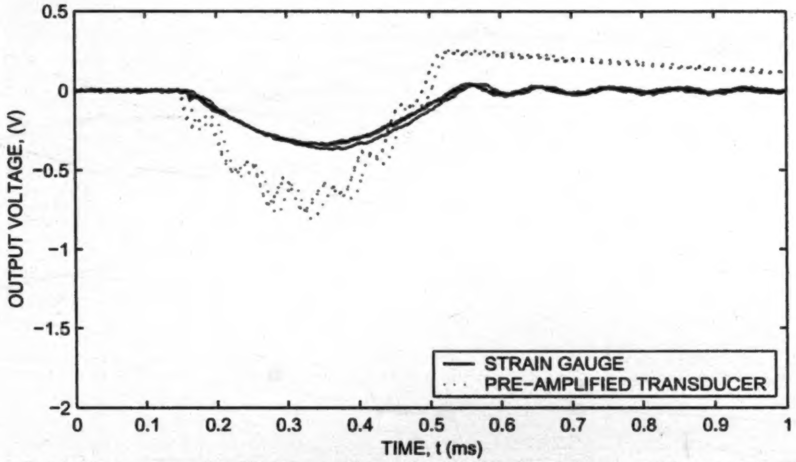

Figure C-14: Response of a Ø3.75mm Extra-Oral Brånemark Implant Mounted in FRB-10 to an Engagement Length of 4.78mm

Appendix D – Strain Gauge Response to Periotest®

The response of the strain-gauged abutment to a Periotest® strike and the post-amplified transducer signal are shown for all in vitro discs evaluated.

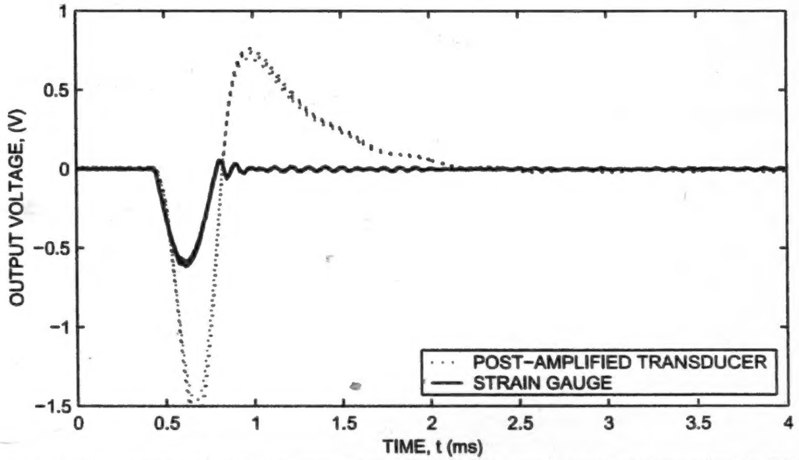

Figure D-1: Response of a Ø3.75mm Intra-Oral Brånemark Implant Mounted in FRB-10 to an Engagement Length of 8.85mm

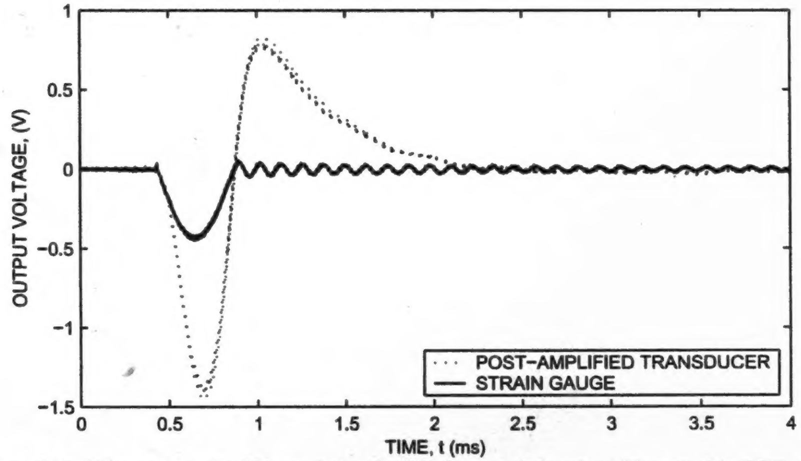

Figure D-2: Response of a Ø4mm Intra-Oral Brånemark Implant Mounted in FRB-10 to an Engagement Length of 8.72mm

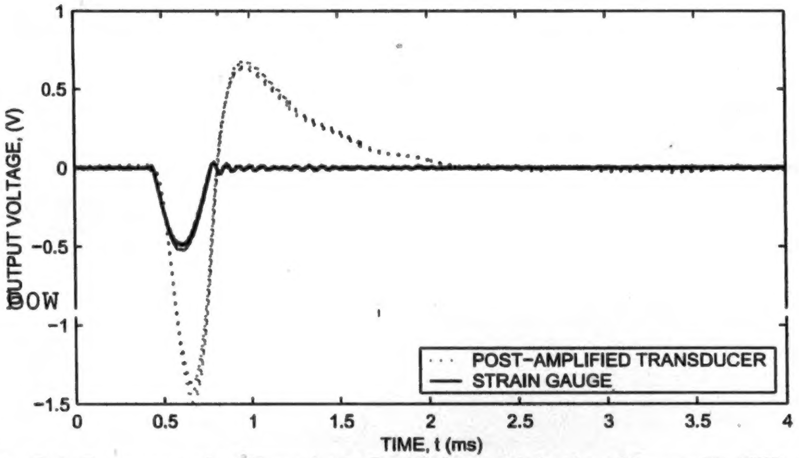

Figure D-3: Response of a Ø5mm Intra-Oral Brånemark Implant Mounted in FRB-10 to an Engagement Length of 9.58mm

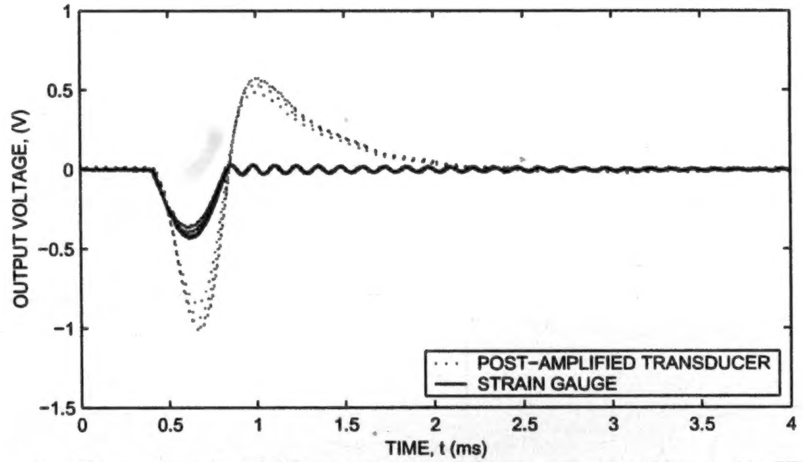

Figure D-4: Response of a Ø3.75mm Intra-Oral Brånemark Implant Mounted in FRB-10 to an Engagement Length of 7.70mm

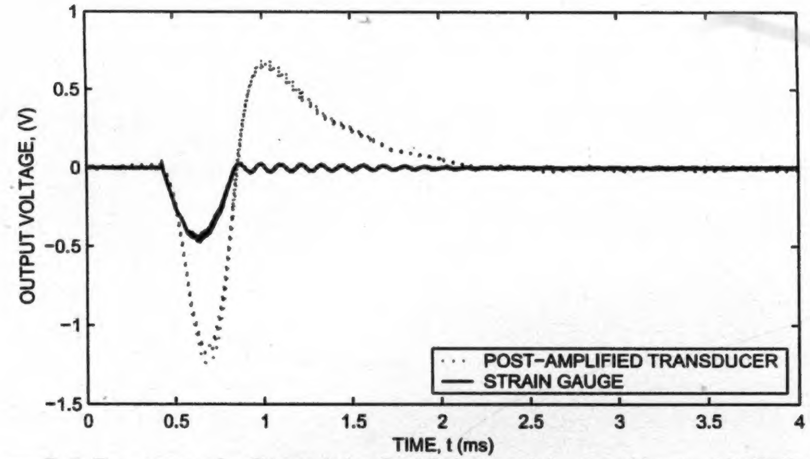

Figure D-5: Response of a Ø4mm Intra-Oral Brånemark Implant Mounted in FRB-10 to an Engagement Length of 1.68mm

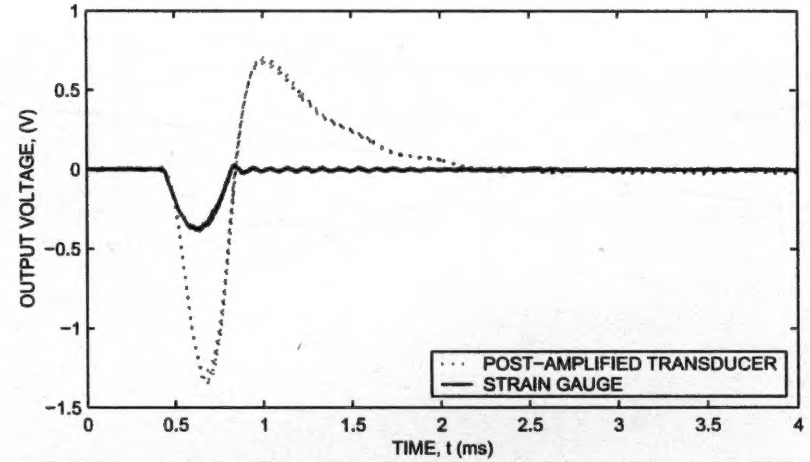

Figure D-6: Response of a Ø5mm Intra-Oral Brånemark Implant Mounted in FRB-10 to an Engagement Length of 8.41mm

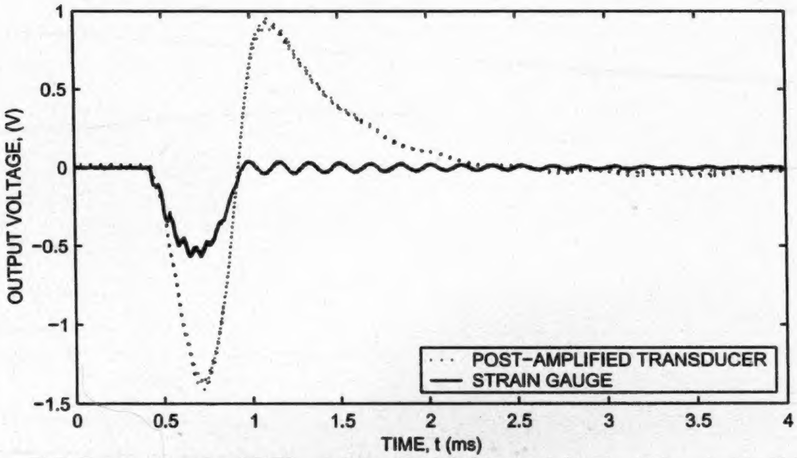

Figure D-7: Response of a Ø3.75mm Intra-Oral Brånemark Implant Mounted in FRB-10 to an Engagement Length of 5.62mm

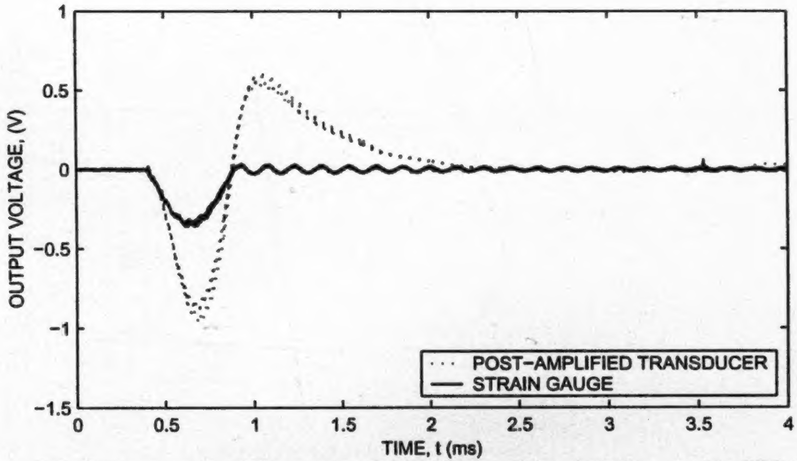

Figure D-8: Response of a Ø4mm Intra-Oral Brånemark Implant Mounted in FRB-10 to an Engagement Length of 5.72mm

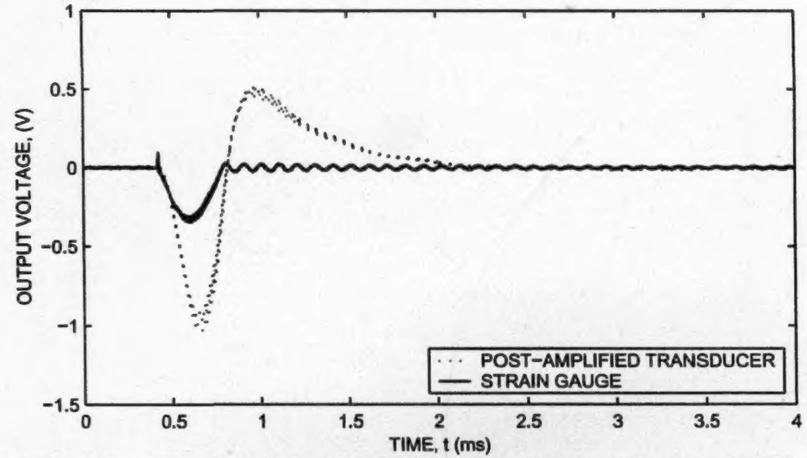

Figure D-9: Response of a Ø5mm Intra-Oral Brånemark Implant Mounted in FRB-10 to an Engagement Length of 6.68mm

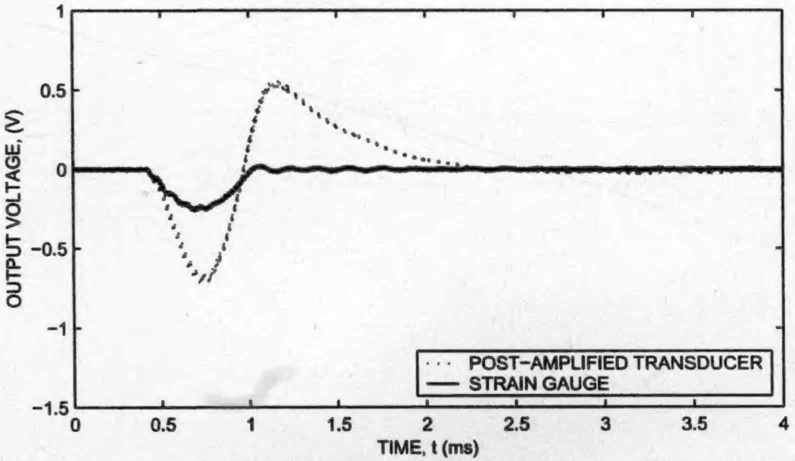

Figure D-10: Response of a Ø3.75mm Extra-Oral Brånemark Implant Mounted in FRB-10 to an Engagement Length of 1.87mm

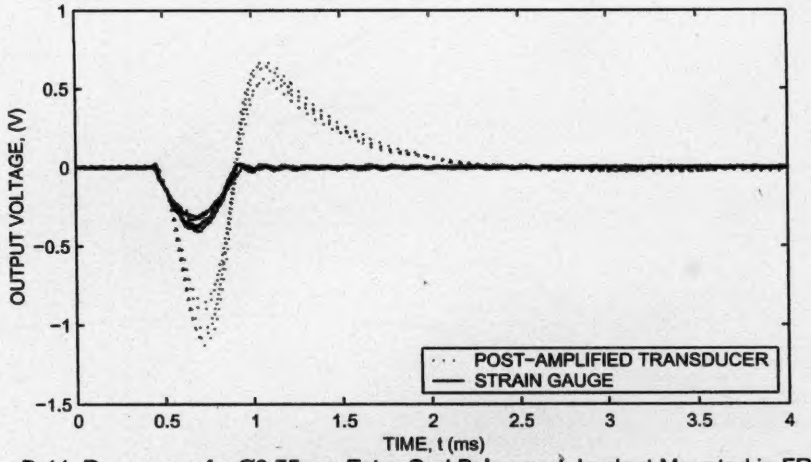

Figure D-11: Response of a Ø3.75mm Extra-Oral Brånemark Implant Mounted in FRB-10 to an Engagement Length of 2.78mm

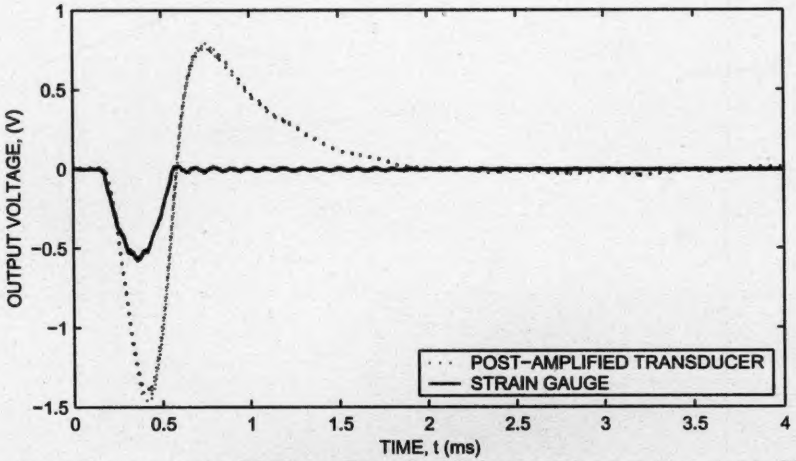

Figure D-12: Response of a Ø3.75mm Extra-Oral Brånemark Implant Mounted in FRB-10 to an Engagement Length of 3.83mm

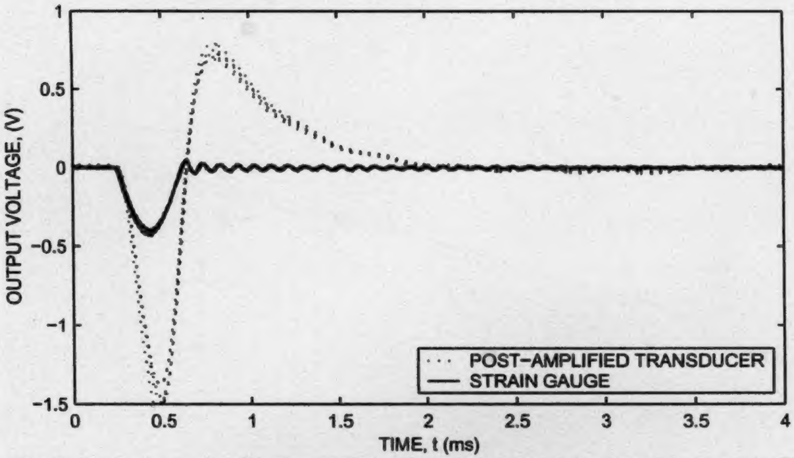

Figure D-13: Response of a Ø3.75mm Extra-Oral Brånemark Implant Mounted in FRB-10 to an Engagement Length of 4.78mm

Appendix E – Strain Gauge Response to Osstell®

This appendix contains the response of the strain-gauged abutment during an Osstell® measurement for all in vitro implant systems evaluated.

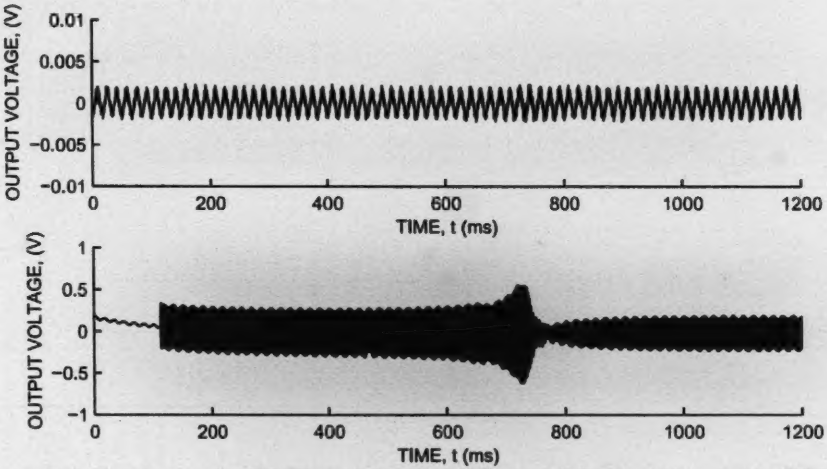

Figure E-1: Response of a Ø3.75mm Intra-Oral Brånemark Implant Mounted in FRB-10 to an Engagement Length of 8.85mm

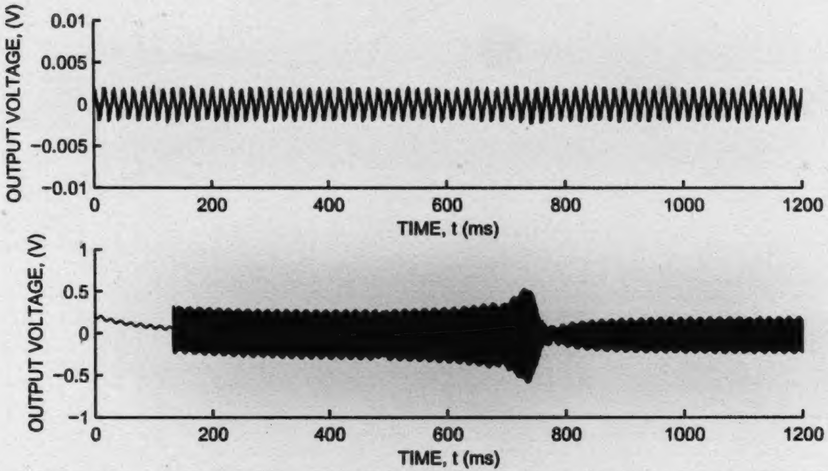

Figure E-2: Response of a Ø4mm Intra-Oral Brånemark Implant Mounted in FRB-10 to an Engagement Length of 8.72mm

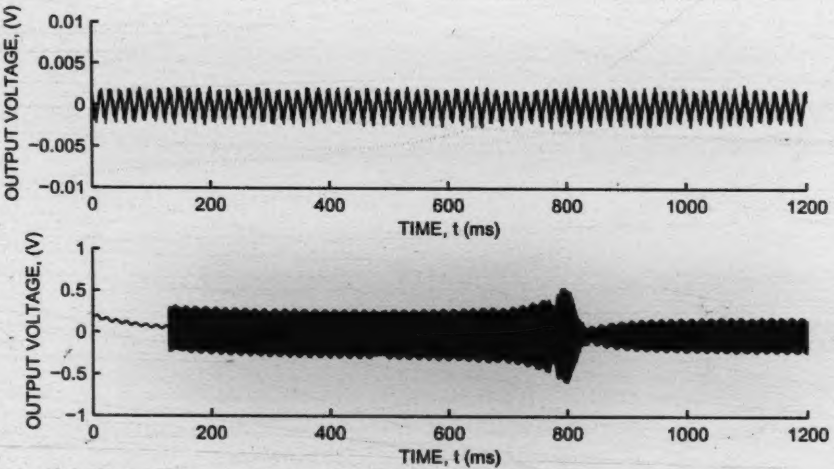

Figure E-3: Response of a Ø5mm Intra-Oral Brånemark Implant Mounted in FRB-10 to an Engagement Length of 9.58mm

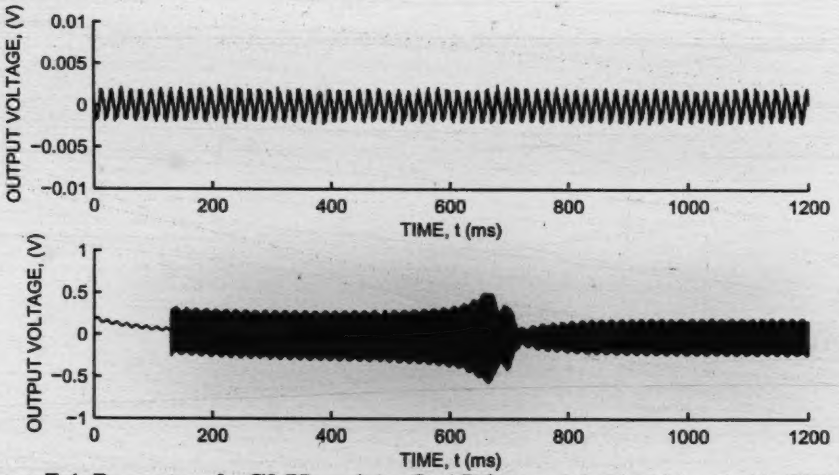

Figure E-4: Response of a Ø3.75mm Intra-Oral Brånemark Implant Mounted in FRB-10 to an Engagement Length of 7.70mm

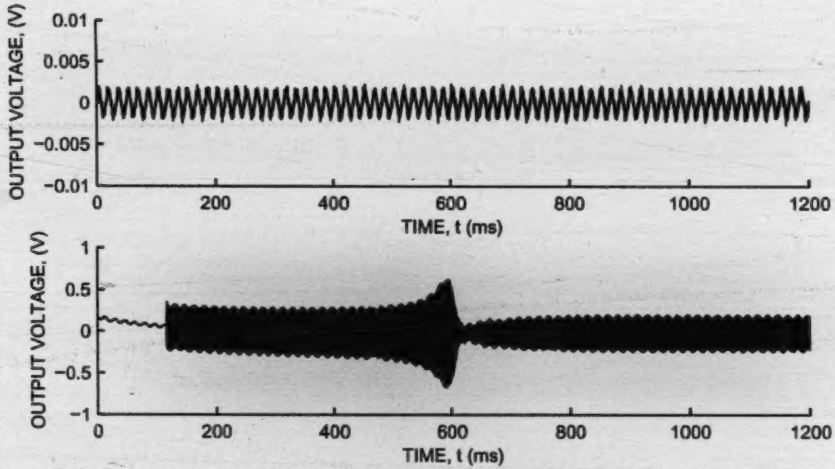

Figure E-5: Response of a Ø4mm Intra-Oral Brånemark Implant Mounted in FRB-10 to an Engagement Length of 1.68mm

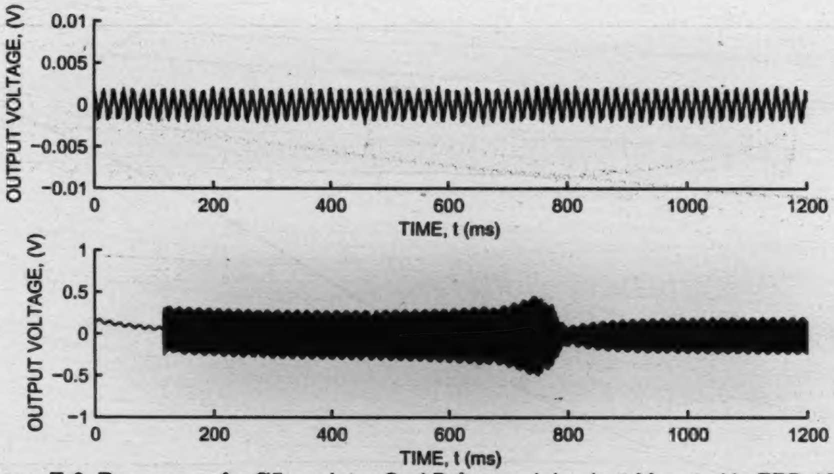

Figure E-6: Response of a Ø5mm Intra-Oral Brånemark Implant Mounted in FRB-10 to an Engagement Length of 8.41mm

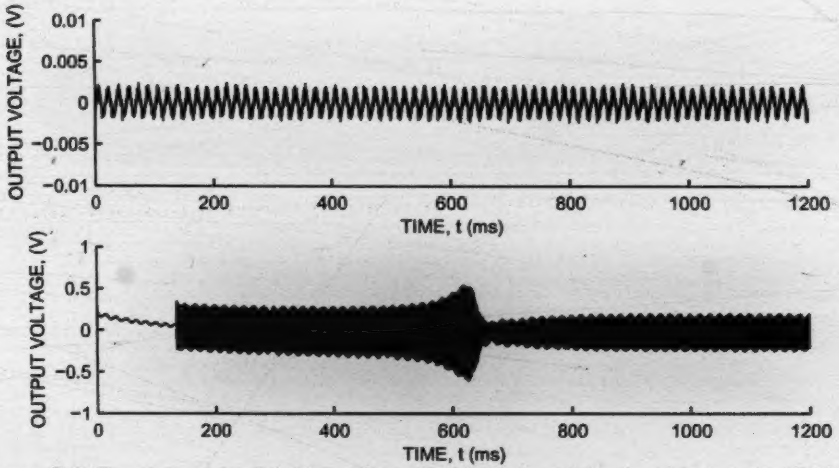

Figure E-7: Response of a Ø3.75mm Intra-Oral Brånemark Implant Mounted in FRB-10 to an Engagement Length of 5.62mm

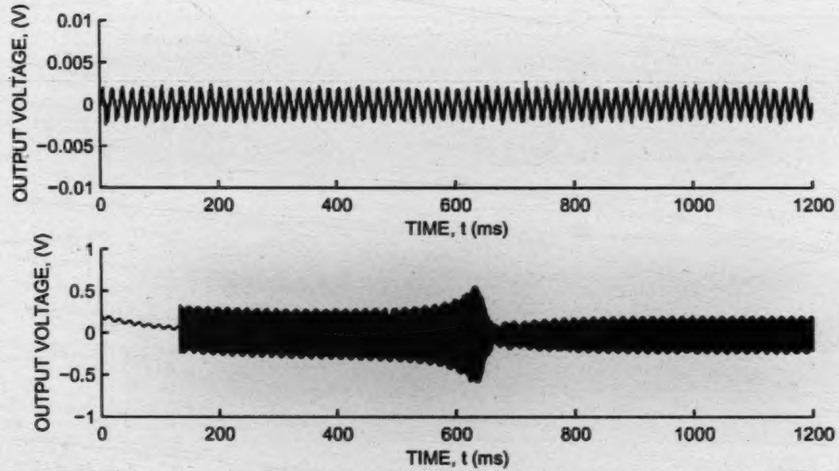

Figure E-8: Response of a Ø4mm Intra-Oral Brånemark Implant Mounted in FRB-10 to an Engagement Length of 5.72mm

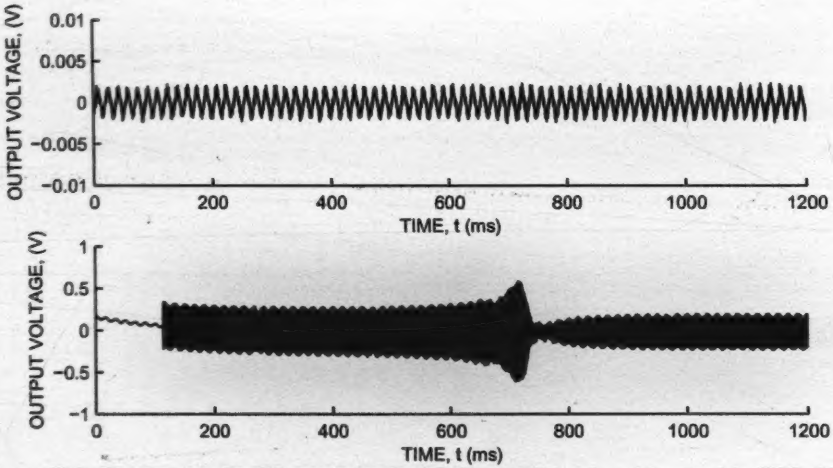

Figure E-9: Response of a Ø5mm Intra-Oral Brånemark Implant Mounted in FRB-10 to an Engagement Length of 6.68mm

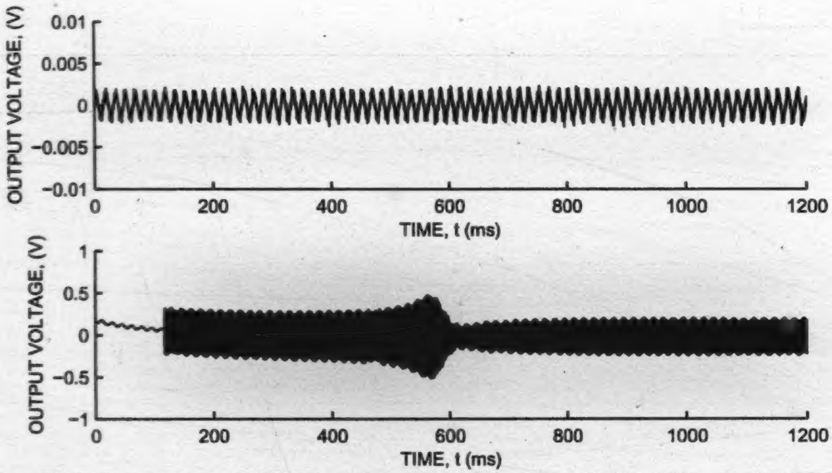

Figure E-10: Response of a Ø3.75mm Intra-Oral Brånemark Implant Mounted in FRB-20 to an Engagement Length of 5.62mm

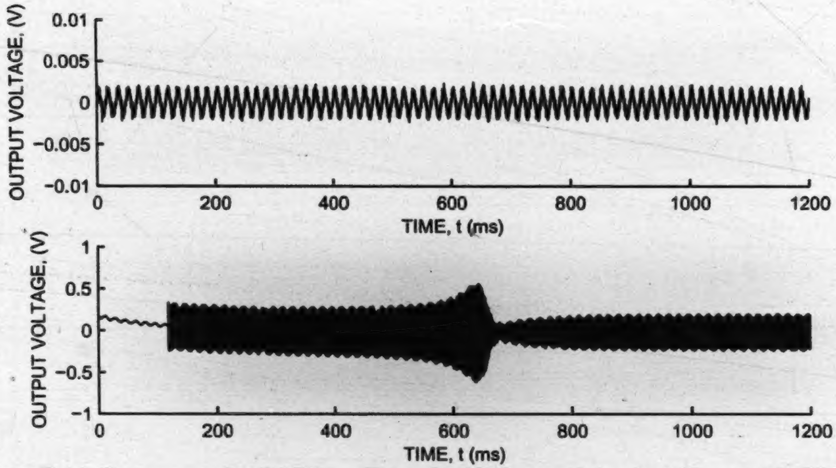

Figure E-11: Response of a Ø3.75mm Extra-Oral Brånemark Implant Mounted in FRB-10 to an Engagement Length of 1.87mm

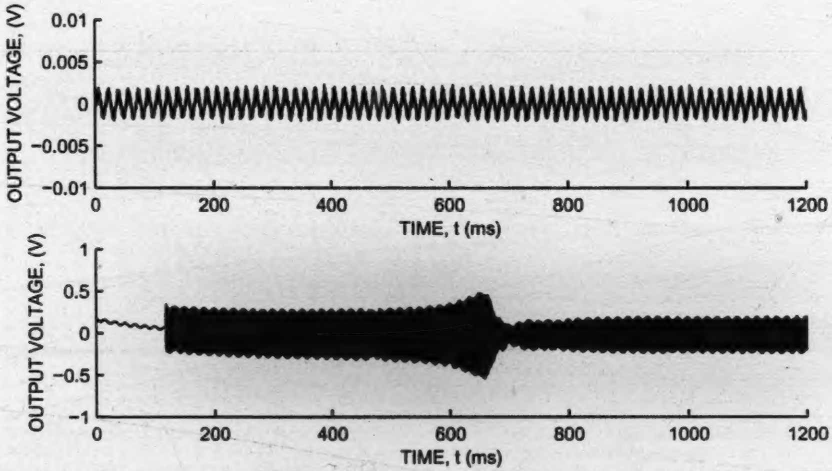

Figure E-12: Response of a Ø3.75mm Extra-Oral Brånemark Implant Mounted in FRB-10 to an Engagement Length of 2.78mm

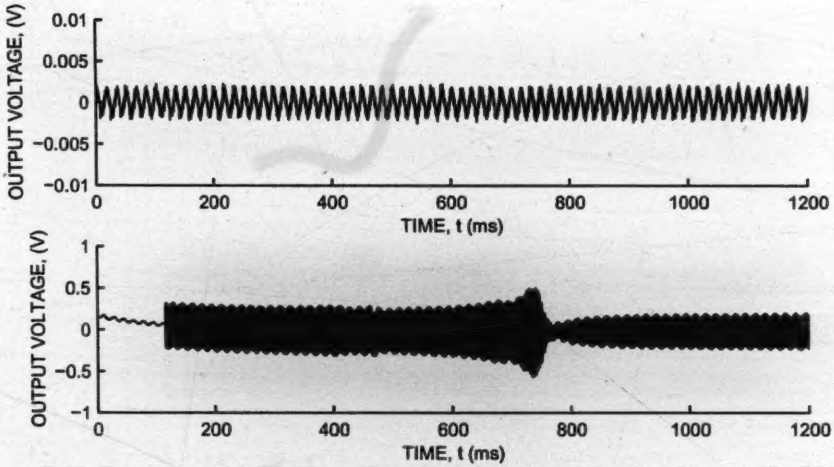

Figure E-13: Response of a Ø3.75mm Extra-Oral Brånemark Implant Mounted in FRB-10 to an Engagement Length of 3.83mm

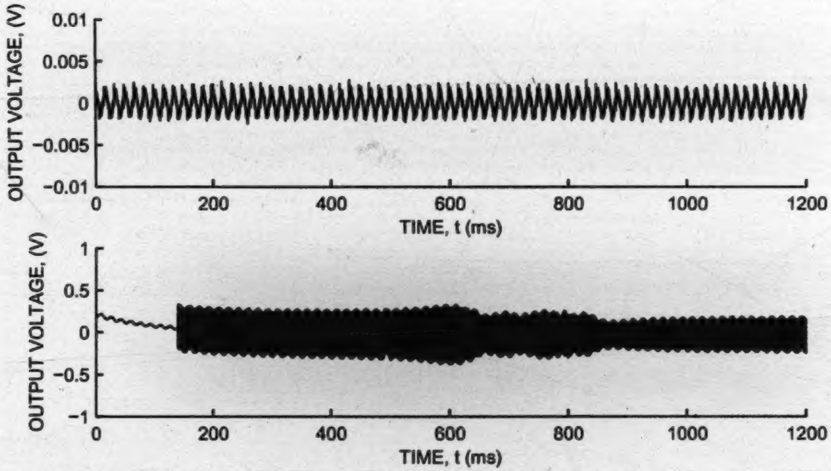

Figure E-14: Response of a Ø3.75mm Extra-Oral Brånemark Implant Mounted in FRB-10 to an Engagement Length of 4.78mm

Appendix F – Periotest® Response to Abutment Length: Giannitsios et. al. Model (2001)

The response of the Periotest® instrument to abutment length are plotted for all in vitro discs evaluated. A curve fit to the Giannitsios et.al. model(2001) is included.

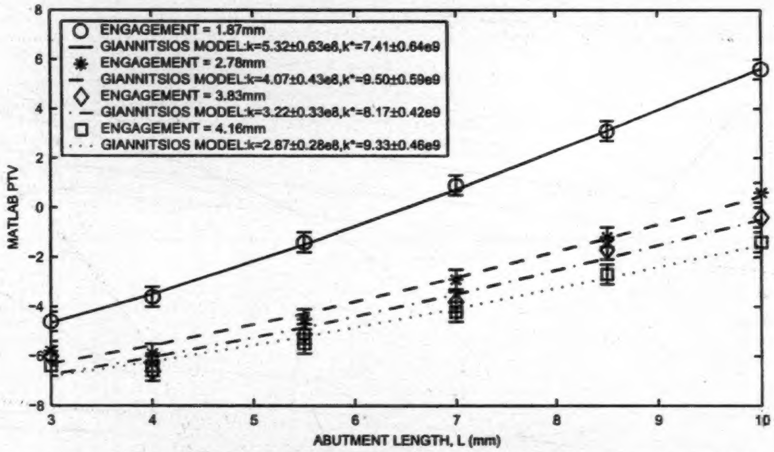

Figure F-1: Periotest® Response to Changes in Abutment Length for Ø3.75mm Brånemark Extra-Oral Implants installed in FRB-10

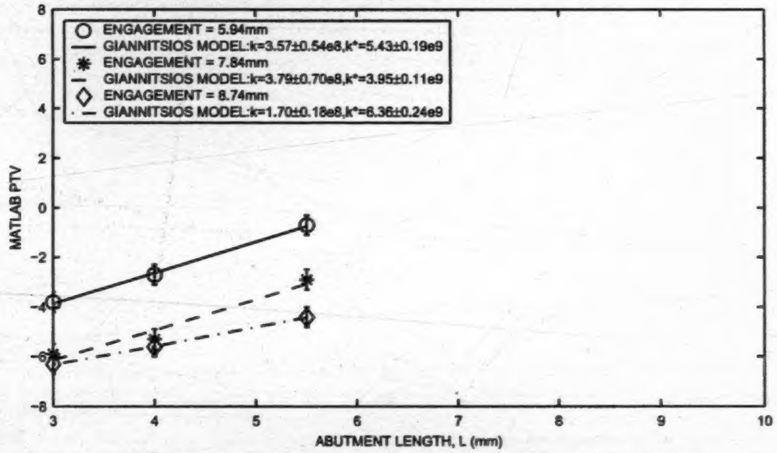

Figure F-2: Periotest® Response to Changes in Abutment Length for Ø3.3mm Brånemark Intra-Oral Implants installed in FRB-10

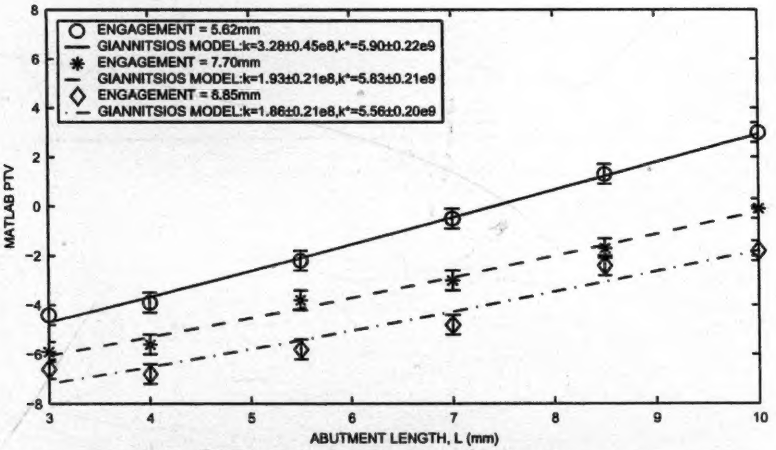

Figure F-3: Periotest® Response to Changes in Abutment Length for Ø3.75mm Brånemark Intra-Oral Implants installed in FRB-10

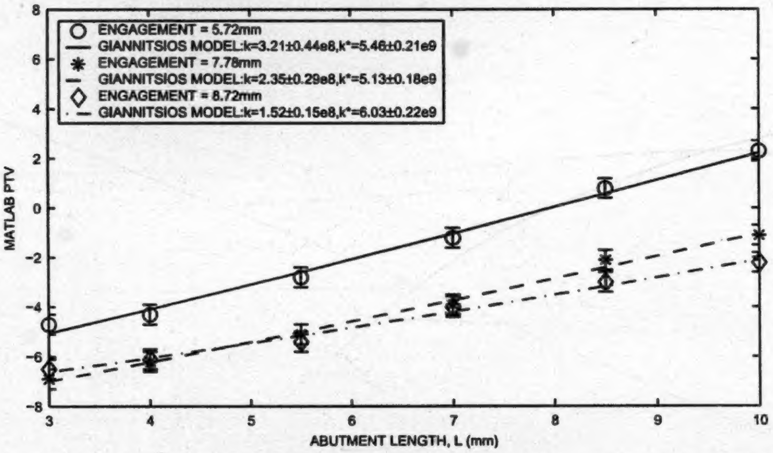

Figure F-4: Periotest® Response to Changes in Abutment Length for Ø4mm Brånemark Intra-Oral Implants installed in FRB-10

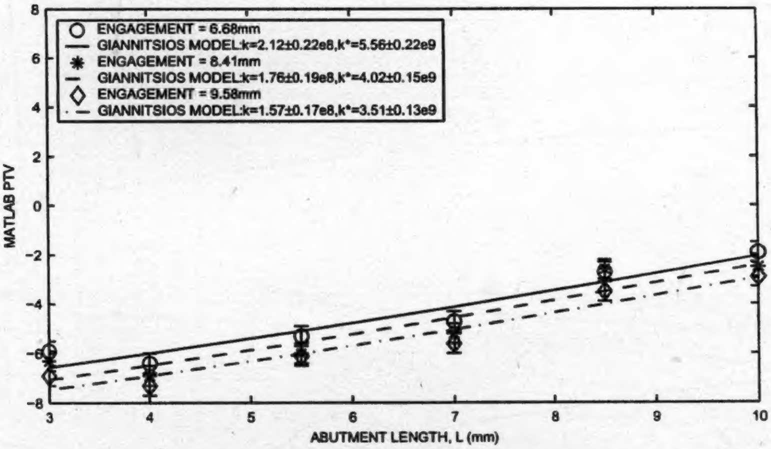

Figure F-5: Periotest® Response to Changes in Abutment Length for Ø5mm Brånemark Intra-Oral Implants installed in FRB-10

Appendix G – Periotest® Response to Abutment Length

A linear curve fit of the Periotest® relationship with abutment length is shown for all in vitro implant systems evaluated.

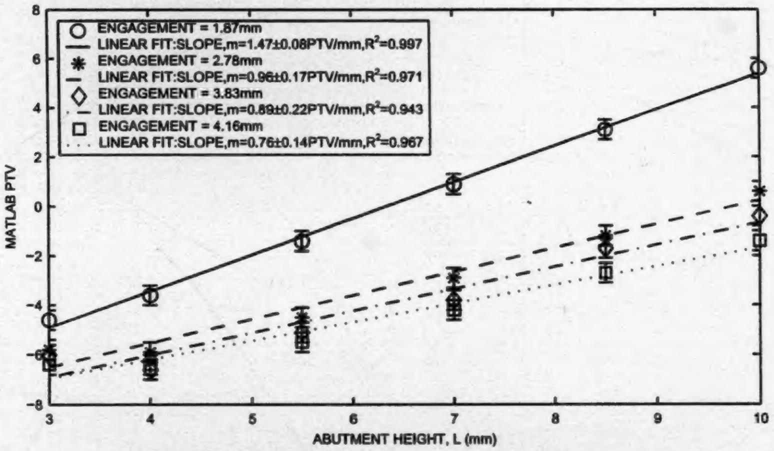

Figure G-1: Periotest® Response to Changes in Abutment Length for Ø3.75mm Brånemark Extra-Oral Implants installed in FRB-10

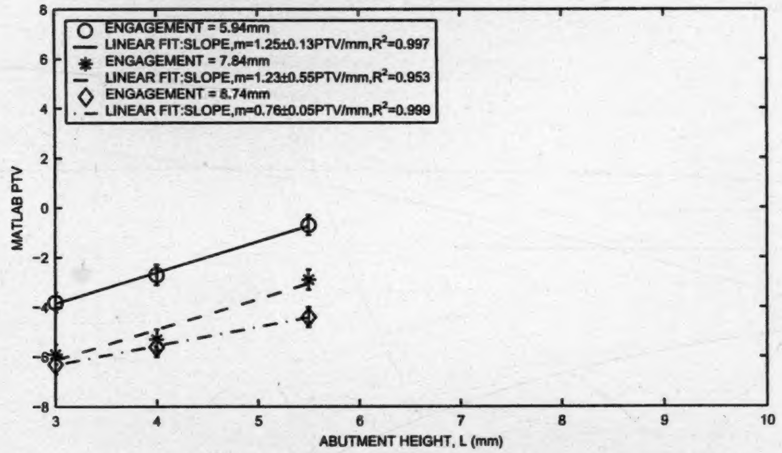

Figure G-2: Periotest® Response to Changes in Abutment Length for Ø3.3mm Brånemark Intra-Oral Implants installed in FRB-10

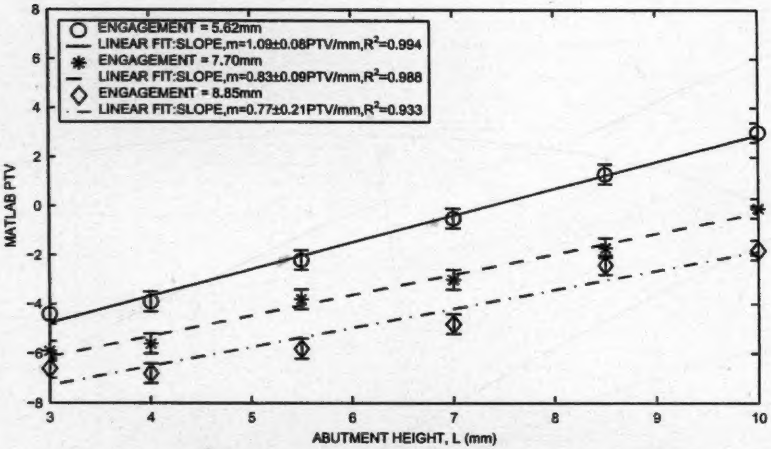

Figure G-3: Periotest® Response to Changes in Abutment Length for Ø3.75mm Brånemark Intra-Oral Implants installed in FRB-10

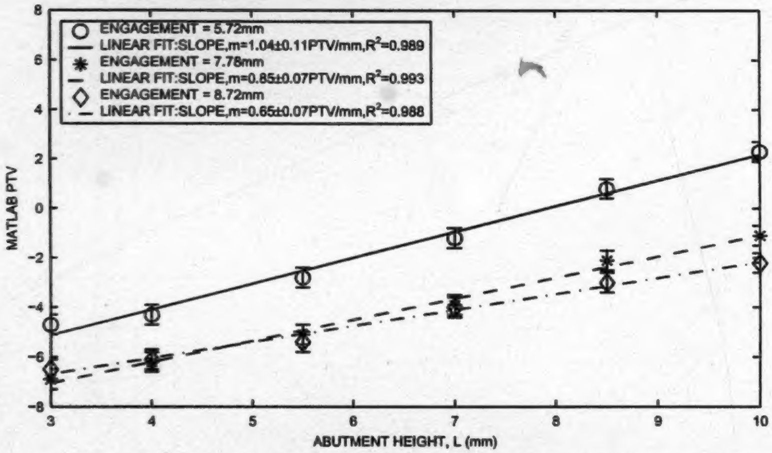

Figure G-4: Periotest® Response to Changes in Abutment Length for Ø4mm Brånemark Intra-Oral Implants installed in FRB-10

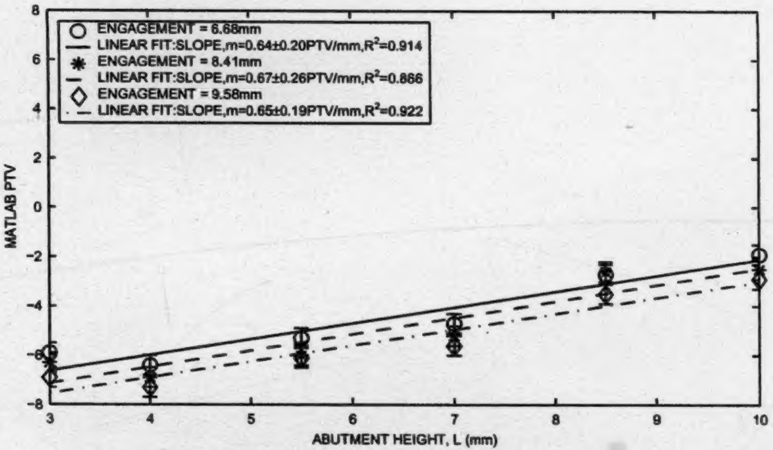

Figure G-5: Periotest® Response to Changes in Abutment Length for Ø5mm Brånemark Intra-Oral Implants installed in FRB-10

Appendix H – Osstell® Response to Abutment Length

This appendix contains the response of the Osstell® instrument to changes in abutment length and includes a linear curve fit.

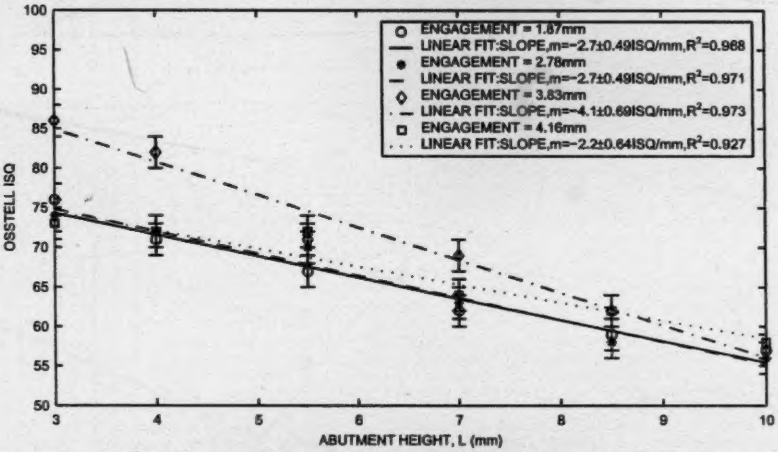

Figure H-1: Osstell® Response to Changes in Abutment Length for Ø3.75mm Brånemark Extra-Oral Implants installed in FRB-10

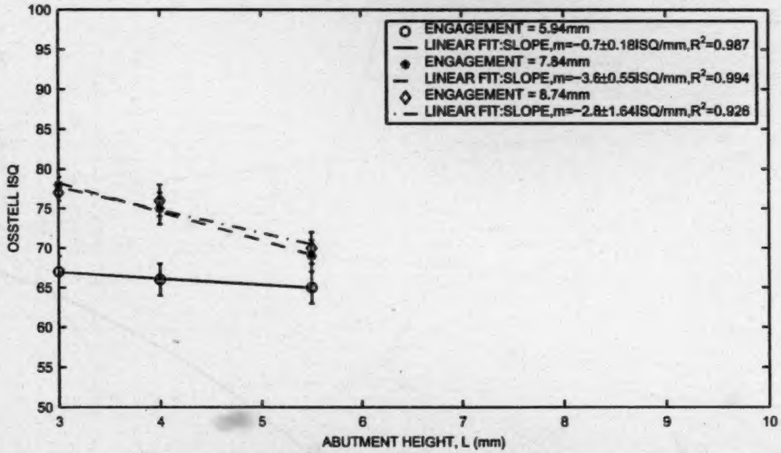

Figure H-2: Osstell® Response to Changes in Abutment Length for Ø3.3mm Brånemark Intra-Oral Implants installed in FRB-10

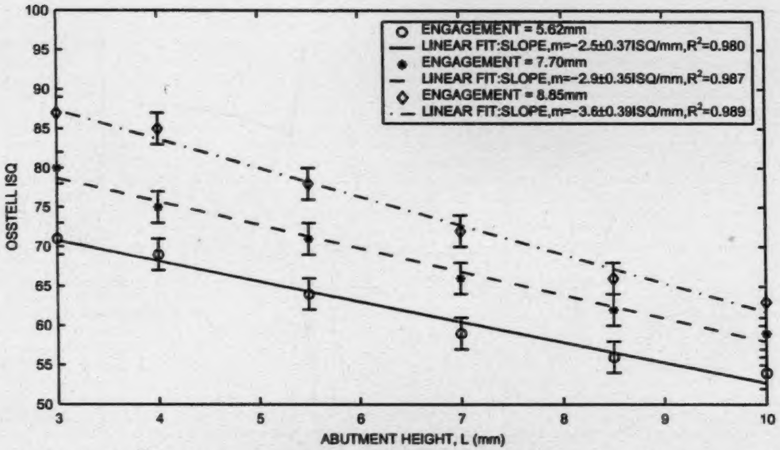

Figure H-3: Osstell® Response to Changes in Abutment Length for Ø3.75mm Brånemark Intra-Oral Implants installed in FRB-10

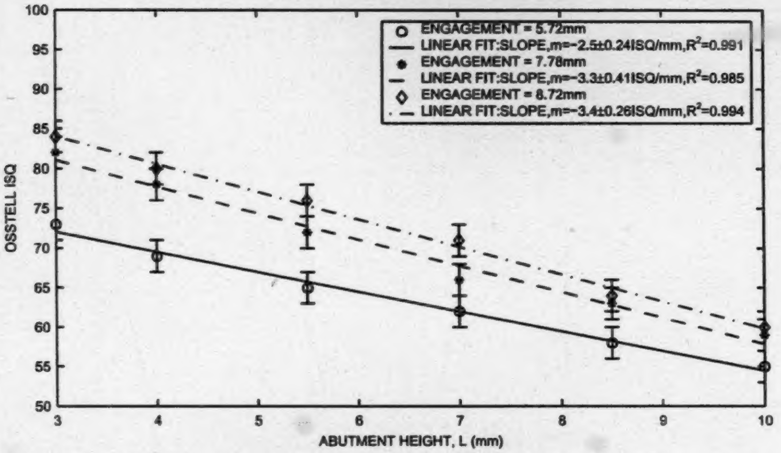

Figure H-4: Osstell® Response to Changes in Abutment Length for Ø4mm Brånemark Intra-Oral Implants installed in FRB-10

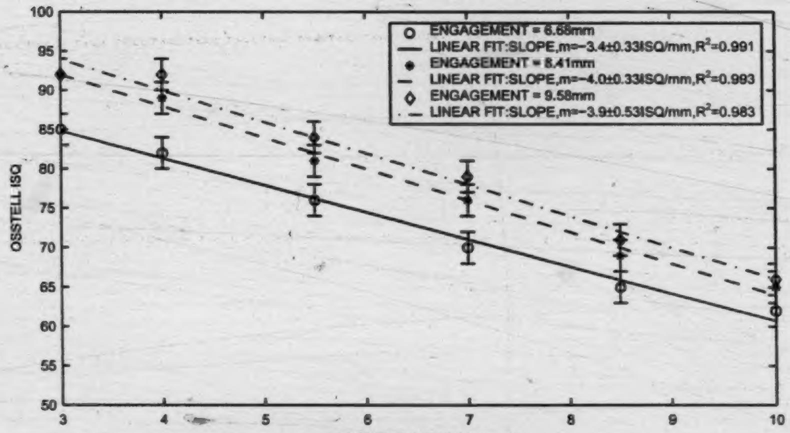

Figure H-5: Osstell® Response to Changes in Abutment Length for Ø5mm Brånemark Intra-Oral Implants installed in FRB-10

Appendix I – Periotest® Response to Engagement Length

The response of the MATLAB PTV to engagement length, and corresponding striking height for all in vitro implant system evaluated are shown below.

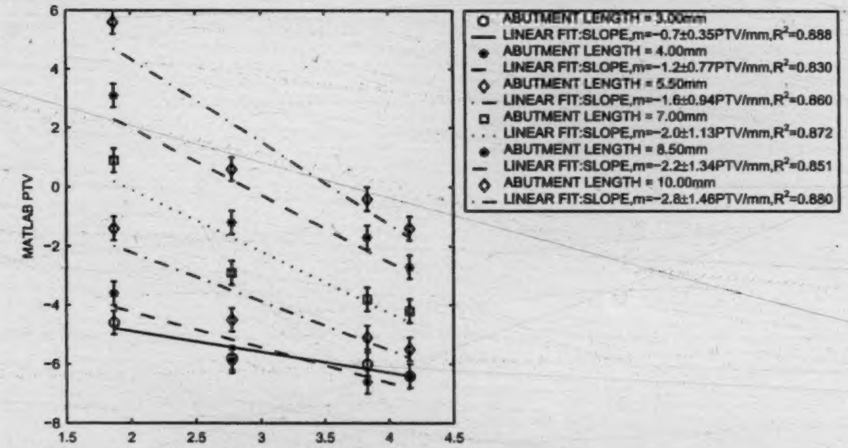

Figure I-1: Periotest® Response to Changes in Engagement Length for Ø3.75mm Brånemark Extra-Oral Implants installed in FRB-10

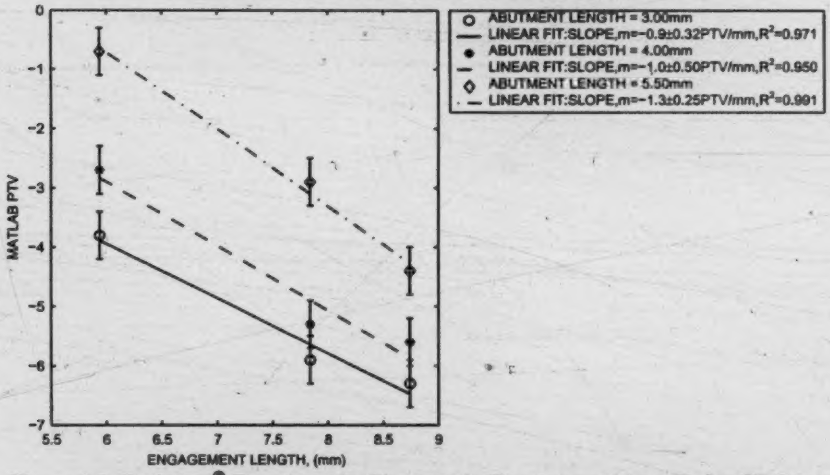

Figure I-2: Periotest® Response to Changes in Engagement Length for Ø3.3mm Brånemark Intra-Oral Implants installed in FRB-10

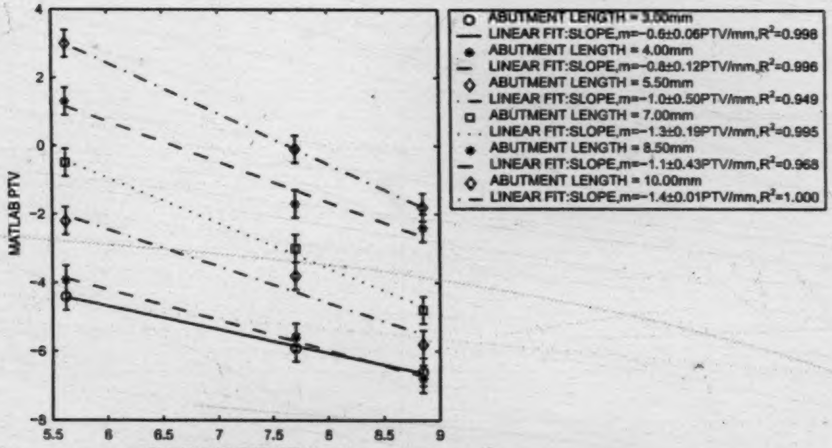

Figure I-3: Periotest® Response to Changes in Engagement Length for Ø3.75mm Brånemark Intra-Oral Implants installed in FRB-10

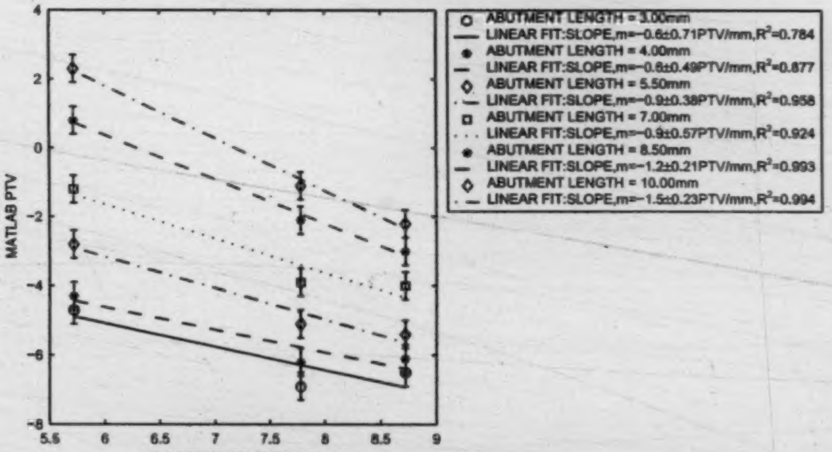

Figure I-4: Periotest® Response to Changes in Engagement Length for Ø4mm Brånemark Intra-Oral Implants installed in FRB-10

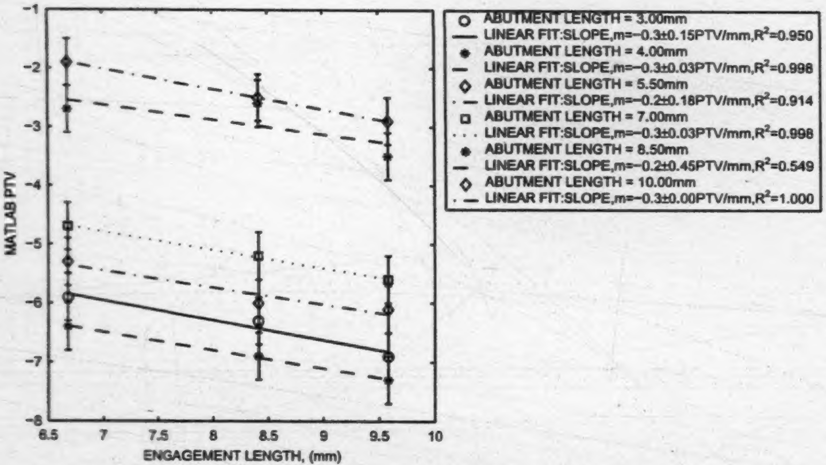

Figure I-5: Periotest® Response to Changes in Engagement Length for Ø5mm Brånemark Intra-Oral Implants installed in FRB-10

Appendix J – Osstell® Response to Engagement Length

This appendix contains the response of the Osstell® instrument to engagement length. A linear regression fit is shown for all in vitro implant systems evaluated.

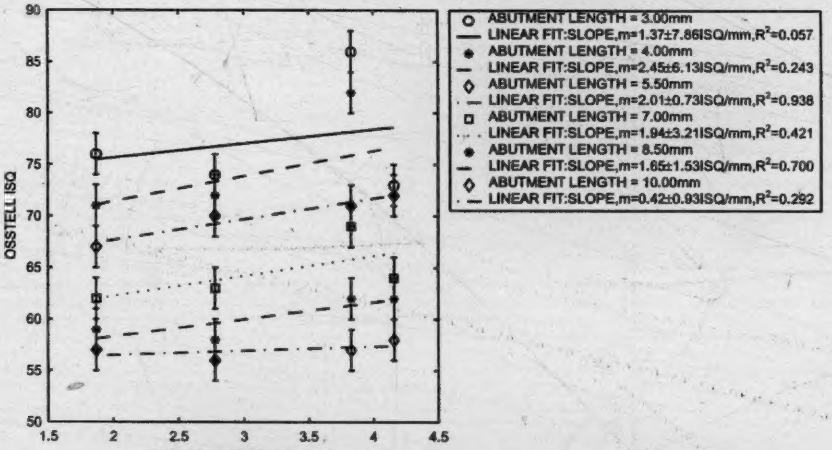

Figure J-1: Osstell® Response to Changes in Engagement Length for Ø3.75mm Brånemark Extra-Oral Implants installed in FRB-10

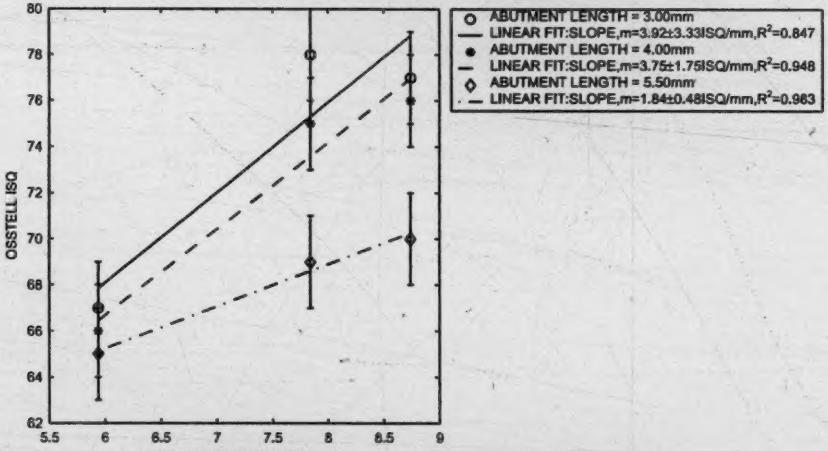

Figure J-2: Osstell® Response to Changes in Engagement Length for Ø3.3mm Brånemark Intra-Oral Implants installed in FRB-10

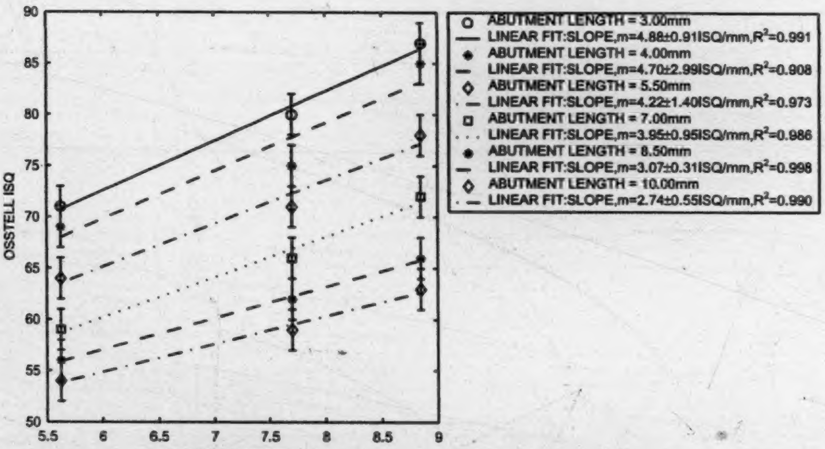

Figure J-3: Osstell® Response to Changes in Engagement Length for Ø3.75mm Brånemark Intra-Oral Implants installed in FRB-10

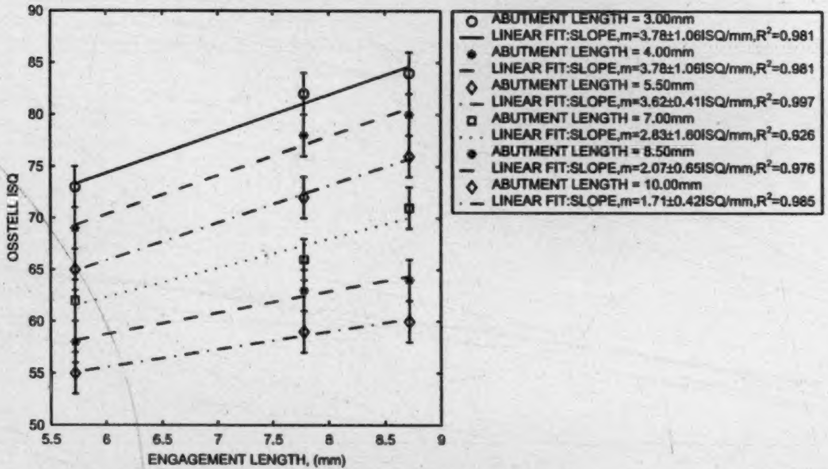

Figure J-4: Osstell® Response to Changes in Engagement Length for Ø4mm Brånemark Intra-Oral Implants installed in FRB-10

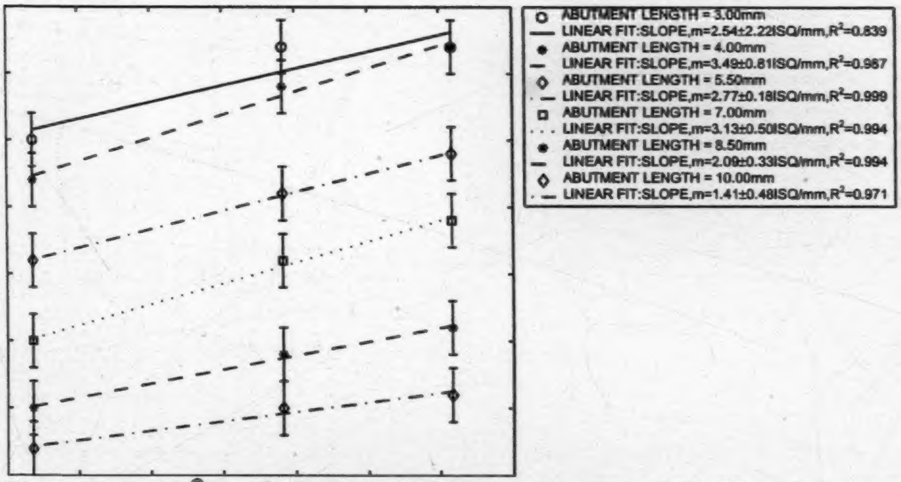

Figure J-5: Osstell® Response to Changes in Engagement Length for Ø5mm Brånemark Intra-Oral Implants installed in FRB-10

Appendix K– Periotest® and Osstell® Response to Implant Diameter

The general trend of the Periotest® and Osstell® instrument to changes in implant diameter, while holding engagement length and abutment height constant.

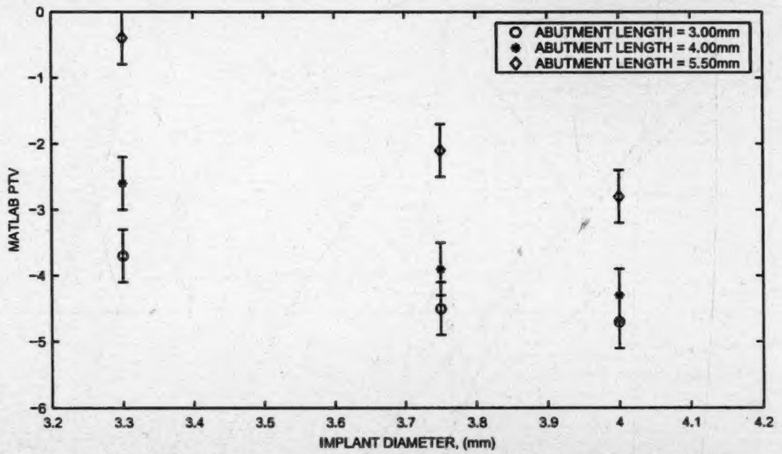

Figure K-1: Periotest® Response to Changes in Implant Diameter for Brånemark Intra-Oral Implants installed in FRB-10 to an Effective Engagement Length of 5.72mm

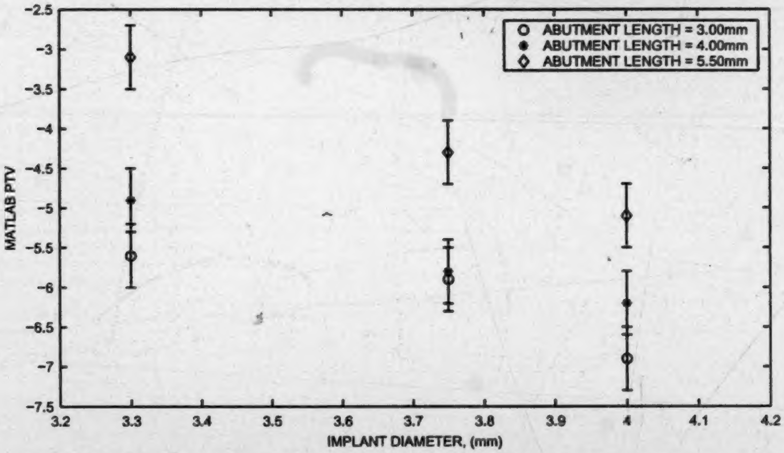

Figure K-2: Periotest® Response to Changes in Implant Diameter for Brånemark Intra-Oral Implants installed in FRB-10 to an Effective Engagement Length of 7.78mm

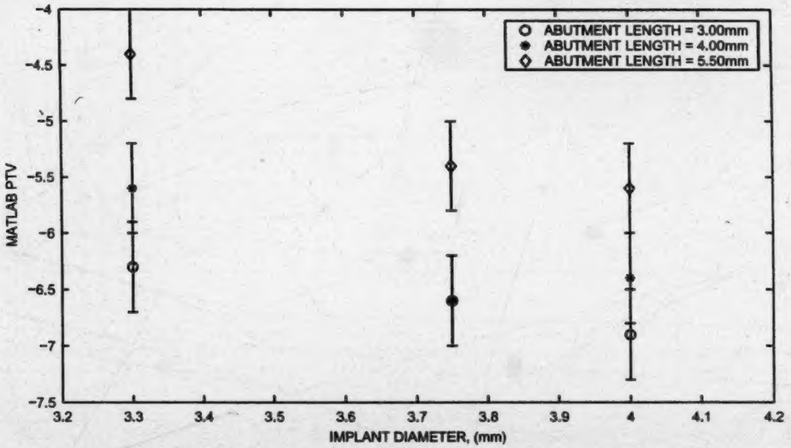

Figure K-3: Periotest® Response to Changes in Implant Diameter for Brånemark Intra-Oral Implants installed in FRB-10 to an Effective Engagement Length of 8.74mm

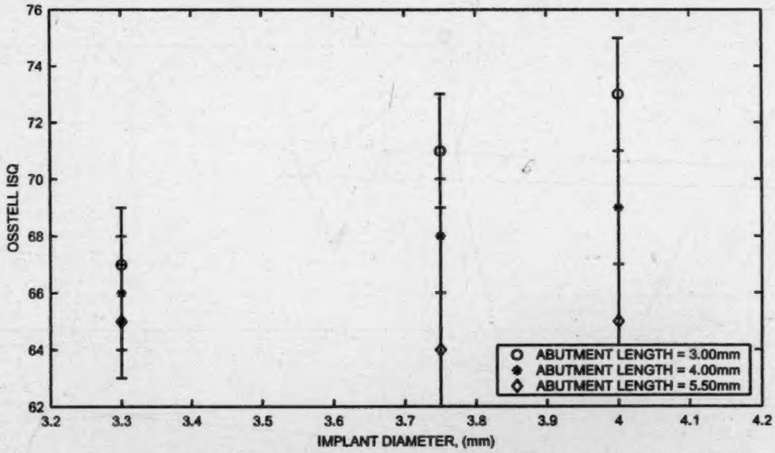

Figure K-4: Osstell® Response to Changes in Implant Diameter for Brånemark Intra-Oral Implants installed in FRB-10 to an Effective Engagement Length of 5.72mm

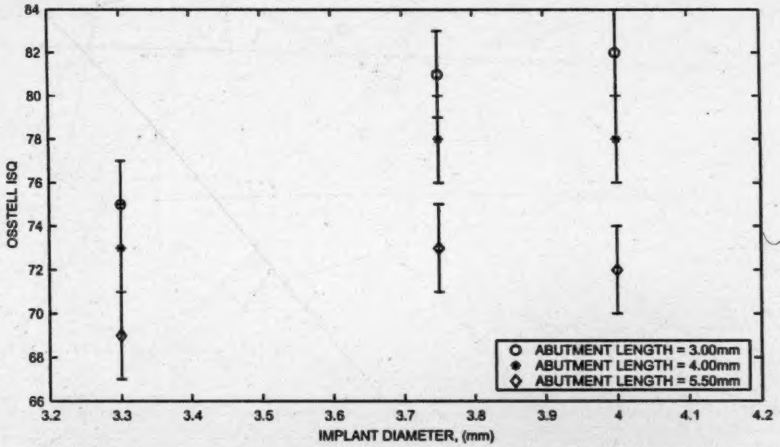

Figure K-5: Osstell® Response to Changes in Implant Diameter for Brånemark Intra-Oral Implants installed in FRB-10 to an Effective Engagement Length of 7.78mm

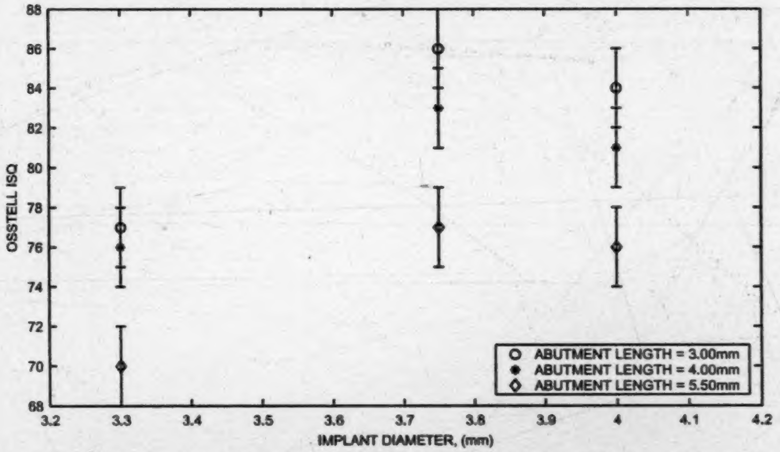

Figure K-6: Osstell® Response to Changes in Implant Diameter for Brånemark Intra-Oral Implants installed in FRB-10 to an Effective Engagement Length of 8.74mm

Appendix L – Giannitios et. al. Model(2001)

Motion of Implant/Abutment System – Giannitsios et. al. Model(2001)

Derivation of Equations Governing Motion

Newton's Laws are used to derive the formulae based on the FBD/MAD shown in Figure 3-19. To complete the model's derivation, assume $x, \dot{x}, \ddot{x} > 0$ when center of gravity moving to the left and $\vartheta, \dot{\vartheta}, \ddot{\vartheta} > 0$ when rotation is counterclockwise.

Sum of Horizontal Forces

$$\boxed{\leftarrow \sum F_h = m\ddot{x} = f(t) - F_{hs} - F_{hc}}$$

Equation L-1

F_{hs} and F_{hc} are the total horizontal spring and horizontal damper forces acting on the implant because of the implant/abutment system translational and rotational displacement, respectively.

$$\begin{aligned}
f_{hs} &= k_{EFFECTIVE}\,\delta_{SPRING} \\
f_{hs} &= [kdy]_{EFFECTIVE}\,[(x-(Q-y)\vartheta)]_{SPRING} \\
F_{hs} &= \int_{y=o}^{y=E} f_{hs} \\
F_{hs} &= \int_{y=0}^{y=E} (x-(Q-y)\vartheta)\,kdy \\
F_{hs} &= kE\left\{x+\left(E/_2-Q\right)\vartheta\right\}
\end{aligned}$$

Equation L-2

$$\begin{aligned}
f_{hc} &= c_{EFFECTIVE}\,\dot{\delta}_{DAMPER} \\
f_{hc} &= [cdy]_{EFFECTIVE}\left[\left(\dot{x}-(Q-y)\dot{\vartheta}\right)\right]_{DAMPER} \\
F_{hc} &= \int_{y=o}^{y=E} f_{hc} \\
F_{hc} &= \int_{y=0}^{y=E}\left(\dot{x}-(Q-y)\dot{\vartheta}\right)\left(\phi/_2\right)cdy \\
F_{hc} &= cE\left(\dot{x}-(Q-y)\dot{\vartheta}\right)
\end{aligned}$$

Equation L-3

Substitution of Equations L-2 and L-3 in Equation L-1 gives rise to one equation of motion.

$$\boxed{\left[\begin{array}{l} m\ddot{x} \\ +kE\left\{x+\left(E/2-Q\right)\vartheta\right\} \\ +cE\left\{\dot{x}+\left(E/2-Q\right)\dot{\vartheta}\right\} \end{array}\right]=f(t)}$$

Equation L-4

Sum of Moments about Center of Mass

Summation of the moments about the center of mass yields Equation L-5.

$$\boxed{\sum M_{CG}=J\ddot{\vartheta}=f(t)(L-Q)+M_s+M_c+M(t)}$$

Equation L-5

The sum of all moments caused by spring forces and damping forces are denoted as M_s and M_c, respectively.

$$\boxed{M_s=\left[\begin{array}{l} kE\left[x\left(Q-E/2\right)+\vartheta\cdot\left(-Q^2+QE-E^2/3\right)\right] \\ -k^{*}E\left(\phi/2\right)^2\vartheta \end{array}\right]}$$

Equation L-6

$$\boxed{M_c=\left[\begin{array}{l} cE\left[\dot{x}\left(Q-E/2\right)+\dot{\vartheta}\cdot\left(-Q^2+QE-E^2/3\right)\right] \\ -c^{*}E\left(\phi/2\right)^2\dot{\vartheta} \end{array}\right]}$$

Equation L-7

Equation L-8 shows substitution of Equations L-6 and L-7 into Equation L-5.

$$\boxed{J\ddot{\vartheta}=\left[\begin{array}{l} f(t)(L-Q)+M(t) \\ +\left[\begin{array}{l} cE\left[\dot{x}\left(Q-E/2\right)+\dot{\vartheta}\cdot\left(-Q^2+QE-E^2/3\right)\right] \\ -c^{*}E\left(\phi/2\right)^2\dot{\vartheta} \end{array}\right] \\ +\left[\begin{array}{l} Ek\left[x\left(Q-E/2\right)+\vartheta\cdot\left(-Q^2+QE-E^2/3\right)\right] \\ -k^{*}E\left(\phi/2\right)^2\vartheta \end{array}\right] \end{array}\right]}$$

Equation L-8

Governing Equations of Motion

The sum of forces and moments about the center of mass can be written in matrix form as shown in Equation L-9.

$$\boxed{\begin{bmatrix} \begin{bmatrix} m & 0\\ 0 & J\end{bmatrix}\begin{Bmatrix}\ddot{x}\\ \ddot{\vartheta}\end{Bmatrix} + E\begin{bmatrix} c & c\left(\frac{E}{2}-Q\right)\\ c\left(\frac{E}{2}-Q\right) & \begin{Bmatrix} c\left(Q^2-QE+\frac{E^2}{3}\right)\\ +c^{\bullet}\left(\frac{\phi}{2}\right)^2\end{Bmatrix}\end{bmatrix}\begin{Bmatrix}\dot{x}\\ \dot{\vartheta}\end{Bmatrix} \\ +E\begin{bmatrix} k & k\left(\frac{E}{2}-Q\right)\\ k\left(\frac{E}{2}-Q\right) & \begin{bmatrix} k\left(Q^2-QE+\frac{E^2}{3}\right)\\ +k^{\bullet}\left(\frac{\phi}{2}\right)^2\end{bmatrix}\end{bmatrix}\begin{Bmatrix}x\\ \vartheta\end{Bmatrix}\end{bmatrix} = \begin{Bmatrix} f(t)\\ f(t)(L-Q)+M(t)\end{Bmatrix}}$$

Equation L-9

These equations that govern the motion of the implant/abutment assume the implant/abutment is a rigid body and vibrates with two degrees of freedom. In addition, small translational and rotational deflections are assumed.

Simplification of Model – Assumptions

If damping is neglected in the vibrating implant/abutment, then the governing equations of motion reduce to Equation L-10.

$$\boxed{\begin{bmatrix} \begin{bmatrix} m & 0\\ 0 & J\end{bmatrix}\begin{Bmatrix}\ddot{x}\\ \ddot{\vartheta}\end{Bmatrix} \\ +E\begin{bmatrix} (k) & k_h\left(\frac{E}{2}-Q\right)\\ k\left(\frac{E}{2}-Q\right) & \begin{bmatrix} k\left(Q^2-QE+\frac{E^2}{3}\right)\\ +k^{\bullet}\left(\frac{\phi}{2}\right)^2\end{bmatrix}\end{bmatrix}\begin{Bmatrix}x\\ \vartheta\end{Bmatrix}\end{bmatrix} = \begin{Bmatrix} f(t)\\ f(t)(L-Q)+M(t)\end{Bmatrix}}$$

Equation L-10

Applied Force and Moment Functions

The applied force and moment functions can take a variety of forms. However, their forms will be restricted to those produced by the Periotest® and Osstell® instruments.

Periotest® Applied Force

Due to the nature of the Periotest® instrument, only a force is applied to the implant/abutment system. The applied force from the Periotest® occurs in the direction of the Periotest® rod. Its magnitude depends on the force interaction between the Periotest® rod and the abutment. For example, if the Periotest® rod remains in contact with the abutment then the applied force can easily be determined as Equation L-11.

$$\boxed{f(t) = -m_{Periotest}\,\ddot{x}_D}$$

Equation L-11

Where $m_{Periotest}$ and $\ddot{x}_D$ are the mass of the Periotest® rod and the acceleration of the abutment at point of contact with the Periotest® rod, respectively.

The mass of the Periotest® rod has been well documented in literature as 8 grams. An expression relating $\ddot{x}_D$ to $x(t)$ and $\vartheta(t)$ from the previously derived governing equations of motion is shown in Equation L-12.

$$\boxed{\ddot{x}_D = \ddot{x}(t) + (L-Q)\ddot{\vartheta}}$$

Equation L-12

Therefore, the governing equations of motion for the implant/abutment system undergoing a Periotest® measurement can be written as Equation L-13.

$$\boxed{\left[\begin{array}{l}\begin{bmatrix} m & 0 \\ 0 & J \end{bmatrix}\begin{Bmatrix} \ddot{x}_D \\ \ddot{\vartheta} \end{Bmatrix} \\ +E\begin{bmatrix} k & k\left(E/2 - Q\right) \\ k\left(E/2 - Q\right) & \begin{bmatrix} k\left(Q^2 - QE + E^2/3\right) \\ +k^{*}\left(\phi/2\right)^2 \end{bmatrix} \end{bmatrix}\begin{Bmatrix} x_D \\ \vartheta \end{Bmatrix}\end{array}\right] = \begin{Bmatrix} -\left(\ddot{x}(t) + (L-Q)\ddot{\vartheta}\right)m_p \\ -\left(\ddot{x}(t) + (L-Q)\ddot{\vartheta}\right)m_p(L-Q) \end{Bmatrix}}$$

Equation L-13

Simplification of Equation L-13 yields Equation L-14.

$$\boxed{\left[\begin{array}{l}\begin{bmatrix} m + m_p & (L-Q)m_p \\ (L-Q)m_p & J + (L-Q)^2 m_p \end{bmatrix}\begin{Bmatrix} \ddot{x}_D \\ \ddot{\vartheta} \end{Bmatrix} \\ +E\begin{bmatrix} k & k\left(E/2 - Q\right) \\ k\left(E/2 - Q\right) & \begin{bmatrix} k\left(Q^2 - QE + E^2/3\right) \\ +k^{*}\left(\phi/2\right)^2 \end{bmatrix} \end{bmatrix}\begin{Bmatrix} x_D \\ \vartheta \end{Bmatrix}\end{array}\right] = \begin{Bmatrix} 0 \\ 0 \end{Bmatrix}}$$

Equation L-14

Appendix M – Least Squares Fit of Periotest® Data

LEAST SQUARES FIT TO DETERMINE k and k^*

```
periotest_stiffness_solver_F.m
%This code solves for k and kstar from Giannitsios et. al. Model(2001)
function [k,kstar,PTVFaulkner]=periotest_stiffness_solver_F(meff,PTV...
      ,implantdiameter,L1,L2)
if length(implantdiameter)==1
    implantdiameter=ones(length(PTV),1)*implantdiameter;
end
options = OPTIMSET('MaxFunEvals',2e10,'MaxIter',1e3);
k=100000;%initial guess of k
kstar=100000;%initial guess of k*
xold=[k,kstar];
xnew=fminsearch('fitting_equation_Faulkner',xold,options,meff,L1,L2,...
      implantdiameter,PTV);
k=xnew(1);
kstar=xnew(2);
for n=1:1:length(L1)
    keff(n)=keff_Faulkner(k,kstar,L1(n),L2(n),implantdiameter(n));
end
for n=1:1:length(L1)
    PTVFaulkner(n)=PTV_Faulkner(k,kstar,meff,L1(n),L2(n),
      implantdiameter(n));
end
```

```
fitting_equation_Faulkner.m
function sse=fitting_equation_Faulkner(x,meff,L1,L2,implantdiameter,PTV)
for i=1:length(PTV)
   fittedcurve(i)=PTV_Faulkner(x(1),x(2),meff,L1(i),L2(i),
      implantdiameter(i));
end
sse=sum((fittedcurve-PTV).^2);%Least Squares Error Term
```

```
keff_Faulkner.m
function keff=keff_Faulkner(k,kstar,L1,L2,implantdiameter)
keff=((k/3*(L2^3-L1^3)+kstar*(implantdiameter/2)^2*(L2-L1))*...
(k*(L2-L1))-(k/2*(L2^2-L1^2))^2)/(k/3*(L2^3-L1^3)...
+kstar*(implantdiameter/2)^2*(L2-L1));
```

```
PTV_Faulkner.m
function PTV=PTV_Faulkner(k,kstar,meff,L1,L2,implantdiameter)
PTV=50000*pi*...
      sqrt(meff/keff_Faulkner(k,kstar,L1,L2,implantdiameter))-21.3;
```

Appendix N – Theoretical Modal Analysis

Modes and Frequencies for a Two DOFS

The mass and stiffness matrices of the Giannitsios et. al. Model(2001) for the Periotest® Motion are given:

$$m = \begin{bmatrix} m_{11} & m_{12} \\ m_{21} & m_{22} \end{bmatrix} = \begin{bmatrix} m_i + m_p & m_i d \\ m_i d & J_G + m_i d^2 \end{bmatrix} \qquad \text{Equation N-1}$$

$$k = \begin{bmatrix} k_{11} & k_{12} \\ k_{21} & k_{22} \end{bmatrix} = \begin{bmatrix} k(\ell_2 - \ell_1) & \frac{k}{2}(\ell_2^2 - \ell_1^2) \\ \frac{k}{2}(\ell_2^2 - \ell_1^2) & \begin{bmatrix} \frac{k}{3}(\ell_2^3 - \ell_1^3) \\ + k^* b^2 (\ell_2 - \ell_1) \end{bmatrix} \end{bmatrix} \qquad \text{Equation N-2}$$

These matrices are derived using Newton's Laws based on the following free body diagram and mass acceleration diagrams of the implant/abutment system undergoing translation and rotation.

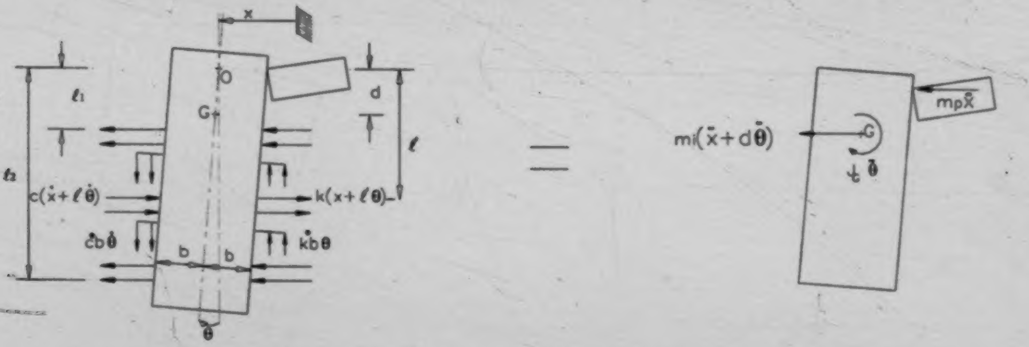

Figure 1: FBD/MAD of Implant/Abutment Model Proposed by Giannitsios et. al. 2001

In order to determine the mode shapes and corresponding frequencies of the implant/abutment system, estimates of the implant/abutment mass, m_i, and rotational inertial, J_G, are required. The masses of Ø3.75mm Intra-Oral Brånemark implant and a regular platform 10mm Intra-Oral abutment were measured and given in Table 1.

Table 1: Mass of Implant and Abutment

Item	Variable	Mass (g)
Ø3.75mm Implant	m_I	0.35
10mm Abutment	m_A	0.65
Implant/Abutment	m_i	1.0

From these masses, an estimate of the center of gravity, G, of the implant/abutment and the rotational inertial property, J_G, are determined in the following manner.

Center of Gravity

If both the implant and abutment are assumed to have *uniform mass distribution*, then an estimate of the center of gravity of the abutment attached to the implant can be calculated using Equation N-3.

$$l_G = \frac{m_A\left(\frac{l_A}{2}+\frac{l_I}{2}\right)}{m_I + m_A} \qquad \text{Equation N-3}$$

Where Table 2 defines the variables.

Table 2: Variable Definitions for Equation 3

Variable	Definition
m_I	mass of Ø3.75mm Implant (0.35g)
m_A	mass of 10mm Abutment (0.65g)
l_A	length of 10mm Abutment (10mm)
l_I	length of Intra-Oral Implant (10mm)
l_G	distance from center of mass of implant to center of gravity of the implant/abutment

With substitutions suggested in Table 2, the center of gravity of the Ø3.75mm Intra-Oral Brånemark implant with a 10mm abutment attached is located $l_G = 6.5mm$ from the center of mass of the implant or $d = 8.5mm$ from the top of the abutment. Given this location of the center of gravity of the implant/abutment, the rotational inertia is calculated by *assuming both the abutment and implant are solid cylinders* using Equation N-4.

$$\begin{aligned} J_G &= J_I^{*} + J_A^{*} = 31.084 g \cdot m^2 \\ J_I &= \frac{m_I l_I^2}{12} = 2.917 g \cdot m^2, J_A = \frac{m_A l_A^2}{12} = 5.417 g \cdot m^2 \\ J_I^{*} &= J_I + m_I l_G^2 = 17.704 g \cdot m^2 \\ J_A^{*} &= J_A + m_A\left(\frac{l_A}{2} - \left\{l_G - \frac{l_I}{2}\right\}\right)^2 = 13.380 g \cdot m^2 \end{aligned} \qquad \text{Equation N-4}$$

The Giannitsios et. al. 2001 model can be rewritten in the following form.

$$\begin{bmatrix} m_{11} & m_{12} \\ m_{21} & m_{22} \end{bmatrix} \begin{Bmatrix} \ddot{x} \\ \ddot{\theta} \end{Bmatrix} + \begin{bmatrix} k_{11} & k_{12} \\ k_{21} & k_{22} \end{bmatrix} \begin{Bmatrix} x \\ \theta \end{Bmatrix} = \begin{Bmatrix} 0 \\ 0 \end{Bmatrix} \tag{Equation N-5}$$

Where m_i and k_i are elements of the mass and stiffness matrix, respectively.

A solution for $x(t)$ and $\theta(t)$ can be found if *simultaneous harmonic motion* is assumed, as shown in Equation N-6.

$$\begin{aligned} x(t) &= X\sin(\omega t) \\ \theta(t) &= \Theta\sin(\omega t) \end{aligned} \tag{Equation N-6}$$

Substitution of Equation N-6 into Equation N-5 yields Equation N-7.

$$\left[\begin{bmatrix} k_{11} & k_{12} \\ k_{21} & k_{22} \end{bmatrix} - \omega^2 \begin{bmatrix} m_{11} & m_{12} \\ m_{21} & m_{22} \end{bmatrix}\right] \begin{Bmatrix} X \\ \Theta \end{Bmatrix} \sin(\omega t) = \begin{Bmatrix} 0 \\ 0 \end{Bmatrix} \tag{Equation N-7}$$

To determine the modes, $\begin{Bmatrix} X \\ \Theta \end{Bmatrix}$, and the corresponding frequency of vibration, ω, requires solution of Equation N-7. The solution of Equation N-7 can be determined using the following 2 steps:

STEP 1) Determine the value of ω^2 from Equation N-8.

$$\det\left[\begin{bmatrix} k_{11} & k_{12} \\ k_{21} & k_{22} \end{bmatrix} - \omega^2 \begin{bmatrix} m_{11} & m_{12} \\ m_{21} & m_{22} \end{bmatrix}\right] = 0 \tag{Equation N-8}$$

Which yields the characteristic polynomial

$$(m_{11}m_{22} - m_{12}m_{21})\omega^4 + (k_{12}m_{21} + k_{21}m_{12} - k_{11}m_{22} - k_{22}m_{11})\omega^2 + (k_{11}k_{22} - k_{12}k_{21}) = 0 \tag{Equation N-9}$$

The solutions of this polynomial are found using the quadratic formula and are given by

$$\omega^2 = \frac{-\begin{pmatrix} k_{12}m_{21} + k_{21}m_{12} \\ -k_{11}m_{22} - k_{22}m_{11} \end{pmatrix} \pm \sqrt{\begin{pmatrix} k_{12}m_{21} + k_{21}m_{12} \\ -k_{11}m_{22} - k_{22}m_{11} \end{pmatrix}^2 - 4(m_{11}m_{22} - m_{12}m_{21})(k_{11}k_{22} - k_{12}k_{21})}}{2(m_{11}m_{22} - m_{12}m_{21})} \tag{Equation N-10}$$

STEP 2) Determine the ratio of the X/θ from Equation N-7

$$X/\theta = \frac{-(k_{12} - \omega^2 m_{12})}{(k_{11} - \omega^2 m_{11})} \tag{Equation N-11}$$

Appendix O – In Vivo Patient Measurements

This appendix contains all of the in vivo data collected from the Periotest® and Osstell® instrument comparison conducted with the approval of 10 BAHA patients cared for under the guidance of COMPRU, Edmonton, Alberta.

The nature of this study was to obtain precise instrument measurements by adjusting the measurement protocol. In hindsight, the protocol should have been extended to ensure the same Periotest® instrument and Osstell® fixture and abutment leads were used with the same patient over this longitudinal study. This protocol was not included because of the strict sterilization protocol in the operating room and in the clinic, and the time requirements to turn-over the instruments for the next patients: at times the sterilization protocol inhibited the same instrument or lead being used with a the same patient. As a result, the plots include an estimated measurement in those cases where measurements were recorded at regular patient visits with different instrumentation than used during the evaluation of the implant system at initial surgery. This measurement is clearly identified.

To accomplish this estimate, a two-sample t-test was performed on both measurements from using the Periotests® (Opt #1 and Opt #3) to evaluate the Periotest® training block, and the Osstell® leads(Fixture: #483, #484 & Abutment: #196, #197, and #501) when evaluating the calibration blocks designed specifically for the Osstell® instrument.

From this statistical analysis, it was determined that the measurements from the Periotests® were significantly different. Therefore, the MATLAB PTV values for Periotest® Opt #1 and Opt #3 were recorded while evaluating the cylinders on one specific Periotest® training block insert. From this procedure, it was determined that the

Opt #3 MATLAB PTV was related to the MATLAB PTV from Opt #1 using the following relationship:

$$OPT\#3_{MATLABPTV} = OPT\#1_{MATLABPTV} - \left(-0.0301(OPT\#1_{MATLABPTV})^2 - 0.3858(OPT\#1_{MATLABPTV}) - 1.5337\right)$$

This relationship was plotted by fitting a second order polynomial to the data and resulted in a high R^2 value, as shown in the figure below.

Approximate Relationship to Estimate Opt#3 PTV from Opt#1

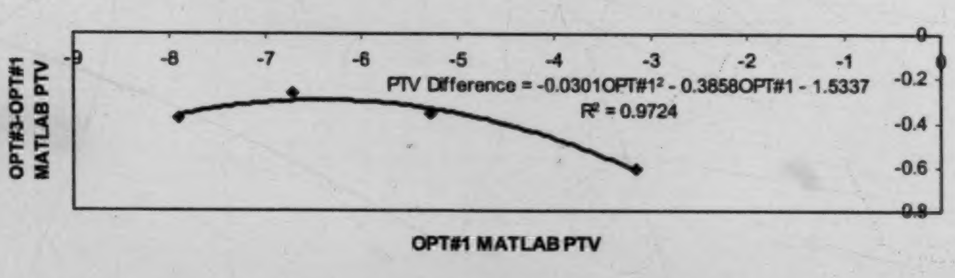

It is important to note that the vertical axis is the difference between the measurements of the two instruments. In addition, recall the repeatability uncertainty of the MATLAB PTV was determined to be ±0.4 PTV.

A similar analysis was performed on the Osstell® transducer leads and resulted in a statistical significant difference only between the fixture transducer leads - #483 and #484. In this case, the relationship between the leads was determined to be:

$$ISQ_{\#483} = ISQ_{\#484} - 4$$

In addition, the Periotest® instruments remained precise because the value of the manufacturer's calibration cap remained consistent throughout the study, to date. The Periotest® measurement values from the Periotest® training blocks could not be used because the properties of the blocks changed slightly during the study. The Osstell® transducer lead and processing unit remained precise during the study because the measurements of the same lead on the same calibration block remained constant. Therefore, the data shown is believed to be recorded using precise instrumentation and any differences in the measurements are a result of the implant interface changing properties.

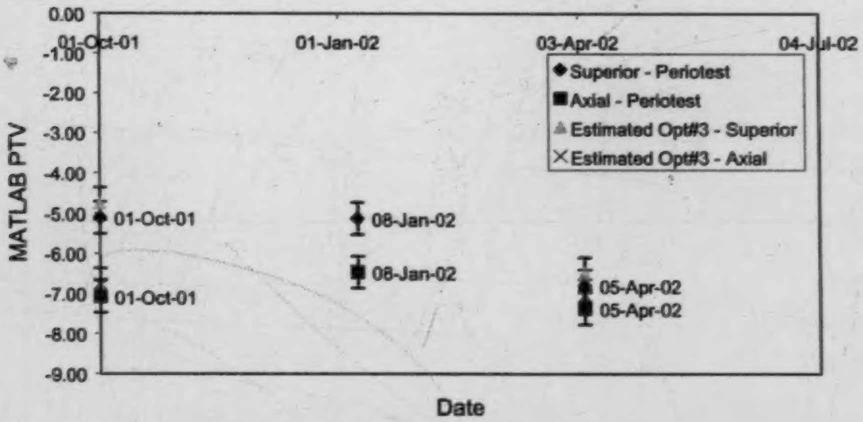

Figure O-1: Periotest® Measurements for BAHA Patient #1

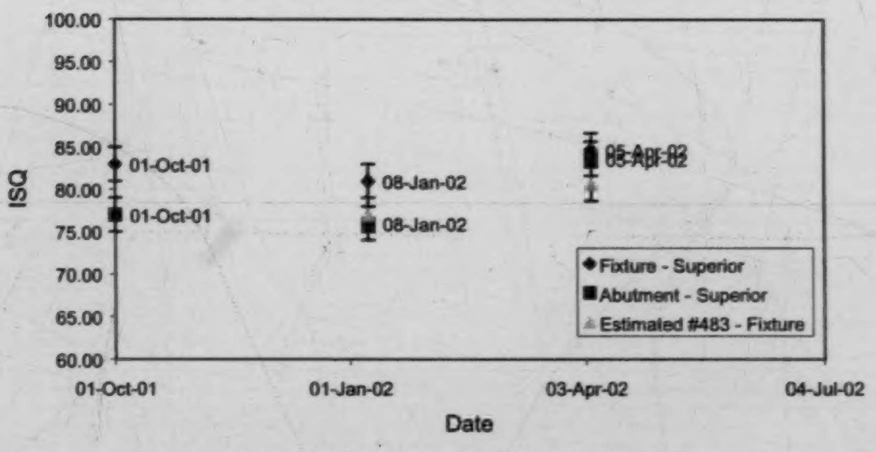

Figure O-2: Osstell® Measurements for BAHA Patient #1

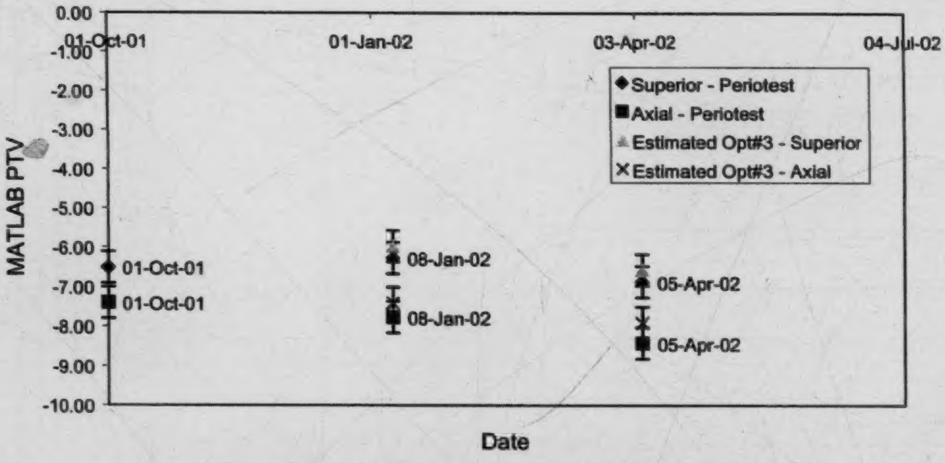

Figure O-3: Periotest® Measurements for BAHA Patient #2

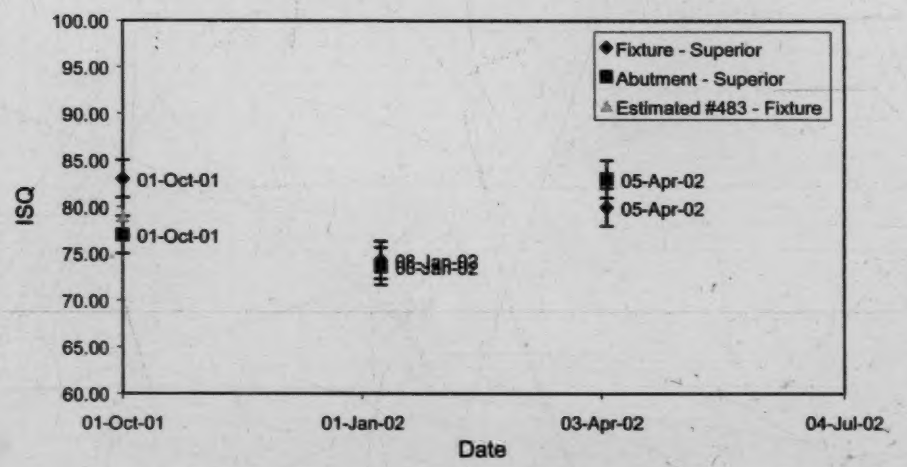

Figure O-4: Osstell® Measurements for BAHA Patient #2

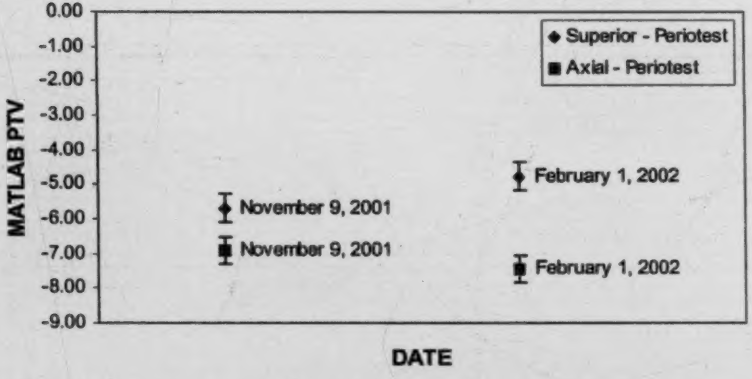

Figure O-5: Periotest® Measurements for BAHA Patient #4

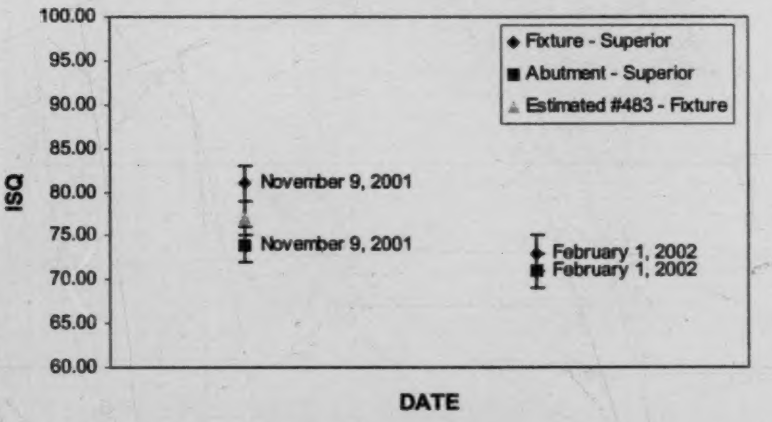

Figure O-6: Osstell® Measurements for BAHA Patient #4

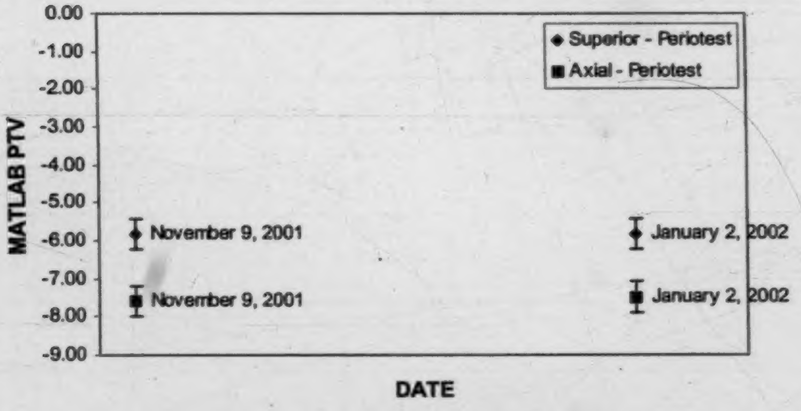

Figure O-7: Periotest® Measurements for BAHA Patient #5

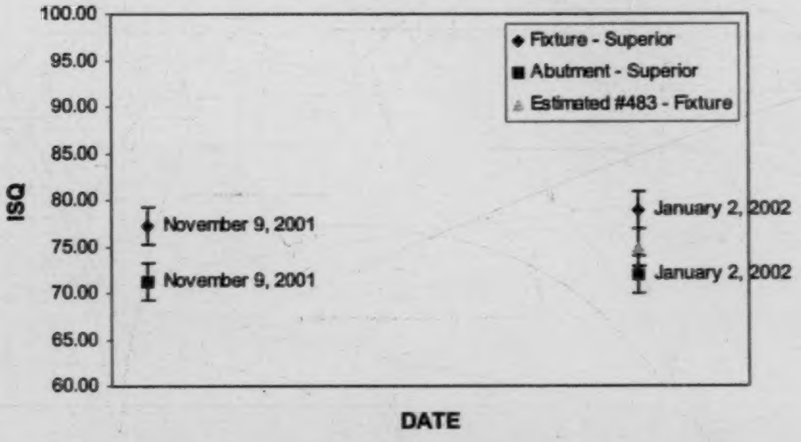

Figure O-8: Osstell® Measurements for BAHA Patient #5

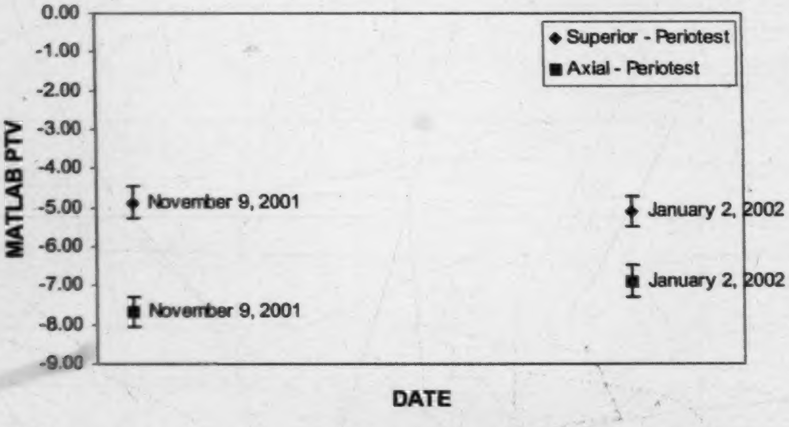

Figure O-9: Periotest® Measurements for BAHA Patient #6

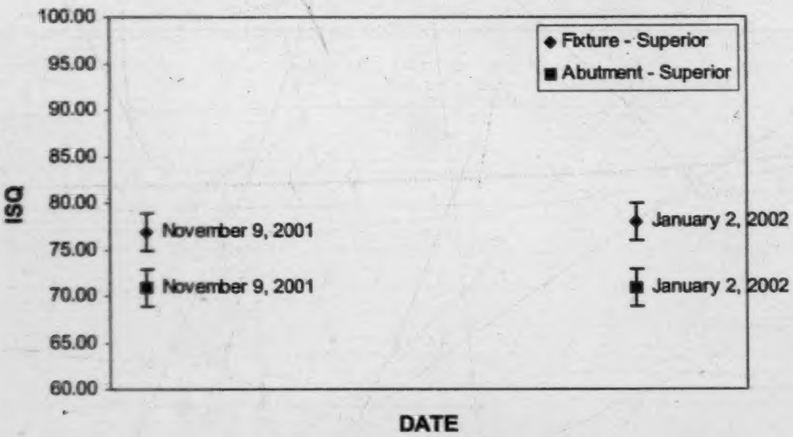

Figure O-10: Osstell® Measurements for BAHA Patient #6

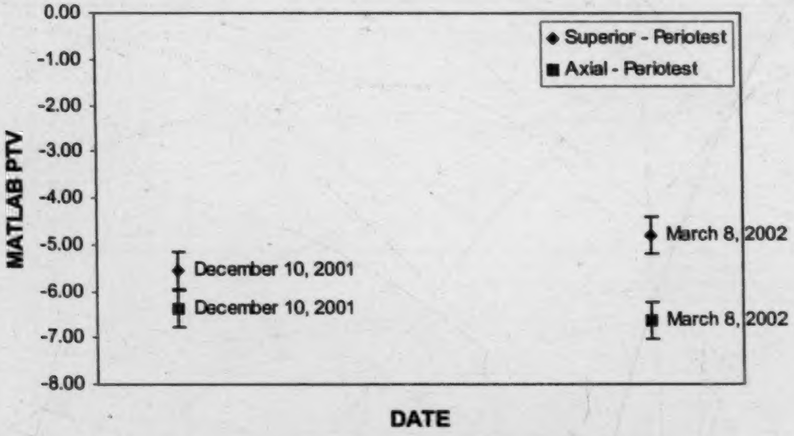

Figure O-11: Periotest® Measurements for BAHA Patient #7

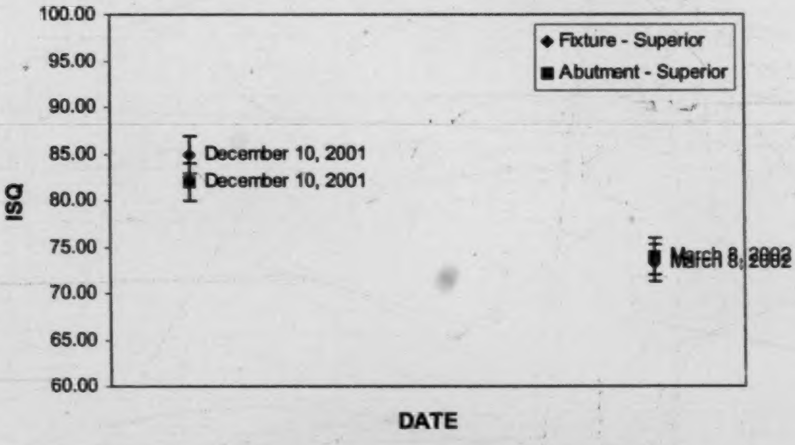

Figure O-12: Osstell® Measurements for BAHA Patient #7

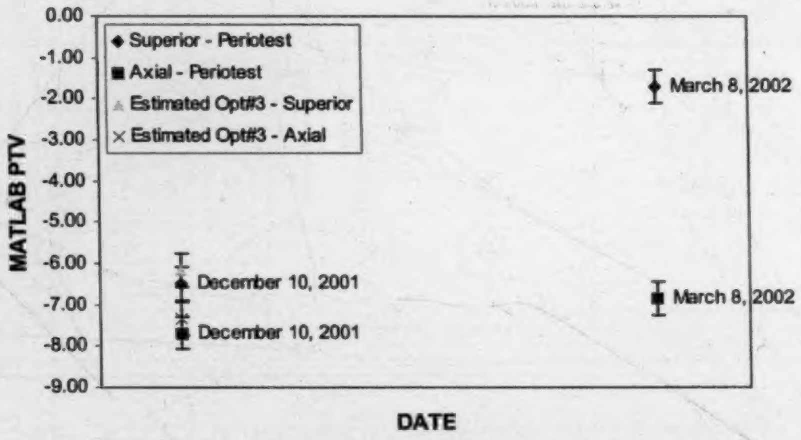

Figure O-13: Periotest® Measurements for BAHA Patient #8

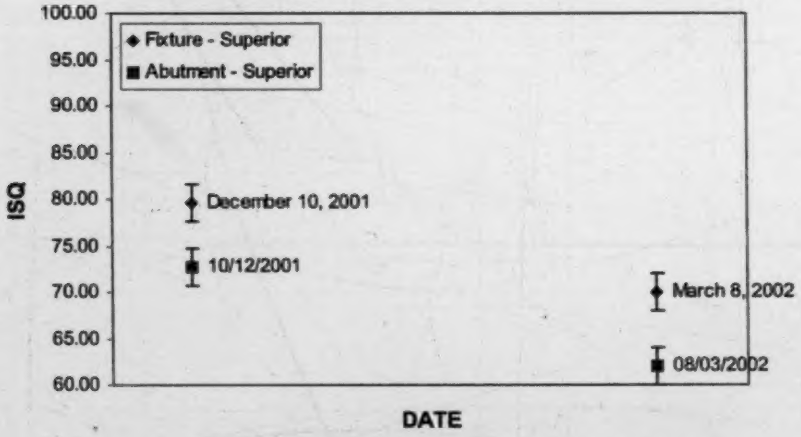

Figure O-14: Osstell® Measurements for BAHA Patient #8

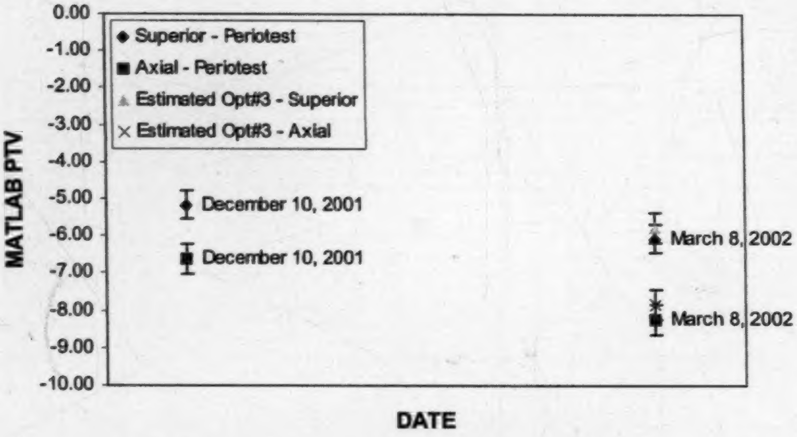

Figure O-15: Periotest® Measurements for BAHA Patient #9

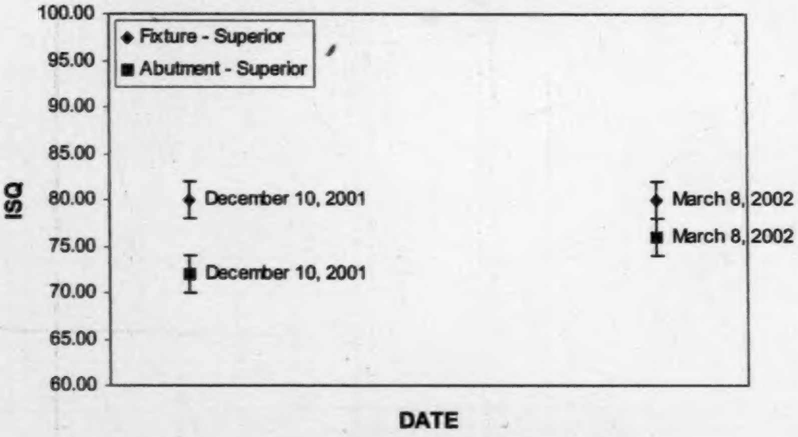

Figure O-16: Osstell® Measurements for BAHA Patient #9

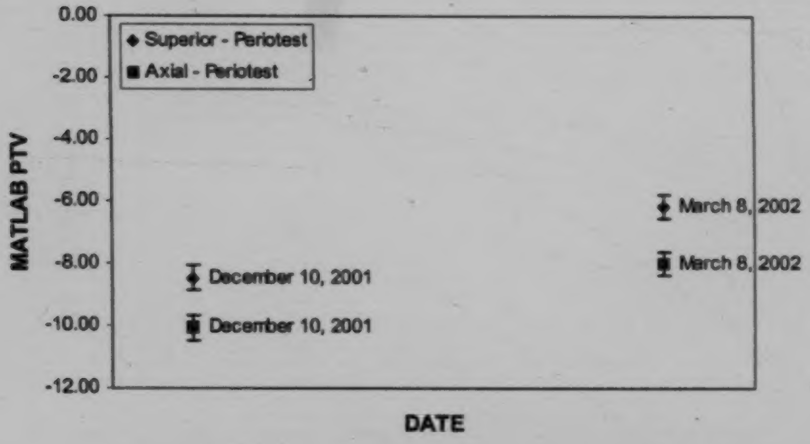

Figure O-17: Periotest® Measurements for BAHA Patient #10

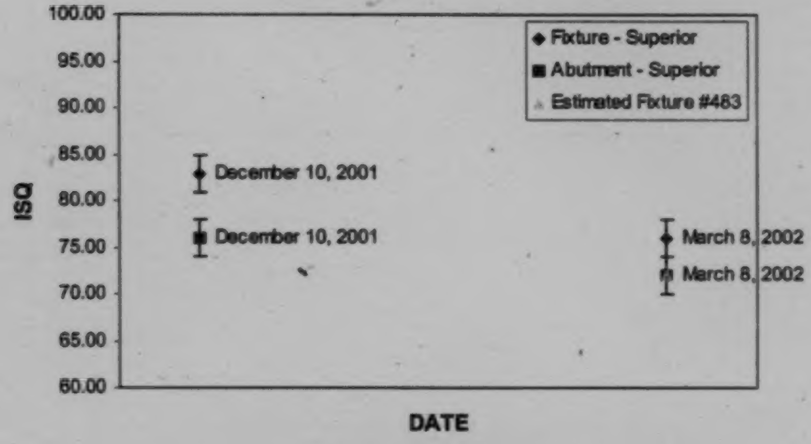

Figure O-18: Osstell® Measurements for BAHA Patient #10